DOCTORAL THESIS

Full Stack 5G Physical Layer Transceiver Design for NOMA in Mobile Heterogeneous Networks

Md Shantanu Islam

A thesis submitted in partial fulfilment of the requirements of Birmingham City University for the degree of Doctor of Philosophy

January 2024

College of Computing,

BIRMINGHAM CITY UNIVERSITY

BIRMINGHAM CITY
University

Abstract

The Fifth Generation (5G) and Beyond 5G (B5G) wireless networks are emerging with a variety of new capabilities, focusing on Massive Machine-Type Communications (mMTC), enabling new use cases and services. With this massive increment of mMTC along with increasing users, higher network capacity is a must for 5G and B5G. The integration of mMTC with traditional user traffic creates a heterogeneous network landscape. To address this challenge, future network designs must prioritize optimizing spectrum efficiency while meeting diverse service demands. Non-Orthogonal Multiple Access (NOMA) stands out as a promising technology for enhancing both system capacity and operational efficiency in such heterogeneous networks. Due to its non-orthogonal resource allocation, NOMA outperforms Orthogonal Multiple Access (OMA) in spectral efficiency, throughput, and user capacity, while also offering superior scalability and adaptability to network heterogeneity. Despite its promising advantages, large-scale implementation of NOMA in cellular systems remains elusive due to various challenges, making it a focal point of current research in cellular network technology.

While there has been considerable progress in implementing NOMA for broadcast and multicast services, notably with Layer Division Multiplexing (LDM) in next-generation digital TV, the challenges of unicast downlink transmission in NOMA remain largely unexplored. Unicast transmission requires a highly tailored network configuration adaptable to individual user requirements and dynamic channel conditions. Clustering users under a single NOMA channel must be both efficient and adaptive to ensure successful transmission, especially for mobile receiver. Besides, the interplay between NOMA and other 5G technologies remains insufficiently explored, in part due to the lack of an established NOMA-5G framework. Specifically, the collective impact of 5G physical layer technologies such as Low-Density Parity Check (LDPC) coding, Multiple-Input Multiple-Output (MIMO) Beamforming, and mmWave transmission on NOMA's performance has not been comprehensively studied. Furthermore, in NOMA schemes involving more than two multiplexed users, known as Multilayer NOMA (N-NOMA), the system becomes increasingly complex and susceptible to noise. While N-NOMA holds considerable promise for scalability, its performance metrics are not yet fully characterized, due to challenges ranging from resource allocation complexities to transceiver design issues. Additionally, existing analytical models for performance evaluation are developed for orthogonal systems, are not fully applicable for assessing NOMA performance. Developing new models that incorporate the impact of non-orthogonality could provide more accurate performance assessments and offer valuable insights for future NOMA research.

Initially this thesis investigates the feasibility of LDM for unicast & multicast downlink transmission scenarios for Internet of Things (IoT)- user pairs. The findings indicate the Core Layer (CL) performance aligns with IoT requirements while Enhance Layer (EL) layer is suitable for users. A specialized Bit Error Rate (BER) expression is formulated to precisely predict CL performance, considering Lower Layer (LL) interference with predefined power ratio. Subsequently, the thesis employs a novel surface mobility model and adaptive power ratio allocation to evaluate LDM pair sustainability under various receiver mobility conditions.

Extending the LDM-Orthogonal Frequency Division Multiplexing (OFDM) model, this thesis presents a Third Generation Partnership Project (3GPP)-compliant 5G transceiver incorporating N-NOMA. This design incorporates a strategically-arranged set of NOMA functionalities and undergoes a rigorous performance evaluation. In particular, the transceiver provides a comprehensive assessment of N-NOMA performance, considering various transmission parameters such as LDPC code rate, MIMO order, modulation schemes, and channel specifications. These considerations not only provide new insights into non-orthogonal access technologies but also highlight dependencies on these factors for network configuration and optimization. To further advance this work, a one-shot N-NOMA multiplexing technique is developed and implemented, simplifying multi-layer standard sequential combiners to reduce transmission latency and transceiver complexity. A more accurate analytical BER expression is also formulated that considers the impact of both residual and non-residual Successive Interference Cancellation (SIC) errors across NOMA layers.

To build upon these advancements, an adaptive Power Allocation (PA) technique is introduced to optimize NOMA cluster sustainability and throughput. Employing a greedy algorithmic approach, this method uses real-time transmission feedback to dynamically allocate power across NOMA layers. In addition, a new Three Dimensional (3D) mobility model has been developed, consistent with existing 3GPP standards, capturing vehicular and pedestrian movement across urban and rural macro & micro-cell environments. When integrated with the PA technique, this model allows for real-time adjustments in the NOMA power ratio, effectively adapting to fluctuating receiver channel conditions.

Collectively, the findings from this research not only indicate significant physical layer performance improvements but also provide new insights into the potential of non-orthogonal access technologies. In the LDM-OFDM setup presented in Chapter 3, the EL layer needs 15 dB more Signal-to-Noise Ratio (SNR) than the CL to achieve the same BER, but allows for higher data rates. When it comes to mobility, IoT movement accounts for about 70% of link terminations in scenarios with similar mobility patterns. The N-NOMA-5G shows significant improvement in low SNR performance compared to existing literature. The 3 layer simulations shows on average a 60% reduction in the SNR requirements to achieve similar BER. The implementation of a one-shot multiplexer has demonstrated a substantial reduction in N-NOMA multiplexing time, particularly with the growing number of NOMA layers, as detailed in Chapter 4. Notably, the simulation outcomes spanning 2 to 10 layers of NOMA multiplexing indicate an remarkable 52% reduction in processing time. This underscores the effectiveness of the one-shot multiplexer in enhancing efficiency, particularly as the complexity of the NOMA setup intensifies. The developed analytical model also shows over 95% similarities with the simulation results. The impact of dynamic PA for both static and mobile receivers demonstrates on average, over 40% improvements in link sustainability time for mobile users and for static users, it achieves optimal PA and fast convergence within just 12 iterations, as detailed in Chapter 5.

Keywords: NOMA, 5G, B5G, BER, SIC, LDM, PA, Link Sustainability, User Mobility.

Acknowledgements

I am deeply grateful to my Director of Studies (DoS), Dr. Raouf Abozariba, for his unwavering support and invaluable guidance throughout this research journey. His willingness to make time, even amidst his demanding schedule, to provide feedback and advice was immensely appreciated. I am truly honoured by the trust and confidence he placed in me and my research during my PhD journey.

I wish to express my profound gratitude to my second supervisor, Professor Taufiq Asyhari. His insights and feedback enriched this research, and his guidance was instrumental in the development of the analytical framework. His contributions were truly invaluable, and I am sincerely appreciative of his involvement.

I extend my heartfelt thanks to my external supervisor and former DoS, Professor Mohammad Patwary. His continuous guidance and insightful ideas laid the foundation for this research. His insistence on depth of understanding and refusal to accept anything less than thorough comprehension nurtured my ability for critical analysis and a more profound grasp of intricate subjects. I am profoundly indebted to him for elevating my research skills and understanding.

My gratitude extends to John Hayes, Abrar Jahin Almazi Bipon, and Dr. Abida Perveen— friends and fellow researchers at the College of Computing, Birmingham City University. A special acknowledgment to John for those extended nights of hard work; together, our combined efforts and shared spirit of collaboration always pushed me forward. I am deeply appreciative of Bipon, who generously offered insights and feedback even before embarking on his own research journey. His unwavering support during challenging times, particularly the rigorous COVID lockdown and the loss of my Aunt, was invaluable.

On a personal note, my wife, Adrita, has been a pillar of support. Balancing the demands of this PhD wouldn't have been possible without her understanding. I'm forever grateful to my parents for their unwavering love. Especially to my father, Md Shahidul Islam, for developing my interest in acquiring education from a very young age and for always motivating me during my educational career. I believe,

without his support and faith in my abilities, my accomplishments in educational journey would not have been possible.

I extend my heartfelt gratitude to the "College of Computing" at Birmingham City University for their unwavering support and adept management, which were instrumental in the timely completion of this research. Additionally, my sincere appreciation goes to Birmingham University for their generosity in providing the PhD studentship and sponsoring this research.

Finally, I would like to say thanks to the examiners for spending their time reviewing this thesis.

Signed: Md Shantanu Islam

Date: January 8, 2024

Declaration of Authorship

I, Md Shantanu Islam, declare that this thesis titled, "Full Stack 5G Physical Layer Transceiver Design for NOMA in Mobile Heterogeneous Networks" and the work presented in it are my own. I confirm that:

- This work was done wholly or mainly while in candidature for a research degree at this University.
- Where any part of this thesis has previously been submitted for a degree or any other qualification at this University or any other institution, this has been clearly stated.
- Where I have consulted the published work of others, this is always clearly attributed.
- Where I have quoted from the work of others, the source is always given. With the exception of such quotations, this thesis is entirely my own work.
- I have acknowledged all main sources of help.
- Where the thesis is based on work done by myself jointly with others, I have made clear exactly what was done by others and what I have contributed myself.

Signed: Md Shantanu Islam

Date: January 8, 2024

List of Publications

Journal:

J01: **Md Shantanu Islam**, Raouf Abozariba, De Mi, Mohammad Patwary, Dazhi He, and A. Taufiq Asyhari, "Design and Evaluation of Multi-layer NOMA on NR Physical Layer for 5G and Beyond", IEEE Transactions on Broadcasting, pp. 1-15, 2023. [*Published*]

Book Chapter:

B01: **Md Shantanu Islam**, Raouf Abozariba, A Taufiq Asyhari, Mohammad Patwary, and Mohammad A Matin, "Feasibility of LDM to Serve User-IoT Pairs in the Future Wireless Network", in A Glimpse Beyond 5G in Wireless Networks. Springer International Publishing 2022, pp. 231-253 [*Published*]

Conference:

C01: **Md Shantanu Islam**, Mohammad Patwary, Roger Tait, and Evtim Peytchev, "Layer division multiplexing for 5G DL transmission within ultra-dense heterogeneous networks", in 2020 IEEE 91st Vehicular Technology Conference (VTC2020-Spring). IEEE, 2020, pp. 1-7 [*Published*]

C02: **Md Shantanu Islam**, John Hayes, Raouf Abozariba, Adel Aneiba, and Taufiq Asyhari, "Evaluating NOMA Link Resiliency Under Mobility: A 5G NR Link-level Simulation", in 2024 IEEE International Conference on Communications (ICC2024) [*Submitted*]

Contents

List of Figures

List of Algorithms

List of Tables

List of Abbreviations

1G First Generation

2D Two Dimensional

2G Second Generation

3D Three Dimensional

3G Third Generation

3GPP Third Generation Partnership Project

4G Fourth Generation

5G Fifth Generation

6G Sixth Generation

A2G Air-to-Ground

AP Access Point

ATSC Advanced Television Systems Committee

AWGN Additive White Gaussian Noise

B5G Beyond 5G

BER Bit Error Rate

BPSK Binary Phase-Shift Keying

BS Base Station

CDL Clustered Delay Line

CDMA Code Division Multiple Access

CL Core Layer

CSI Channel State Information

DL-SCH Downlink Shared Channel

EL Enhance Layer

eMBB Enhanced Mobile Broadband

eMBMS evolved Multimedia Broadcast Multicast Service

FD Full-Duplex

FDM Frequency Division Multiplexing

FDMA Frequency Division Multiple Access

FPGA Field-Programmable Gate Array

GB Grant Based

GF Grant Free

HARQ Hybrid Automatic Repeat Request

HD Half-Duplex

HDTV High-Definition Television

IoT Internet of Things

IRS Intelligent Reflecting Surfaces

KPI Key Performance Indicator

LAN Local Area Network

LCS Local Coordinate System

LDM Layer Division Multiplexing

LDPC Low-Density Parity Check

LL Lower Layer

LoS Line of Sight

LTE Long Term Evolution

M-PLP Multiple Physical Layer Pipe

M2M Machine to Machine

MA Multiple Access

MBMS Multimedia Broadcast Multicast Services

MC-MTC Massive and Critical MTC

MCSs Modulation and Coding Schemes

MEC Mobile Edge Computing

MIMO Multiple-Input Multiple-Output

MISO Multiple-Input Single-Output

mMIMO massive MIMO

mMTC Massive Machine-Type Communications

MTC Machine Type Communication

N-NOMA Multilayer NOMA

NFFT Non-Uniform Fast Fourier Transform

NGDPA Normalized Gain Difference PA

NGMA Next Generation Multiple Access

NLoS Non-Line of Sight

NOMA Non-Orthogonal Multiple Access

NR New Radio

NSA Non-Standalone

O2I Outdoor to Indoor

OFDM Orthogonal Frequency Division Multiplexing

OFDMA Orthogonal Frequency-Division Multiple Access

OMA Orthogonal Multiple Access

OTFS Orthogonal Time Frequency Space

P2MP Point-to-Multi Point

P2P Point-to-Point

PA Power Allocation

PDSCH Physical Downlink Shared Channel

PIN Positive Intrinsic Negative

PL Pathloss

QAM Quadrature Amplitude Modulation

QoS Quality of Service

QPSK Quadrature Phase-Shift Keying

RIS Reconfigurable Intelligent Surface

RMa Rural Macro

SA Standalone

SC-FDMA Single Carrier FDMA

SER Symbol Error Rate

SIC Successive Interference Cancellation

SISO Single-Input Single-Output

SNR Signal-to-Noise Ratio

SQAM Square QAM

SVD Singular Value Decomposition

TDL Tapped Delay Line

TDM Time Division Multiplexing

TDMA Time Division Multiple Access

THz Terahertz

UAV Unmanned Aerial Vehicle

UE User Equipment

UHD Ultra-High-Definition

UHDTV Ultra-High-Definition Television

UL Upper Layer

UMa Urban Macro

UMi Urban Micro – Street Canyon

URLLC Ultra-Reliable Low-Latency Communication

VLC Visible Light Communications

WCDMA Wideband CDMA

Wi-Fi Wireless Fidelity

List of Notations

(x, y)	Coordinate in Two Dimensional (2D) plane
α_i	NOMA i-th layer Power
δ	Dirac Delta Function
$\mathbf{H}$	Channel Matrix
$\mathbf{N}_0$	Noise Matrix
ρ	SNR
τ	Path Delay
θ	Angle between transmit beam and user location
C	Channel Capacity
d	Distance
dB	Decibel
EB	Exabytes
f_c	Carrier frequency
f_d	Doppler frequency
g_i	Power ratio between i-th and $(i-1)$-th NOMA layer
I	In-phase carriers
p_n	Noiser Power
p_t	Transmit Power
Q	Quadrature-phase carriers

t	Time
x	Transmit Bit
y	Received Bit

This dissertation is dedicated to my dad Md Shahidul Islam, mom Mowsumi Nargis, aunt Ferdousi Begum and mentor Prof. M Mofazzal Hossain.

Chapter 1

Introduction

1.1 Background & Motivation

Mobile communication technologies have seen remarkable advancements over the years. Starting with the foundational voice services of First Generation (1G), advancing to the text and low-speed data offerings of Second Generation (2G), the multimedia services of Third Generation (3G), and culminating in the high-speed data transmissions of Fourth Generation (4G), each iteration marked a pivotal leap in technological evolution. With Fifth Generation (5G) now widely deployed, it offers enhanced functionalities specifically designed for Internet of Things (IoT), augmented reality, virtual reality, and an array of cloud-driven applications [1–3]. The constraints of the 4G architecture have been surmounted, ushering in an era of advanced applications and services [4]. Parallelly, Multiple Access (MA) technologies have matured alongside these generations, acting as a foundational element in the evolution of cellular networks. Each generation distinctly adopts a specific MA technology, as depicted in figure 1.1.

The 5G technology in use today faces challenges in accommodating the diverse needs of emerging services, especially given their varied requirements and the swift addition of new users. In 2022, there was a 39% year-on-year surge in mobile network traffic, culminating in a staggering 100 EB/month [5]. The swift rise of the IoT, which includes smart cities, homes, and advanced transportation systems, combined with the spread of smart devices, suggests an imminent connectivity demand that might soon overwhelm current networks [6,7]. Projections for 2023 estimate the global mobile devices count at 13.1 billion, with internet-enabled devices expected

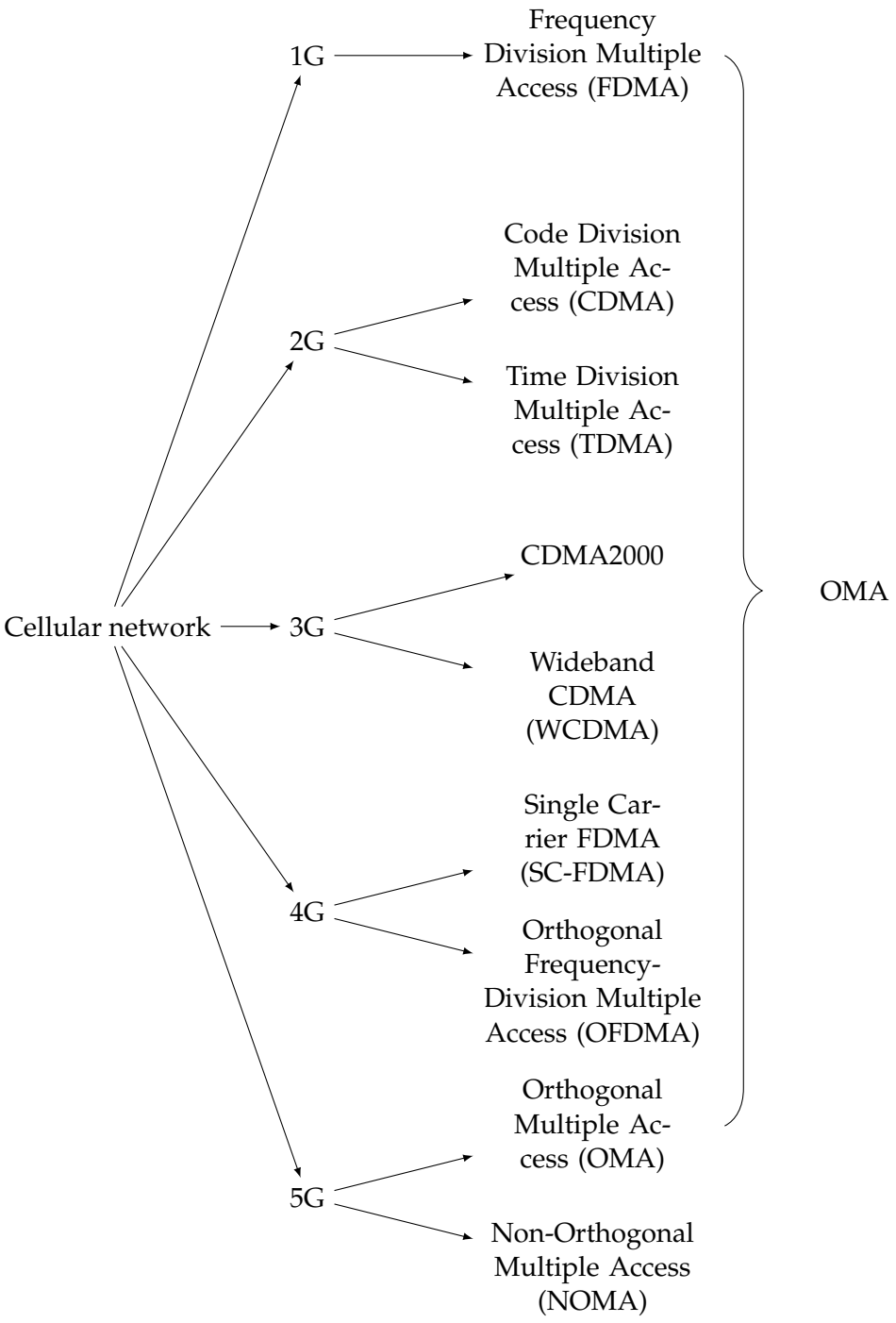

FIGURE 1.1: Evolution of MA technology with each cellular generation

to jump from 18.4 billion in 2018 to a projected 29.3 billion [8]. This rapid growth, fuelled by a world still progressing towards total connectivity, hints that both 4G and 5G networks might soon be strained beyond their intended capacities. Such a situation highlights the urgent need for novel solutions to address 5G challenges and set the stage for upcoming Sixth Generation (6G) networks [9].

The advent of 5G marks a significant leap in mobile communications. However, the full scope of its capabilities, especially concerning MA techniques, is yet to be completely realized. This is where the role of NOMA becomes crucial. The conventional OMA methods, which were pivotal for previous generations, are now showing their constraints, particularly when managing a large array of devices that demand high-speed, concurrent connections [10].

At its core, NOMA is designed to permit multiple users to utilize the same radio resources. Such a strategy offers benefits like improved spectral efficiency, minimized transmission delays and queuing, and expanded connectivity [11, 12]. Despite the well-established theoretical foundations of NOMA, its practical integration within the 5G and Beyond 5G (B5G) physical layer presents intricate challenges that are a subject of ongoing research [10, 13].

The evolution from 5G to B5G and, eventually, 6G is not merely about achieving faster speeds or accommodating more devices. It is about architecting a network that is intelligent, adaptive, and discerning in prioritizing diverse communication needs. For instance, it is crucial that a remote surgery procedure gets network priority over routine video streaming. Similarly, ensuring seamless communication for critical IoT devices in densely populated urban areas is paramount.

In this evolving landscape, delving deep into the capabilities of NOMA within the 5G physical layer is not just an academic pursuit but a critical necessity. As global initiatives, such as the "6G Flagship" in Finland and Terahertz (THz) communication studies in the USA, gain momentum [9], the research and advancements in 5G and NOMA will undoubtedly influence the future of mobile communications. The goal is to ensure that upcoming networks are not only faster but also smarter, more efficient, and truly prepared for the demands of an increasingly connected world.

In conclusion, the exploration of NOMA's performance within the 5G physical layer presents a multitude of challenges. However, addressing these challenges

head-on will pave the way for groundbreaking innovations in cellular communications, setting the stage for a future where connectivity is seamless, efficient, and universal.

1.2 Problem Statement

The advancement of wireless communication has positioned NOMA as a pivotal component in shaping future wireless infrastructures. Its potential was evident when NOMA, using Successive Interference Cancellation (SIC) for interference cancellation, was introduced as the future cellular radio access technology in [13]. Multiple research efforts have underlined the superiority of NOMA over OMA in terms of spectral efficiency, throughput, and user capacity [14–17]. This prominence was further validated when Layer Division Multiplexing (LDM), a subtype of NOMA, was integrated into the Advanced Television Systems Committee (ATSC) 3.0 broadcasting standard [18], setting high anticipations for its role in the evolution of 5G.

Yet, challenges arise when attempting to integrate NOMA seamlessly into the New Radio (NR) architecture, particularly in the domain of downlink unicast transmission [14–17]. Although recent studies have extensively examined the advantages of NOMA in broadcast transmission, unicast downlink NOMA remains comparatively unexplored [19,20]. Due to the receiver-specific nature of unicast transmission, two distinct challenges arise. First, unicast NOMA demands precise user grouping to cater to diverse Quality of Service (QoS) requirements. Second, the influence of receiver mobility on NOMA performance remains unclear. In light of these challenges, effective power distribution between NOMA layers becomes essential for dependable transmission. This necessitates Power Allocation (PA) methods adaptable to the fluctuating conditions of mobile receivers.

5G introduced advanced technologies like Multiple-Input Multiple-Output (MIMO) beamforming, mmWave transmission, Polar and Low-Density Parity Check (LDPC) channel coding. Yet, the integration of NOMA with these technologies remains an area yet to be thoroughly examined [12, 15]. These innovations hold the promise to elevate NOMA performance, potentially streamlining its adoption in both uplink and downlink transmissions, paving the way for its inclusion in forthcoming 5G and

B5G standards. Such technologies could boost NOMA performance, paving its way into 5G and B5G standards, especially in low-Signal-to-Noise Ratio (SNR) regions favouring Multilayer NOMA (N-NOMA). While NOMA's true capabilities may be realized in N-NOMA, current studies often limit their scope to theoretical considerations due to the intricate signal processing complexities and sensitivity to noise in both transmitters and receivers. This gap in practical research on NOMA and N-NOMA explains the absence of an official NR framework integrating NOMA. Even though the recent Third Generation Partnership Project (3GPP) release 16 released a study on 2-layer Upper Layer (UL) NOMA [21], an established framework for 5G downlink transmission still remains elusive. This underscores the pressing need to develop a comprehensive 5G physical layer transceiver that efficiently incorporates NOMA.

1.3 Research Question

Given the rapid advancements in mobile communication technologies, particularly the evolution from 1G to 5G, and the pivotal role of NOMA in shaping the future of wireless infrastructures, there arises a pressing need to understand its full potential and challenges within the 5G framework. The integration of NOMA with emerging 5G technologies, such as MIMO beamforming, mmWave transmission, Polar, and LDPC channel coding, presents a myriad of opportunities and complexities. Furthermore, the influence of receiver mobility on NOMA performance, especially in the context of downlink unicast transmission, remains a significant area of concern.

Against this backdrop, the central research question that this study aims to address is:

How can NOMA be effectively incorporated into the 5G physical layer downlink transceiver architecture? What are the potential advantages, including improved spectral efficiency and throughput, and the challenges, such as SNR-data rate trade-offs and increased multiplexing complexity, associated with its adoption in wireless communication systems?

This research question will guide the exploration of:

- The practical integration challenges of NOMA within the 5G and B5G physical layer.
- The symbiotic potential of combining NOMA with advanced 5G technologies.
- The impact of receiver mobility on NOMA performance and the development of adaptive PA methods tailored for dynamic channel conditions.
- The theoretical and practical considerations of N-NOMA extending the scope and potential of NOMA beyond the current 2 layer approach.

By addressing this research question, the study aims to bridge the existing gaps in the literature, provide insights into the practical challenges and solutions associated with NOMA, and set the foundation for its efficient integration in future wireless communication systems.

1.4 Aim & Objectives

Aim

To investigate and optimize NOMA technologies for enhancing spectrum efficiency and operational performance in 5G and B5G networks, particularly in the context of downlink unicast transmission.

Objectives

1. **Investigate LDM-Orthogonal Frequency Division Multiplexing (OFDM) Framework:** To thoroughly investigate the LDM-OFDM framework for unicast and multicast downlink transmission scenarios, with a focus on SNR and Bit Error Rate (BER) performance across different layers.
2. **Develop & Evaluate N-NOMA-5G Transceiver:** To design a 3GPP-compliant 5G transceiver that incorporates all necessary NOMA functionalities. The objective also includes rigorously assessing its performance metrics under various conditions such as LDPC code rate, MIMO order, modulation schemes, and channel specifications, and optimizing the transceiver model to reduce multilayer challenges and complexity.

3. **Formulate Analytical Models:** To develop accurate analytical models for BER, taking into consideration the additional interference that results from non-orthogonal resource sharing.

4. **Assess Mobility Impact for Unicast Transmission:** To evaluate the impact of receiver mobility on link sustainability and link termination. This involves developing specialized mobility models that simulate urban and rural scenarios for motorized and pedestrian movement.

5. **Optimize PA:** To introduce an adaptive PA technique to dynamically allocate power across NOMA layers, thereby enhancing cluster sustainability and throughput. This technique will be optimized for both dynamic and static channel conditions.

1.5 Research Methodology

The research methodology adopted for this study is a structured and iterative approach, designed to ensure a comprehensive exploration of the research problem and its potential solutions. The methodology is described into distinct phases, each building upon the previous, to ensure a systematic progression towards the research aim. The phases of the methodology are visually represented in Figure 1.2.

1.5.1 Initial Literature Review

The research commences with an exhaustive review of existing literature in the domain NOMA, LDM and 5G physical layer. This phase aims to understand the current state of knowledge, identify seminal works, and discern gaps in the existing body of literature.

1.5.2 Define Initial Research Problem

Post the literature review, the primary research problem is articulated. This problem statement is rooted in the identified knowledge gaps and serves as the foundation for subsequent phases.

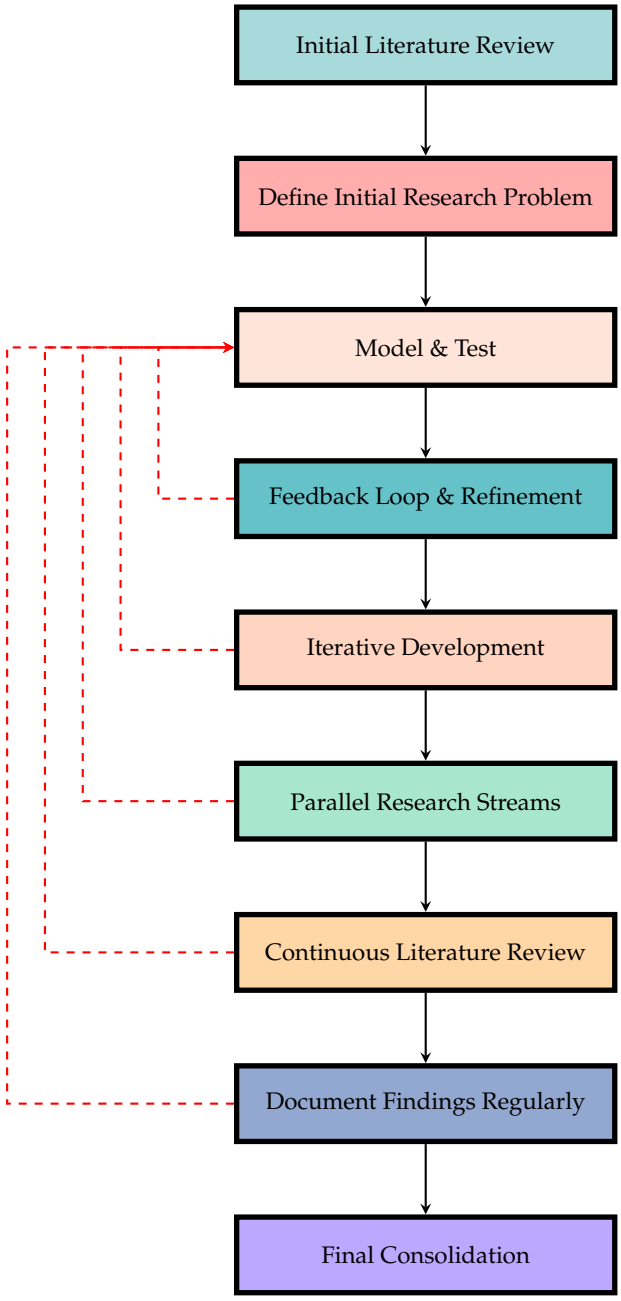

FIGURE 1.2: Research methodology

1.5.3 Model & Test

Upon defining the research problem, a model representing the problem is formulated. This model is then subjected to rigorous testing to validate its accuracy and reliability. Both analytical methods and comprehensive simulations are employed for validation.

1.5.4 Feedback Loop & Refinement

The results from the testing phase are critically analysed, leading to feedback that informs refinements in the model. This iterative feedback mechanism ensures that the model evolves to be a robust representation of the research problem.

1.5.5 Iterative Development

Building upon the feedback loop, the research adopts an iterative development approach. This ensures continuous improvement and adaptation of the model in response to new findings and insights.

1.5.6 Parallel Research Streams

As the research progresses, parallel streams of inquiry may emerge, necessitating simultaneous exploration. These streams, while distinct, are interconnected and contribute to the holistic understanding of the research problem.

1.5.7 Continuous Literature Review

To ensure the research remains aligned with contemporary developments in the field, a continuous literature review is conducted. This ongoing review ensures that the research is informed by the latest findings and theories in the domain.

1.5.8 Document Findings Regularly

Throughout the research process, findings are meticulously documented. This not only aids in maintaining clarity and direction but also facilitates the dissemination of knowledge through academic publications.

1.5.9 Final Consolidation

The culmination of the research process is the final consolidation phase. Here, all findings, models, and insights are synthesized to present a comprehensive solution to the initial research problem. This phase also sets the stage for future research directions.

In conclusion, the adopted research methodology is a dynamic and iterative process, ensuring a thorough exploration of the research problem and the development of robust solutions.

1.6 Contributions to Knowledge

Throughout the course of this doctoral research, a series of pivotal advancements have been made in the realm of wireless communication, particularly concerning the integration of NOMA technologies. This section methodically outline the principal contributions of this thesis.

Integration of LDM in Unicast/Multicast Transmission Framework

- Advancement of a unified framework for downlink unicast/multicast transmissions, aiming to cater to both human users and IoT devices across urban and rural landscapes, thereby enhancing spectral efficiency and strengthening coverage range.
- An analytical framework to evaluate Core Layer (CL) BER within an uncoded OFDM transceiver framework.
- Introduction of a detailed mobility model employing a Local Coordinate System (LCS), which sketches out the trajectories of mobile users in varied terrains—rural, urban, and highways—by leveraging random waypoint, Manhattan, and freeway mobility models. This model is adept at assessing path loss and predicting change in channel conditions as users transition from their original locations.
- Assessment of sustainable link duration for mobile LDM pairs, which lays the foundation for optimized user pairing based on spatial positioning and mobility patterns.

N-NOMA-5G Transceiver Design

- A novel NOMA-aided 5G NR-compliant transceiver design is developed, incorporating NOMA and MIMO functionalities into the NR physical layer, facilitating heterogeneous transmission by overlapping multiple NOMA layers within a single communication channel.
- An enhancement to the N-NOMA multiplexer design is introduced, utilizing a one-shot method that reduces both the complexity and latency relative to conventional sequential combiners.
- A closed-form BER expression is formulated, accommodating both residual and non-residual errors from SIC. This also incorporates the gains from MIMO, offering a novel analytical tool for N-NOMA system assessment.
- Extensive evaluations of BER across varying modulation orders, channel coding rates, MIMO orders, and NOMA layers within diverse Clustered Delay Line (CDL) and Tapped Delay Line (TDL) channels. These evaluations empirically substantiated the practicality and efficacy of the suggested transceiver design and analytical framework.

Adaptive PA for Downlink N-NOMA

- An adaptive PA algorithm is developed specifically designed for downlink N-NOMA transmission. This algorithm adopts a greedy strategy, leveraging transmission feedback for dynamic power distribution among NOMA layers.
- A comprehensive analytical model to depict Three Dimensional (3D) user movement is also developed. Using the 3GPP-endorsed path loss model, it integrates probabilistic selections of Line of Sight (LoS) and Non-Line of Sight (NLoS) transmissions to compute the SNR for each user that mimic real world implementation. This SNR then interfaces with the proposed 5G transceiver model, providing insights into the mobile user performance in the suggested transmission framework, both with and without the adaptive PA.

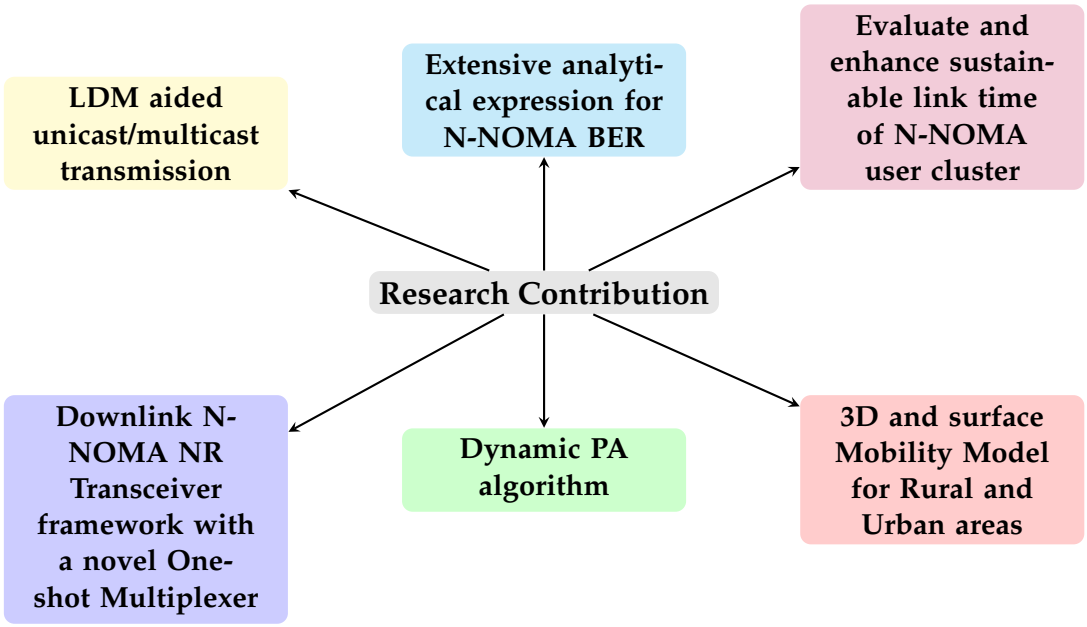

FIGURE 1.3: Research contribution

- Validated the efficacy of the proposed model via simulations, showcasing significant improvements in link sustainability for mobile users and efficient power optimization for static users within a few iterations.

1.7 Organisation of Thesis

The structure of this thesis is meticulously crafted to ensure an incremental understanding of the research theme.

Chapter 2: 5G Physical layer & NOMA: State-of-the-Art is an exploration into existing knowledge. The chapter delves into the concept of NOMA, discusses its various types, and describes the adaptation of LDM in the ATSC 3.0. It provides a window into the challenges inherent to NOMA and outlines the advancements in 5G physical layer technologies. The chapter wraps up by identifying gaps in the current literature and elaborating on the distinctive contributions.

Chapter 3: Convergence of Machine to Machine (M2M) & Mobile Communication Using LDM for Unicast/Multicast Transmission delves into the potential applications of LDM in both rural and urban future scenarios. It examines the integration of LDM with the uncoded OFDM framework, providing an in-depth analysis of the CL BER formulations. Further, the chapter addresses the specific challenges

associated with maintaining LDM pair sustainability for unicast service delivery. Comprehensive PA algorithms utilising surface mobility model for mobile receiver have been developed to extend sustainable link time, enhancing the suitability of LDM for downlink cellular networks. The insights and findings from this chapter have been published in [C01, B01].

Chapter 4: Design & Evaluation of N-NOMA on NR Physical Layer for 5G & Beyond offers insights into the layered structure of the NOMA 5G transceiver model and elaborates on the nuances of the N-NOMA 5G model. The chapter introduces the one-shot multiplexing technique tailored for N-NOMA and presents a comprehensive BER model that accounts for interference from both UL and Lower Layer (LL). The insights from this chapter have culminated in the publication [J01]."

Chapter 5: Adaptive PA to Enhance N-NOMA Link Time concentrates on the optimization of PA for N-NOMA layers, with an emphasis on augmenting the cluster link duration. Multiple algorithms are introduced with the intent to optimize the N-NOMA PA for maximizing throughput in static receivers and sustaining link duration for mobile receivers. User mobility is depicted using a 3D model adhering to the 3GPP path loss models. The findings and insights from this chapter have culminated in the publication [C02].

Concluding the thesis, **Chapter 6: Conclusion and Future Works** offers a concise recap of the findings and insights from previous sections. It underscores how the study meets its intended research objectives and provides suggestions for potential future research in this area.

Chapter 2

5G Physical layer & NOMA: State-of-the-Art

2.1 Introduction

The rapid and continuous progression of wireless communication technologies can be attributed to several factors. Primarily, there is an unyielding demand for elevated data rates [22, 23]. Additionally, we are witnessing an exponential surge in the number of new users and services. These users and services come with a diverse range of QoS expectations [23–25]. As we transition into the 5G era and look beyond, the exploration of innovative MA techniques becomes paramount to meet these demands [12, 26]. Among the myriad of techniques, NOMA emerges as a frontrunner, capturing significant attention due to its potential to increase system capacity and spectral efficiency [27].

The efficacy of NOMA is rooted in its capacity to facilitate multiple users in concurrently utilizing identical resources, such as time, frequency, and code. This concurrent utilization is realized by superimposing multiple signals within either the power or code domain [28, 29]. A significant advancement for NOMA was its incorporation as LDM in the ATSC 3.0 standard, a protocol designed for downlink TV broadcasting [18, 30–32]. This successful deployment of LDM has ignited global scholarly interest, prompting investigations into the diverse applications of NOMA in emerging wireless communication frameworks [10, 33]. The pioneering large-scale application of a NOMA technique in a practical setting forms the foundational inspiration for this thesis.

The ongoing evolution of the 5G wireless network highlights a broad array of applications and forward-thinking business approaches. As we build upon the foundations set by 4G Long Term Evolution (LTE) systems, there is a push for a network with enhanced capabilities. This advancement is pivotal for next-level multimedia services, such as Ultra-High-Definition (UHD) video, 3D visuals, augmented reality, and immersive virtual reality experiences [34, 35]. To navigate the future challenges of 5G and its successors, strategies include expanding to frequency bands above 6GHz, increasing the density of small cells, and integrating the newest technologies [36, 37].

NOMA is expected to play a crucial role in future 5G releases, targeting enhanced spectrum efficiency [10, 35, 38]. The deployment of both Point-to-Point (P2P) and Point-to-Multi Point (P2MP) transmission types is vital for delivering diverse services under the 5G framework [39]. With NOMA leading the way, these services can be provided more efficiently, resulting in increased network capacity. While the traditional OMA scheme has its merits, its limitations are evident [10, 40, 41]. NOMA, with its controllable interference and non-orthogonal resource allocation, offers numerous advantages over OMA [42–46].

In the following sections, a deep dive into the nuances of NOMA will be undertaken. This exploration will encompass its diverse aspects, with a special emphasis on LDM. Furthermore, light will be shed on the latest downlink 5G transceiver design and all the relevant technologies. This chapter is designed to lay a robust foundation, facilitating a holistic understanding of the current state-of-the-art in both NOMA and 5G domains.

2.2 Non-Orthogonal Multiple Access

NOMA represents a paradigm shift in the domain of wireless communication, offering innovative solutions to address the ever-growing demand for high data rates and system capacity. As wireless networks evolve, there is an increasing need for techniques that can efficiently utilize the available spectrum [10]. NOMA, with its unique multiplexing approach, stands out as a promising candidate to meet these demands [10, 29]. This section provides an in-depth exploration of NOMA, its core

principles, the spectrum of variants proposed in scholarly literature, and its prospective role in shaping the future of cellular networks.

2.2.1 Principle of NOMA

NOMA offers a novel approach to resource allocation for multiple users, differentiating itself significantly from traditional methods like OMA. At its core, NOMA allows for the simultaneous transmission of signals, setting them apart by varying power levels, as opposed to OMA which allots exclusive resources for each user [47]. This paradigm shift can be visualized in Figure 2.1, wherein multiple users share the same communication channel, with UE-X representing user X. Each user signal, though overlapping with others, possesses a unique power level that facilitates its identification at the receiving end.

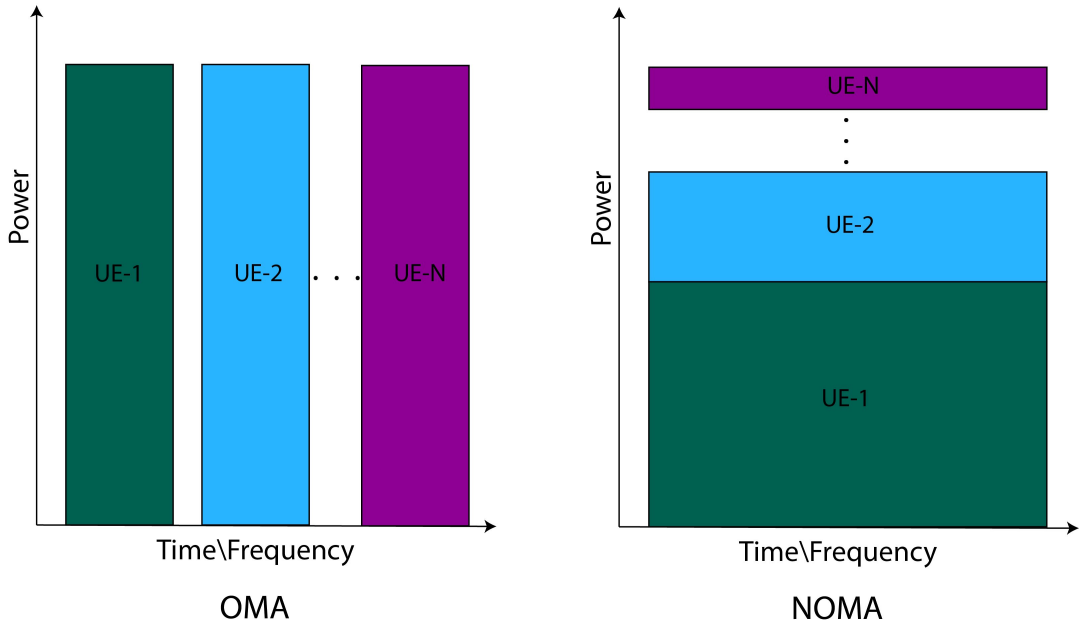

FIGURE 2.1: Resource allocation: OMA *vs.* NOMA

The allure of NOMA lies in its potential to maximize spectral efficiency [48,49]. It achieves this by permitting multiple users to coexist within the confines of the same frequency band. As a result, the system can support a higher user density without the need for additional bandwidth. This approach addresses the ever increasing demand for data in modern communication networks, optimizing the use of available

spectral resources. The multiplexing technique of uplink and downlink NOMA are different which is explained in the next section [50–52].

Uplink NOMA

In the uplink NOMA, multiple users concurrently transmit their data to a Base Station (BS)/Access Point (AP) utilizing a common frequency slot. The intricacy of this system lies not in the transmission, but in the reception and decoding. Each participating user is not required to be aware of other users sharing the frequency [53]. This lack of awareness does not introduce complexities at the user end because the transmitter design they employ aligns seamlessly with the conventional OMA system [54].

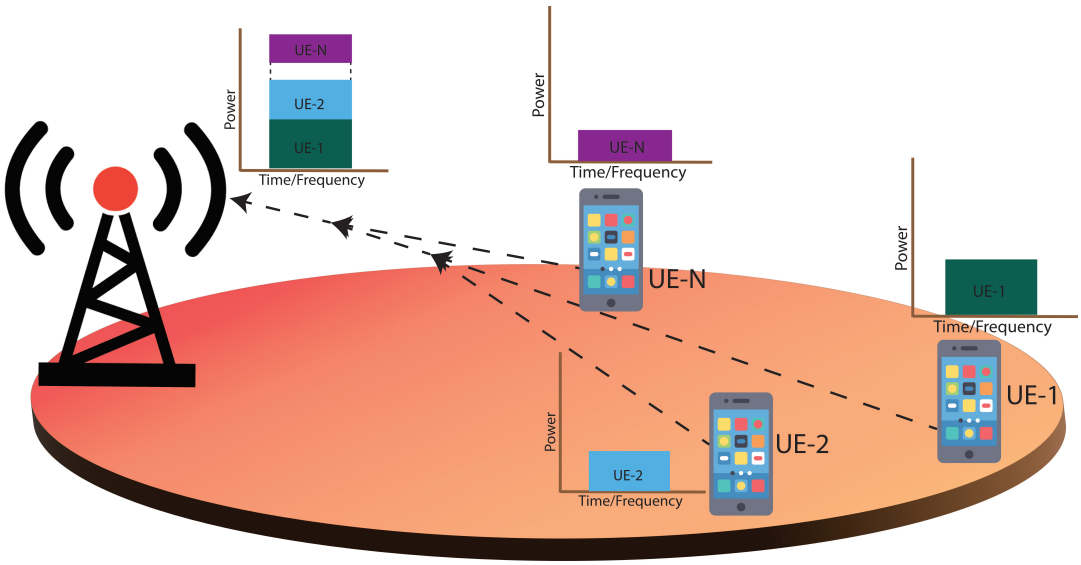

FIGURE 2.2: Uplink NOMA transmission

When each user dispatches their respective signal, it is done so with an allocated power level over the shared traffic channel. As these transmissions are synchronized, by the time they reach the BS or AP, they transform into a singular, composite signal over the channel [55]. This resultant signal, therefore, is an aggregation of individual user data interleaved with the interference from every other user transmitting over the same traffic channel as shown in Figure. 2.2.

The primary challenge, and indeed the sophistication of uplink NOMA, surfaces at the detection phase at the BS. Given the interwoven nature of the received signal,

it becomes imperative for the receiver to distinguish and decode each user data accurately [56]. The key to this discrimination is the pre-known power levels of each user transmission. With this knowledge, the receiver applies a sequential decoding process.

The receiver begins by targeting the user signal with the highest power within the composite transmission. By decoding this dominant signal first, its contribution can be effectively isolated and then subtracted from the combined signal. This operation is defined as SIC simplifies the composite signal, making the subsequent user signals progressively detectable. Through a series of iterative decoding and subtractions, the receiver systematically extracts and reconstructs the data from all users.

Downlink NOMA

In contrast to uplink NOMA, where multiple users send data to a singular destination using a shared traffic channel, downlink NOMA operates differently. Here, data is transmitted from one source but is directed towards several users [57]. This core distinction translates into a different multiplexing mechanism for NOMA. Consequently, there emerges a requisite for distinct and specialized transmitter and receiver designs tailored for downlink NOMA [58].

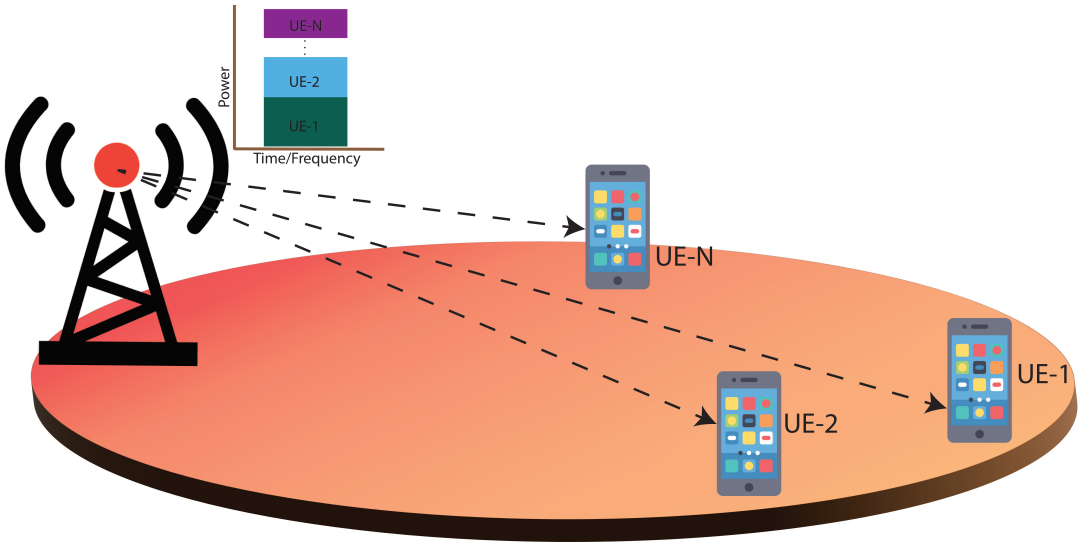

FIGURE 2.3: Downlink NOMA transmission

Considering the transmitter in downlink NOMA, it is imperative to multiplex the signals of all NOMA layers into a composite signal before transmission as shown

in Figure 2.3. During this process, PA to individual NOMA layers is strategically determined. This decision hinges on multiple factors, such as the specific channel conditions each user faces and their corresponding QoS. Typically, the layer with highest PA is called the UL, meant for users contending with the most challenging channel conditions. Conversely, subsequent LL, which cater to users with comparatively better channel conditions, are allotted reduced power [59, 60]. This configuration ensures NOMA optimally capitalizes on the inherent diversity and variability of channel conditions within its user cluster.

NOMA Multiplexing

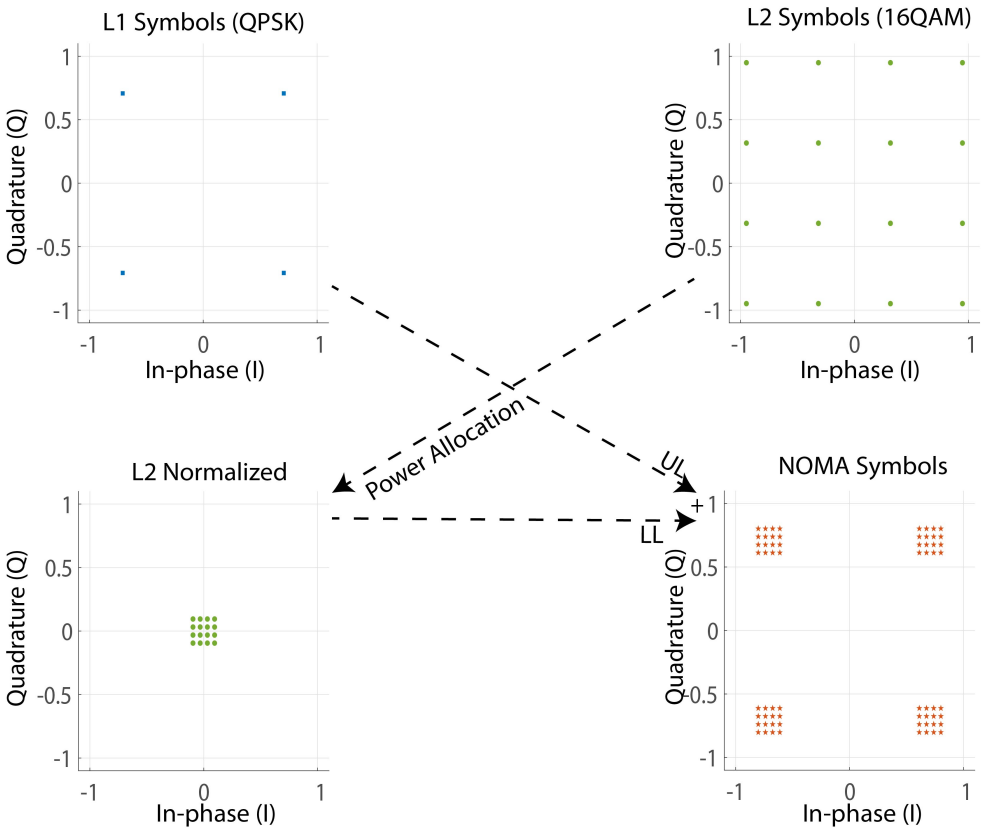

FIGURE 2.4: NOMA multiplexing process

Figure 2.4 illustrates a 2-layer NOMA multiplexing method. In this representation, the UL employs a Quadrature Phase-Shift Keying (QPSK) modulation, which is overlaid with a 16 Quadrature Amplitude Modulation (QAM) signal in the LL. The power ratio between the LL and UL is $-5\ dB$. This configuration yields a combined signal with a potential of $4 \times 16 = 64$ unique values. To begin, the LL signals

are scaled by their power coefficients to diminish the overall power of the LL in the merged signal. Subsequently, a symbol-wise addition is performed between the UL and the attenuated LL symbols. The resulting signal is termed as NOMA symbols.

To extract individual user data from this NOMA signal at the destination, the receiver employs the SIC technique, a process that is discussed in the next section.

SIC

The NOMA system stands apart due to its unique approach to interference. Instead of avoiding interference like in OMA, NOMA uses it, but in a controlled way. SIC is the main tool that enables this approach [13].

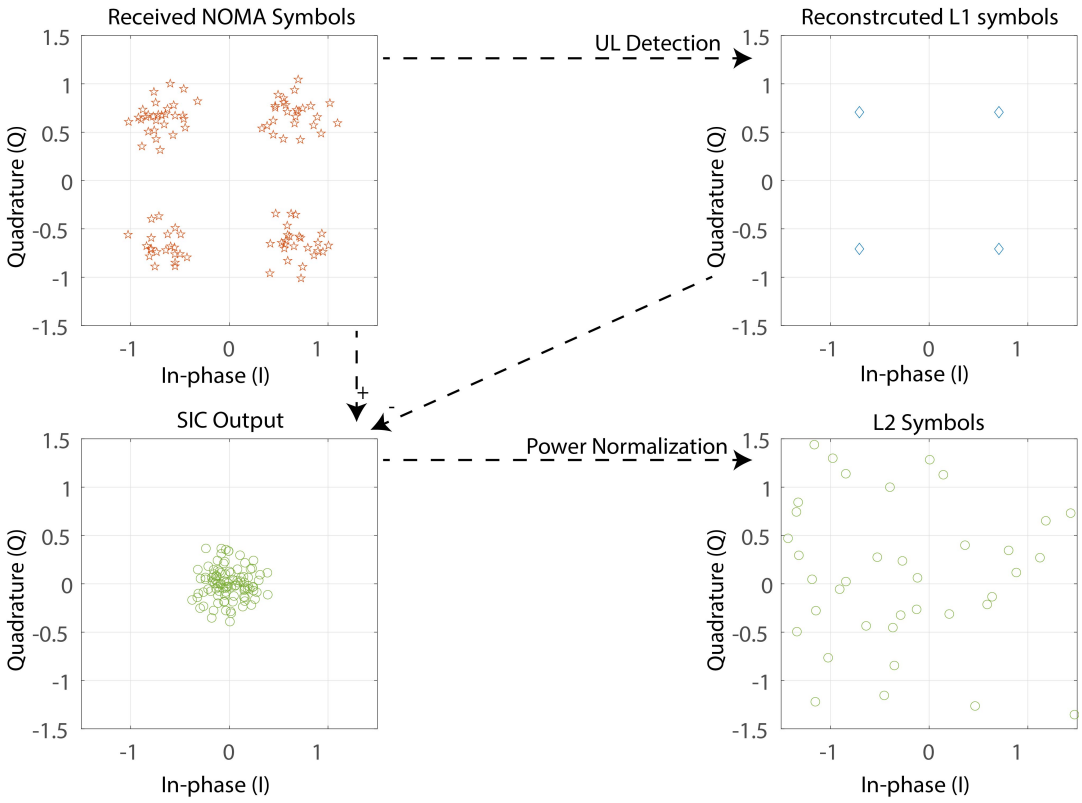

FIGURE 2.5: The process of SIC in NOMA

The SIC allows a receiver to decode multiple overlapping signals, starting with the strongest one [61]. Once the strongest signal is decoded, it is subtracted from th e total received signal. This process is then repeated for the next strongest signal, and so on, until all signals are extracted and decoded [62]. Figure 2.5 illustrates this for a 2-layer NOMA received signal over noisy channel. Here, the receiver first identifies and decodes the UL data (QPSK). Following this, the reconstructed UL

signal is subtracted from the total received NOMA signal. The remaining signal is then adjusted using the power ratio coefficient, from which the LL signal (16 QAM) is then detected.

For SIC to work effectively, it requires [63, 64]:

- Clear information about the power allocated to each layer set by the transmitter, ensuring accurate decoding of the dominant signal.
- A strategy to decode signals in order of their power levels, beginning with the most dominant.
- The ability to accurately subtract a decoded signal from the combined received signal.

SIC offers several benefits when used in NOMA systems [63]:

- Efficiency: It enables more users to operate on a single frequency, leading to higher overall system performance.
- Fairness: Allowing users with varying channel conditions to use the same frequency ensures a more balanced system.
- Flexibility: SIC can be integrated with other techniques such as MIMO, LDPC, POLAR channel coding, higher order QAM to further enhance its effectiveness [65].

But, there are some hurdles too:

- Latency: In systems like N-NOMA, SIC can be time-consuming due to its sequential nature.
- SNR Demands: For NOMA users with SIC, a higher SNR is required compared to OMA users to get the same level of performance.

Even with these obstacles, SIC remains essential for NOMA, enabling it to handle multiple users simultaneously and thus maximizing both system capacity and fairness.

NOMA PA

PA in NOMA is like giving everyone the right volume to hear a concert perfectly based on where they are sitting. In downlink transmissions, the BS sends a combined signal. LL users first decode signals meant for the UL users. After successfully decoding that, they can retrieve their own data. In contrast, UL users can directly detect the data intended for them.

The concept of power ratio becomes central in this context. It determines how power is distributed between different layers or users in the NOMA system [66]. However, dynamic user conditions mean this ratio can shift, potentially causing disruptions and compromised signal quality. Fine-tuning this ratio for optimal transmission becomes a complex task given the variables involved.

Several studies have addressed this complexity. For example, [67] and [68] devised PA strategies for two-user systems to maximize data transfer rates. Meanwhile, [69] integrated user selection with PA, drawing from user feedback to ensure consistent data rates across varying channel condition. In a distinct approach, [70] developed a PA strategy based on outage probability for two-layer systems and introduced a method to model user locations. Further expanding on PA techniques, [71] and [72] innovated methods aimed at energy efficiency and optimizing data transfer in next-generation downlink transmission.

2.2.2 Types of NOMA

NOMA has seen multiple adaptations and designs to better serve various communication scenarios. Here, are some of the prevalent NOMA types:

- **Power-domain NOMA:** The most prevalent variant, power-domain NOMA, allocates different power levels to users for multiplexing [73–75]. In the decoding process, the user with the strongest signal strength is prioritized. By employing techniques like SIC, the receiver can then decode subsequent users based on decreasing signal power.

- **Code-domain NOMA:** Here, multiplexing is achieved through the application of distinct spreading codes for different users. It draws parallels to CDMA.

However, the distinct feature of code-domain NOMA is the use of non-orthogonal codes, allowing for a greater number of users to be supported compared to traditional CDMA [74,76].

- **Spatial-domain NOMA:** Rooted in the principles of MIMO technology, spatial-domain NOMA exploits the spatial domain for user multiplexing [77]. This method harnesses the unique Channel State Information (CSI) associated with each user, making it particularly suitable for environments with a rich scattering and diverse user distribution.

- **Hybrid NOMA:** As the name suggests, hybrid NOMA merges attributes from different NOMA types [78]. The integration is done in a way to capitalize on the strengths of each individual type, offering both versatility and improved performance. For instance, one might combine power-domain with spatial-domain NOMA to gain both power and spatial multiplexing benefits.

Choosing the appropriate NOMA variant hinges on various factors. These encompass the structure of the network, the distribution and mobility of users, the prevailing environmental conditions, and the overarching objectives of the communication network. Some scenarios might benefit from the fine-grained power control of power-domain NOMA, while others with diverse user distributions might find spatial-domain NOMA more advantageous. As research in this domain progresses, it is likely that more refined and novel variants of NOMA will emerge to cater to the evolving needs of wireless communication.

Among the various types of NOMA, LDM distinguishes itself as a power domain NOMA technique designed for downlink transmissions, which adopts a non-linear PA mechanism. What sets LDM apart in the realm of real-world applicability is its recognition and subsequent adoption by ATSC 3.0. This significant endorsement marks LDM as the first NOMA method to be officially incorporated into the next-generation digital TV broadcasting standards [79].

This transition to practical application by such a prominent broadcasting standard showcases the potential and viability of LDM. The acceptance of LDM by ATSC 3.0 serves as the primary catalyst for this thesis. This research navigates through the intricacies of LDM as implemented in ATSC 3.0. The study further delves into the

challenges, solutions, and technical considerations necessary for its effective deployment in upcoming wireless communication paradigms, notably 5G and B5G.

2.2.3 Layer Division Multiplexing

Introduced as a power-domain NOMA technology, LDM emerged in the realm of cloud transmission, characterized by its flexible multilayer system. This system employs spectrum overlay technology, facilitating the concurrent delivery of multiple program streams [80]. Owing to its superior flexibility and performance benefits compared to traditional OMA methods, LDM was subsequently incorporated into the physical layer architecture of ATSC 3.0 [32]. Within the ATSC 3.0 framework, LDM combines services into two distinct layers, namely CL and Enhance Layer (EL), enabling transmission over a singular traffic channel. While the CL data can be decoded by perceiving the EL data as interference, the EL data necessitates signal cancellation techniques for decoding [18]. Such an innovative approach underscores the potential of LDM in augmenting the capacity of upcoming heterogeneous cellular networks.

LDM in ATSC 3.0 Architecture

The ATSC 3.0 transceiver architecture, illustrated in Figure 2.6, incorporates a two-layer LDM [30]. Within this system, the CL is granted a higher PA than the EL, with a logarithmic power ratio between EL to CL. Such a PA minimizes interference of the EL on the CL. This configuration ensures that CL data remains detectable in low SNR channels without necessitating SIC. Consequently, the power-rich CL is employed to transmit High-Definition Television (HDTV) mobile services to an array of devices including indoor, portable, and handheld receivers. Conversely, the EL caters to high data rate services, such as Ultra-High-Definition Television (UHDTV) or multiple HDTV transmissions, targeting users with good channel conditions typically associated with stationary receiver. In these terminals, the operational SNR typically remains elevated, a result of large and possibly directional receive antennas [81].

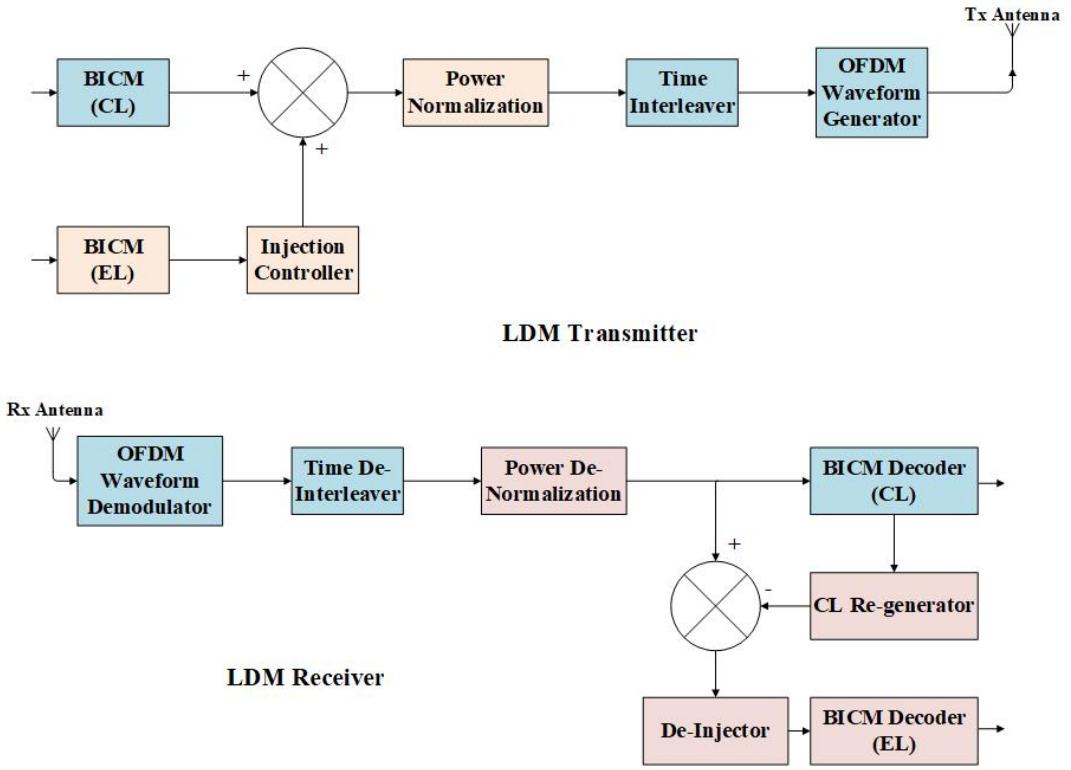

FIGURE 2.6: ATSC 3.0 transceiver framework

Since adapting LDM into ATSC 3.0 physical layer design, much work has been done on finding LDM performance for downlink broadcast transmission. In [30], LDM and Time Division Multiplexing (TDM) performance over Additive White Gaussian Noise (AWGN), Rician, and Rayleigh channels are compared. Their results show that LDM has a gain of 5.4, 5.1, and 8.4 dB average reception power, respectively. As EL requires a portion of the total transmission power, the addition of EL reduces the SNR of CL transmission. So the additional EL transmission comes at the cost of reduced CL transmission performance. Reference [82] investigated this performance trade-off between CL and EL where capacity and coverage performance of EL at the cost of that of CL is shown for ATSC 3.0. Their work shows a better performance of LDM compared with TDM and Frequency Division Multiplexing (FDM). The authors in [83] proposed a Multiple Physical Layer Pipe (M-PLP) configurations based on multi-layer LDM and did capacity analysis of this configuration to determine the lower capacity bound (approximately 1 Mbps) of CL. In [84] the authors showed that LDM CL provides higher channel capacity than TDM/FDM at

low SNR, and EL can do the same at high SNR condition. In [31], the CL performance for mobile and indoor devices shows that it can deliver Half-Duplex (HD) program. The successful integration of LDM into ATSC 3.0 and its advantage over OMA transmission motivated researchers to investigate the possibilities of LDM in 5G network.

LDM in 5G

The successful integration of LDM into ATSC 3.0 and its advantage over OMA transmission has spurred interest in the potential of LDM for 5G. Given the notable capacity gain of LDM over TDM and FDM, it is increasingly being considered for 5G deployment. Numerous studies have explored the feasibility of employing LDM for P2MP and broadcast transmission within 5G wireless communication.

In the study by Zhang et al. [85], the authors evaluated the BER performance and the necessary SNR threshold for the successful detection of an LDM P2MP transmission using the LTE evolved Multimedia Broadcast Multicast Service (eMBMS) specification. Their findings underscored a significant increase in network capacity when compared to TDM and FDM, albeit with increased transmitter complexity. Another research [86] highlighted that LDM demands less power for both unicast and broadcast transmissions compared to TDM/FDM. Additionally, it offers enhanced robustness against imperfect CSI, which are commonly encountered in real-world systems.

Zhang et al. [14] proposed a unicast-broadcast transmission scenario for 5G Multimedia Broadcast Multicast Services (MBMS), demonstrating a substantial capacity gain with LDM over OMA transmission. In a parallel vein, Iradier et al. [15] introduced a PHY/MAC architecture for unicast-broadcast convergence using LDM, integrated with Hybrid Automatic Repeat Request (HARQ). This model surpassed the throughput of the TDM system. Xue et al. [16] further delved into network throughput, analysing the influence of the power ratio between EL and CL on SNR and throughput. Collectively, these studies affirm that LDM is adept at catering to a diverse range of devices and enhancing network capacity.

The existing literature underscores the proficiency of LDM in serving a diverse array of devices and augmenting network capacity. While a significant portion of research has predominantly concentrated on leveraging LDM for broadcast multimedia transmission, such findings have paved the way for the exploration of alternative applications where LDM might exhibit potential. The fusion of unicast and multicast transmissions, considering the heterogeneity of service requirements, has the potential to catalyze the widespread implementation of LDM/NOMA in 5G and B5G networks. Nevertheless, there exists a discernible void in analytical models that aptly capture the performance of LDM within the OFDM framework, which is imperative for validating future research. Furthermore, in anticipation of a future where the majority of receivers might exhibit varying degrees of mobility, determining the impact of user mobility on the sustainability of LDM pairings is of paramount importance.

2.2.4 Recent Advances in NOMA Implementation

NOMA has gained significant interest from research communities in recent years, mainly due to its potential applicability in B5G and 6G use case scenarios. As the wireless communications landscape evolves towards more advanced and ubiquitous systems, it is crucial to explore innovative approaches to maximize spectral efficiency and user connectivity. NOMA, with its ability to facilitate concurrent transmission for multiple users over a single channel, presents an attractive solution to many of the challenges foreseen in next-generation networks. In this context, several areas have been identified where NOMA can play a transformative role, some of which are discussed below.

NOMA-Based Unmanned Aerial Vehicle (UAV)-Aided Communications

In next-generation wireless networks, UAV-aided communications stand out due to their mobility and adaptability [87–89]. Serving as BSs, relays, and users, UAVs enable applications like wireless service recovery, traffic offloading, environmental surveillance, and cargo transport. This is largely attributed to their LoS dominated

Air-to-Ground (A2G) channel. Yet, challenges like resource optimization, interference management, and latency persist [12].

Research such as [90] delves into multi-UAV-enabled downlink NOMA, suggesting user-centric and UAV-centric strategies. Another avenue, [91], examines the potential of uplink NOMA in energy-restricted UAV systems. However, it focuses only on scenarios involving a single UAV. Further investigation is needed to assess performance in scenarios with a large number of UAVs. The study in [92] presents a cooperative NOMA method for uplink to tackle A2G interference, allowing specific BSs to decode and relay signals from a static UAV. The authors in [93] investigate cellular-connected UAV trajectory design, utilizing NOMA to manage interference. Despite these recent developments, current research in this field remains largely theoretical. Most studies concentrate on analytical models that demonstrate potential rather than practical implementation. Establishing a concrete NOMA transmission framework would enable future researchers to assess performance more accurately, paving the way for turning these theoretical models into real-world applications.

NOMA-Enhanced Robotic Communications

The rise of connected robots in wireless networks signifies a shift towards network-based communications over isolated onboard computing, promising cost-effectiveness but with its challenges [94]. Initiatives like [95, 96] integrate NOMA to overcome these hurdles. Specifically, [95] emphasizes indoor robot path planning using NOMA for communication but their approach is reliant on perfect geographic knowledge, rendering them unsuitable for unknown or new areas. This limitation is particularly significant in various applications, such as search and rescue missions, where the geographic landscape may not be precisely mapped or familiar.

Massive and Critical MTC

The momentum towards digitization in domains like smart cities and Industry 4.0 in the 6G era underscores the relevance of Machine Type Communication (MTC) [97]. While addressing the need for Massive Machine-Type Communications (mMTC), 6G also brings strict QoS demands. Approaches like Grant Free (GF) random access

and NOMA are gaining traction, especially with power balancing in varied channels [98]. The emergence of semi-GF NOMA as seen in [99] offers a confluence of Grant Based (GB) and GF methods, catering to the dual "massive" and "critical" KPIs for Massive and Critical MTC (MC-MTC) [100]. These studies can be further validated through an established NOMA-5G framework, which would allow for the consideration of various practical scenarios. These include LoS/NLoS connectivity, imperfect CSI, as well as varying channel coding and modulation orders.

Mobile Edge Computing (MEC) Networks

MEC champions decentralized computing, prioritizing high-speed data and reduced latency [101]. Compared to OMA, NOMA enhances task transmission and result notifications. This facilitates better resource allocation in MEC networks, enhancing computational outcomes. Researches like [102–105] delve into the synergy between NOMA and MEC, probing into performance metrics, resource distribution, and latency reduction in MEC with NOMA. The research presented in these papers primarily concentrate on 2 user NOMA which can be further extended into N-NOMA that can provide support for more users.

2.2.5 Interplay between NOMA and Other Emerging Physical Layer Techniques

Ensuring compatibility between new and existing technologies is crucial, particularly as 6G is anticipated to merge a multitude of physical layer techniques. This section delves into the fusion of NOMA with other emerging physical layer methods, offering insights from contemporary research in the domain.

Reconfigurable Intelligent Surface (RIS)-NOMA

Recent progress in metasurfaces has showcased RIS [106], often labeled as Intelligent Reflecting Surfaces (IRS) [107], as central components for forthcoming wireless frameworks. At its core, an RIS is a custom-designed surface embedded with numerous cost-effective, tunable components like Positive Intrinsic Negative (PIN)

diodes, overseen by advanced mechanisms such as Field-Programmable Gate Array (FPGA). By fine-tuning the phase and amplitude responses of these elements, RIS can transform incoming wireless signals, leading to a radical shift in the radio environment [108].

There is an inherent charm in fusing RIS with NOMA [109]. At its core, the superiority of NOMA over OMA is based in the distinct channel conditions of users. This distinction might not always be evident. Yet, through strategic placement of RIS and careful adjustment of their reflection coefficients, this channel diversity can be magnified, further boosting NOMA efficacy. In addition, RIS has the capability to metamorphose channels, advocating for an intelligent QoS-based NOMA operation. Numerous studies have looked into the promise of this synergy. For instance, a study [110] established the superiority of centralized deployment strategies, regardless of the access scheme. Building on this, another work [111] investigated the ideal RIS deployment in multi-user downlink networks, revealing distinct advantage of NOMA. Further studies delved into the duality of STAR-RIS systems [112–114] and the computational challenges presented by RIS-assisted Multiple-Input Single-Output (MISO) downlink NOMA networks [115–117].

Orthogonal Time Frequency Space (OTFS)-NOMA

OTFS modulation is emerging as a beacon for high-mobility users [118–120]. The essence of OTFS lies in its ability to position high-mobility user signals in the delay-Doppler domain, transmuting time-fluctuating channels into static ones. Yet, its performance is bound to its resolution. Addressing this, a novel OTFS-NOMA system was proposed [121], aiming to elevate spectral efficiency. Venturing into MIMO domains, there is a shift towards beamforming strategies tailored for OTFS-NOMA systems [122], maintaining QoS for high-mobility users while boosting data rates for others.

Full-Duplex (FD)-NOMA

FD emerges as a cornerstone for next-generation wireless networks, offering simultaneous downlink and uplink transmissions. Blending FD with NOMA can significantly elevate resource efficiency, but it also invites interference challenges [123]. To counteract these, robust resource allocation strategies are imperative. Studies have delved into optimizing these allocations [123], evaluated the outage performance of FD-NOMA versus its HD counterpart [124], and proposed relay selection methods for HD relay-assisted NOMA networks [125]. The results are unanimous in underlining FD NOMA's potential, especially in low SNR environments [126].

Visible Light Communications (VLC)-NOMA

For indoor environments, VLC is capturing interest due to its myriad advantages [127]. However, its narrow modulation bandwidth calls for advanced MA techniques. Here, NOMA offers an appealing solution. The authors in [128] have ventured into evaluating the performance of NOMA-VLC systems, indicating a clear edge over OMA-based systems. Another study [129] in the realm of MIMO-VLC systems introduced the Normalized Gain Difference PA (NGDPA) method, accentuating the merits of intertwining NOMA with traditional VLC setups.

2.3 5G Physical Layer

The emergence of 5G represents a significant advancement in wireless communication, offering unparalleled data rates and minimal latency relative to earlier generations. While we are yet to fully exploit the potential of 5G, numerous promising physical layer technologies, including NOMA, VLC, and RIS, are on the horizon for implementation. The technology's widespread global deployment is evident [130]. The Non-Standalone (NSA) version of 5G, designed for a smooth and cost-efficient transition from its predecessors, has been widely adopted in many countries, making up a significant part of the 5G coverage [131]. Notably, regions like the USA and China have initiated public 5G Standalone (SA) deployments [5]. The rise of

local 5G networks presents an intriguing alternative to conventional Wireless Fidelity (Wi-Fi) for Local Area Network (LAN) applications [132]. In response to these developments, 3GPP has released various versions of the 5G transceiver model, incorporating state-of-the-art technologies such as MIMO and mmWave, and catering to a range of channel, transmission, and mobility scenarios. This study delves into the viability of NOMA for downlink unicast/multicast transmission, and subsequent sections will explore the contemporary 3GPP transceiver design for Downlink Shared Channel (DL-SCH).

2.3.1 5G Downlink Transceiver Framework

Matlab has introduced a comprehensive 5G toolbox, facilitating end-to-end simulations that encompass the latest 3GPP releases. In alignment with their 5G toolbox and the 3GPP Release 16, Figure 2.7 depicts the standard downlink transceiver model [133,134]. All the component of this 5G transceiver model is briefly described in the following sections.

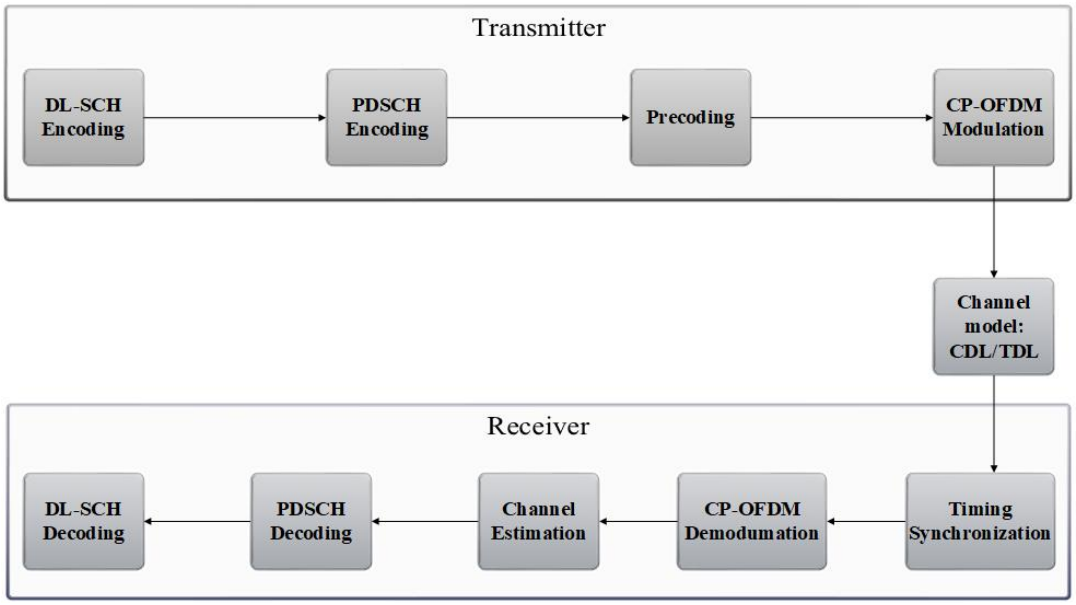

FIGURE 2.7: 5G transceiver model following 3GPP release-16

Transmitter Side Operations

- **DL-SCH Encoding:** The DL-SCH is tasked with transmitting user data and control information. It utilizes sophisticated coding techniques like LDPC and

polar coding to maintain data integrity and incorporates HARQ for error rectification [135, 136].

- **Physical Downlink Shared Channel (PDSCH) Encdoing:** The PDSCH transmits the data processed by the DL-SCH. It maps the data to the suitable physical resources. The supported modulation techniques include QPSK and (16, 64, 256) QAM [137].

- **MIMO Precoding:** MIMO precoding is a technique that leverages multiple antennas at both the transmitter and receiver to improve communication performance. Precoding is the process of shaping the transmitted signals in a way that optimizes the received signal quality, taking into account the channel conditions.

- **OFDM Modulation:** OFDM is a modulation scheme used in 5G to efficiently transmit data over frequency-selective channels. The cyclic prefix is added to each OFDM symbol to combat inter-symbol interference caused by multipath propagation.

Channel Model

In wireless communication, signals often traverse multiple routes before arriving at the receiver due to a phenomenon termed multipath propagation. This can lead to interference and a reduction in signal quality. The 3GPP release 16 provides an extensive model for various transmission scenarios, such as Rural Macro (RMa), Urban Macro (UMa), Urban Micro – Street Canyon (UMi), and Outdoor to Indoor (O2I), encompassing both LoS and NLoS communications [138].

In a typical multi-antenna scenario within a multipath channel, signals from multiple transmitting antennas are sent at different angles and undergo multipath propagation. Consequently, a receiver is likely to perceive multiple versions of each transmitted signal. These versions can have varying delays and noise levels, depending on the type and number of reflecting objects [139]. The accepted models for such multipath channels are TDL for single antenna transmissions and CDL for MIMO transmissions [140, 141].

- **TDL Channel Model:** The TDL channel model, commonly referenced in 3GPP specifications, represents a series of discrete taps in time domain, where each tap has a certain power level associated with it. This model is particularly useful for scenarios where multipath components are well-separated in the delay domain, and thus can be distinctly identified. Different versions of the TDL model are characterized by different numbers of taps, different delay spreads, and different power levels for each tap. For instance, in 3GPP NR specifications, we encounter variants such as TDL-A, TDL-B, up to TDL-E, each suited for different propagation conditions and scenarios.

- **CDL Channel Model:** The CDL model is another approach to represent multipath propagation channels. Unlike the TDL model which focuses on distinct taps, the CDL model emphasizes clusters of rays. Each cluster consists of multiple rays, and each ray within a cluster can have its own delay, angle of arrival, and angle of departure. 3GPP has also detailed multiple versions of the CDL model, such as CDL-A, CDL-B, and so on, to cater to a variety of scenarios from urban to rural, from LoS to NLoS conditions.

Key parameters for all TDL and CDL channel models are explained in the Table 2.1 [138].

Receiver Side Operations

- **Timing Synchronization**: Ensures that the receiver is synchronized with the transmitter, allowing for accurate decoding of the received signals.

- **OFDM Demodulation**: Removes the cyclic prefix and demodulates the OFDM symbols to retrieve the transmitted data.

- **Channel Estimation**: Estimates the channel conditions to optimize the decoding process.

- **PDSCH Decoding**: Decodes the data from the PDSCH, retrieving the original data and control information.

- **DL-SCH Decoding**: Further processes the decoded data, applying error correction and other techniques to ensure data integrity.

Model	**LoS/NLoS**	**No. of Tap/Cluster**	**Normalized delay**	**Power in [dB]**
TDL-A	NLoS	1	0.0000	-13.4
		10	1.5375	-15.9
		20	4.7966	-18.9
TDL-B	NLoS	1	0.0000	0
		10	0.3697	-3
		20	3.6187	-11.4
TDL-C	NLoS	1	0.0000	-4.4
		10	0.7935	-7.1
		20	5.6077	-17.1
TDL-D	LoS	1 (LoS path)	0.0000	-0.2
		1 (Rayleigh)	0.0000	-13.5
		10	7.937	-23.6
TDL-E	LoS	1 (LoS path)	0.0000	-0.03
		1 (Rayleigh)	0.0000	-22.03
		10	2.6426	-22.3
CDL-A	NLoS	1	0.0000	-13.4
		10	1.5375	-15.9
		20	4.7966	-18.3
CDL-B	NLoS	1	0.0000	0
		10	0.3697	-3
		20	3.6187	-11.4
CDL-C	NLoS	1	0.0000	-4.4
		10	0.7935	-7.1
		20	5.6077	-17.1
CDL-D	LoS	1 (LoS path)	0.0000	-0.2
		1 (Laplacian)	0.0000	-13.5
		10	7.937	-23.6
CDL-E	LoS	1 (LoS path)	0.0000	-0.03
		1 (Laplacian)	0.0000	-22.03
		10	2.6426	-22.3

TABLE 2.1: TDL & CDL channel model parameters

The 5G downlink transceiver model is a complex system that incorporates a variety of advanced methods to ensure efficient and dependable data transmission. The combination of these elements enables 5G to satisfy the rigorous demands of contemporary wireless communication, delivering superior performance at low SNR. This also enhances the viability of NOMA deployment, as NOMA typically necessitates higher SNR values compared to OMA.

2.4 Summary

The evolution of wireless communication has been marked by continuous advancements and innovations, with the integration of NOMA and the development of the 5G physical layer being at the forefront of this progression. This chapter delves into the state-of-the-art technologies and methodologies that underpin NOMA and the 5G physical layer, highlighting the pivotal role they play in shaping the future of wireless communication.

NOMA, as a key MA technique, has garnered significant attention for its potential to enhance spectral efficiency and cater to a massive number of users simultaneously. Its integration into the 5G framework promises to address the ever-growing demands for higher data rates, better QoS, and more reliable communication. The chapter further explores the successful incorporation of LDM into the ATSC 3.0 framework and its implications for 5G systems. LDM's potential in enhancing downlink broadcast transmission, its performance trade-offs, and its capacity gains over traditional multiplexing techniques are discussed in detail.

Furthermore, the chapter provides an in-depth analysis of the 5G physical layer transceiver model, emphasizing its intricacies and the underlying processes that drive its functionality. Key technological components such as MIMO systems, LDPC codes, OFDM, and varying modulation orders are explored, shedding light on their roles in optimizing data transmission, enhancing signal integrity, and ensuring robustness against channel imperfections.

Navigating through the chapter, it is evident that the current research landscape is rich with innovations aimed at pushing the boundaries of wireless communication. This state-of-the-art review not only offers a comprehensive understanding of

the current technological landscape but also sets the stage for this thesis's contributions. By understanding the latest works and principles in the domain, this thesis aims to carve out a niche, offering novel insights and solutions that can further the cause of next-generation wireless systems.

While the integration of NOMA into the NR architecture presents numerous benefits, current research exhibits distinct gaps in fully understanding and applying this technology, especially in the context of downlink unicast transmission. Key observations from the literature are as follows:

1. **Unicast downlink NOMA Under-researched:** Despite the growing literature on the benefits of NOMA in broadcast transmission, its application in unicast downlink remains less scrutinized [14–17, 19, 20]. The unique challenges associated with unicast transmissions, such as the need for precise user grouping and understanding the impacts of receiver mobility on NOMA performance, demand attention.

2. **PA for Mobile Users:** The mobile nature of receivers further complicates the application of NOMA in downlink. Given these dynamics, the power distribution between NOMA layers requires adaptable PA techniques that can respond to varying mobile conditions to ensure reliable transmission.

3. **Integration with Advanced 5G Technologies:** While 5G has brought forth groundbreaking technologies such as MIMO beamforming and LDPC channel coding, the synergy between these innovations and NOMA remains underexplored [12, 15]. Harnessing these technologies may significantly enhance NOMA performance, ensuring its broader adoption in both uplink and downlink transmissions, making it a staple in future 5G and B5G standards.

4. **Limited Practical Research on N-NOMA:** The potential of NOMA might be fully harnessed by practical implementation of N-NOMA. However, many studies on this subject remain confined to theoretical domains due to challenges like complex signal processing and noise sensitivities in communication equipment. This theoretical inclination contributes to the lack of a formal NR framework that integrates NOMA.

5. **Absence of an Established 5G Framework:** Even with the 3GPP release 16 initiating a study on 2-layer UL NOMA [21], the industry lacks a comprehensive framework for 5G downlink transmission. This underscores the imminent necessity for the development of an efficient 5G physical layer transceiver with integrated NOMA capabilities.

In the subsequent chapter, the focus shifts to a comprehensive LDM-OFDM framework specifically designed for downlink unicast and multicast transmissions. This intricate framework is complemented by an analytical model that precisely measures the CL BER performance. Further deepening the investigation, a Two Dimensional (2D) surface model and a strategic PA algorithm are introduced. These advancements aim to enhance the sustainability of LDM pairs, ensuring a resilient communication experience.

Chapter 3

Convergence of M2M & Mobile Communication Using LDM for Unicast/Multicast Transmission

3.1 Introduction

Building on the insights from the previous chapter , the integration of LDM into ATSC 3.0 marks a pivotal advancement for next-generation digital TV broadcasting. Motivated by that success, many have investigated the possibility of using LDM in P2MP and broadcasting transmission in 5G downlink wireless communication which is discussed in Section 2.2.3. Collectively, these investigations affirm the potential of LDM in 5G and beyond in enhancing network capacity. Nevertheless, while the focus so far has leaned towards broadcast/multicast services, there is a significant research gap regarding the role of LDM role in unicast transmission, presenting a plethora of issues yet to be unravelled.

The intrinsic design of LDM is tailored for a heterogeneous group of receivers, given its unique SNR requirements and transmission rates [142]. Therefore a successful convergence depends on pairing devices that have heterogeneous requirements and without potential use-case scenarios, the proposed framework holds little significance. Potential user groups in future wireless networks were identified, and a unique unicast/multicast convergence was suggested between IoT devices (utilizing CL) and human users User Equipment (UE) (employing EL). The value of

this pairing becomes evident particularly when there is substantial downlink transmission needed for IoT devices. Potential scenarios for such downlink-heavy IoT communication in future urban and rural areas are discussed in Section 3.2.

In the next section, a framework is developed that integrates a 2-layer LDM within OFDM for downlink transmission and is tailored to accommodate various channel models. This simulation structure offers insights into the behaviour of LDM across a spectrum of transmission settings. To confirm the accuracy and applicability of this framework, there is an additional analytical model is derived to assess LDM CL BER in Section 3.4. Constructed through a process of trial and error, this model is anchored in the established BER expression for uncoded OFDM OMA transmission. Within this model, the additional interference from EL during the CL detection phase are accounted. As a result, this structure stands as a valuable reference. The results from the developed simulation and analytical model are compared and discussed in Section 3.5.

Broadcast/multicast transmissions are different from unicast transmissions, especially when using LDM [143]. The challenge with unicast transmission via LDM is the necessity for UE pairing, which becomes more complex with mobile receivers due to dynamic channel conditions which is explored in Section 3.6. There, a surface mobility model has been constructed to depict UE movement within the transmission beam. This model operates under the presumption that the beam is aimed directly at the initial position of UE. The findings indicate a strong dependency between UE mobility and the sustainable link time of LDM pair. An algorithm has been created to address these challenges, aiming to prolong the link time. This is achieved by adjusting the power distribution between CL and EL layers, allowing LDM to be optimized in fluctuating channel conditions. To better accommodate the mobility of IoT device receivers, the mobility model has been expanded to consider both types of users. An analytical model has also been formulated to examine the correlation between link duration and the mobility patterns of each UE type. The ramifications of receiver mobility are elaborated upon in Section 3.7, further emphasizing the potential of LDM in unicast/multicast transmission scenarios. The chapter wraps up in Section 3.8, providing an overview of the main contributions, discoveries, and limitations of the research detailed in this chapter.

3.2 Downlink-Heavy IoT Communication

The development of wireless communication, particularly with the introduction of 5G, has led to a significant transformation in MTC, marked by a rapid increase in the number of IoT devices for a diverse range of applications [144, 145]. Historically, MTC was perceived to be predominantly uplink-centric. However, emerging applications and use cases such as cloud controlled drone, autonomous vehicular movement, and multisensory reconfigurable IoT implementation suggest a significant need for downlink data transmissions [146]. This section delves into potential scenarios where downlink transmission becomes pivotal for MTC, considering both urban and rural contexts.

3.2.1 Urban Area

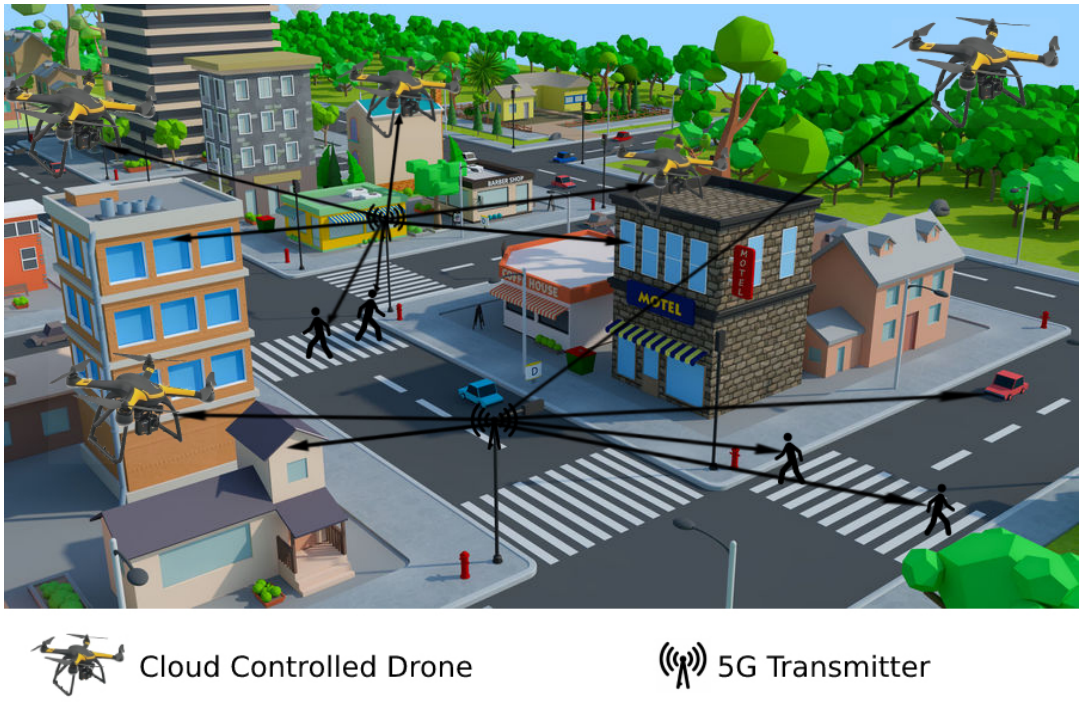

FIGURE 3.1: Downlink transmission model for IoT devices in urban areas.

Urban environments, characterized by high device density, are anticipated to be the epicenters of advanced communication systems. As illustrated in Figure 3.1, the urban landscape of the future is poised to witness a proliferation of autonomous

vehicle systems and cloud-controlled drones, necessitating robust downlink communication. The integration of small cells or picocells into the urban cellular infrastructure, especially in 5G networks, will further enhance the efficiency of these transmissions. Existing urban fixtures, such as lamp-post-mounted radio-heads, will play a pivotal role in facilitating this communication model [147].

Cloud-controlled drones, governed by centralized systems, will be heavily reliant on downlink communication for real-time control. Similarly, autonomous vehicles will depend on continuous traffic updates and control directives from cloud systems to navigate urban terrains. These applications necessitate Ultra-Reliable Low-Latency Communication (URLLC). Moreover, managing the capacity due to the massive device density in urban areas presents a significant challenge. LDM CL, with its reliability and minimal latency, emerges as a viable solution to address these challenges, enhancing system capacity.

3.2.2 Rural Area

Contrasting the urban landscape, rural areas present a unique set of IoT applications. As depicted in Figure 3.2, the future of rural areas is poised to embrace advanced farming and agricultural systems, heavily reliant on IoT sensors. Cloud-controlled drones will play a pivotal role in real-time monitoring and control in agricultural settings.

IoT sensors in rural settings will be instrumental in monitoring various agricultural parameters, such as water flow rates, storage conditions, and other agriculture-centric metrics. These multifunctional devices, capable of self-reconfiguration based on cloud directives, underscore the importance of robust downlink communication in rural scenarios. One notable distinction in rural network configurations is the deployment of large coverage cells, enhancing the sustainability of UE-IoT pairings, especially in mobile scenarios. The LDM CL, with its reliability in varying channel conditions, emerges as a promising solution for these challenges in 5G downlink communication for MTC.

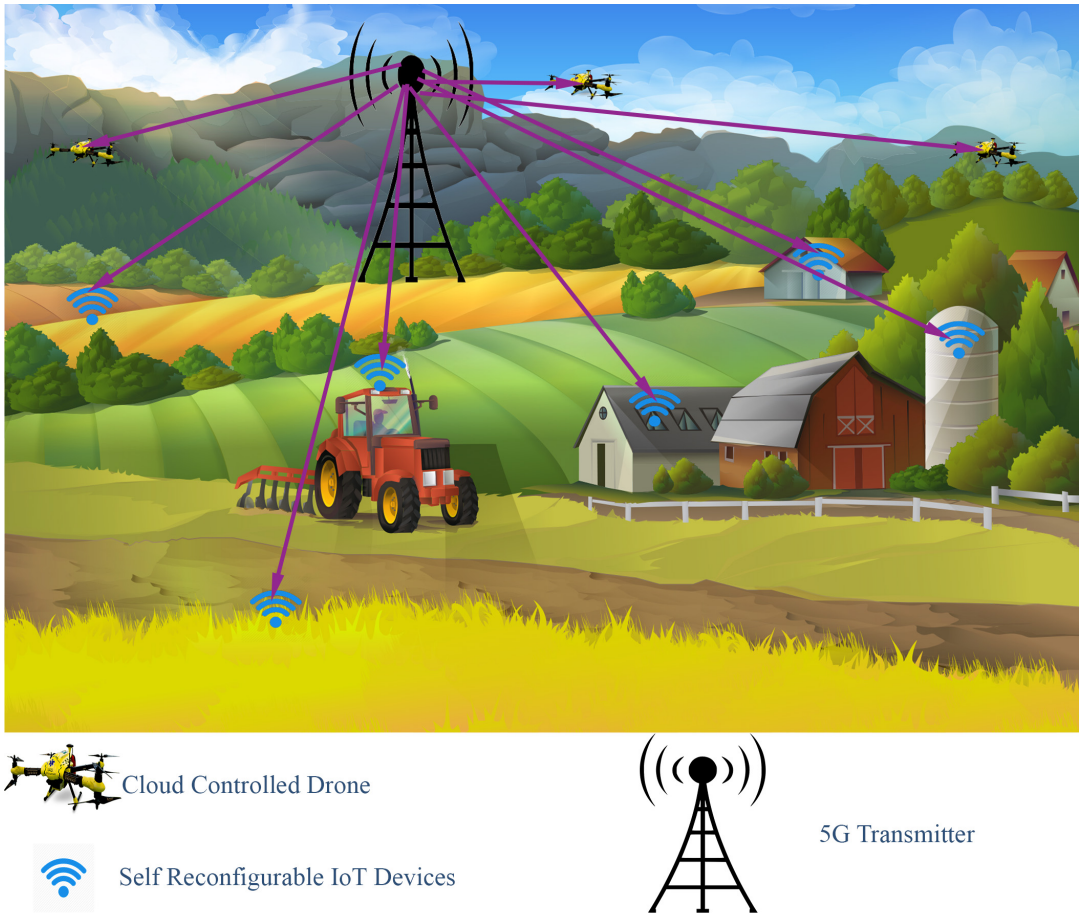

FIGURE 3.2: Downlink transmission model for IoT devices in rural areas.

3.3 LDM-OFDM System Model

A framework for the OFDM physical layer is developed to adapt LDM for 5G and B5G. This section elaborates on the detailed structure of the proposed framework for the AWGN, the fading channel, and massive MIMO (mMIMO) transmission.

3.3.1 System Model (AWGN Channel)

Consider a transmission scenario where a BS provides services to users and IoT devices. IoT devices, denoted as IoT-1, IoT-2, and IoT-3 in Figure 3.3, are small devices necessitating real-time communication. These IoT devices are presumed identical in their requirements and capacities but are situated in distinct locations, thus experiencing different channel conditions. All three IoT devices are assumed to need the same information, so a single multicast channel can cater to all three devices using

OMA transmission. In this scenario, IoT devices necessitate real-time communication and possess limited computational capacity. The detection process for these devices should be fast and simple. The other device in Figure 3.3 is a UE. It is assumed that the UE demands a high data rate transmission, such as multimedia communication, and is proximate to the transmitter, thus experiencing favorable channel conditions (high SNR). Moreover, the UE boasts significant computational capacity, and its requirements are more latency-tolerant, making it suitable for EL transmission. The lines in Figure 3.3 depict the LDM signal with an AWGN channel and LoS communication. These lines originate from a single LDM data channel transmission reaching all four devices from the BS. Hence, this scenario serves all four receivers using a single channel, whereas an OMA transmission system might necessitate two or more channels. As this model leverages the capabilities of a NOMA technique, there is no need for time or frequency sharing. The communication is uninterrupted, and all devices utilize the entire time and frequency slot of the employed traffic channel.

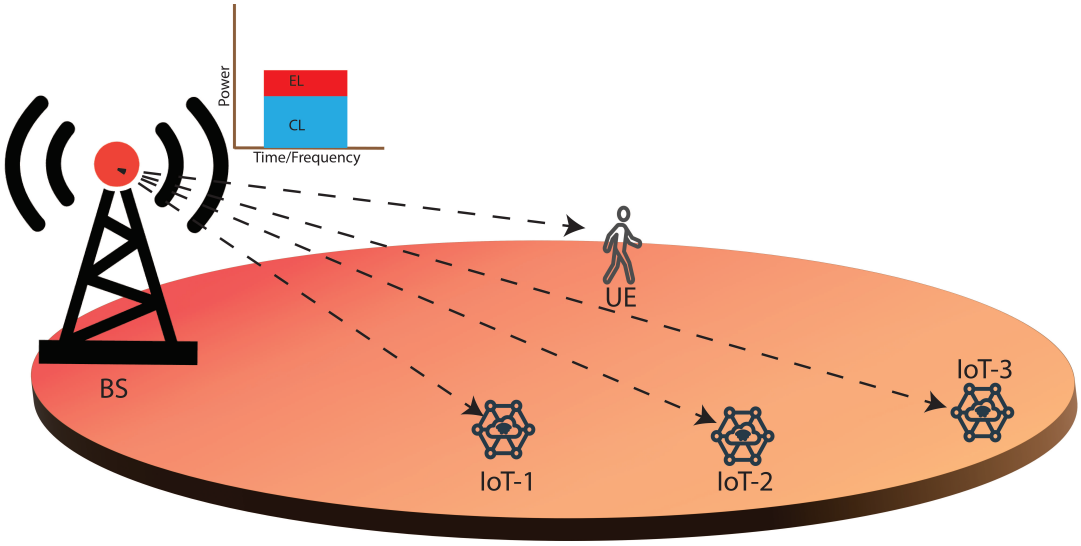

FIGURE 3.3: LDM aided Unicast-Multicast transmission scenario

Transmitter Framework with LDM Superposition

An OFDM system with QAM modulation is employed to evaluate the system, as depicted in Figure 3.4. To analyze the performance of LDM in the proposed framework, channel coding has been excluded. Figure 3.4 illustrates that the CL and EL

bits are processed concurrently. The transmission bit rate of CL and EL can differ as different QAM modulation scales M can be employed for each layer. Both data sets are converted into QAM symbols, ensuring each frame contains an identical number of QAM symbols. Upon obtaining the QAM modulation of CL and EL data, both symbol sets are combined using LDM superposition to yield an equal number of LDM symbols. The power of the EL symbol is reduced during the superposition process to occupy a smaller power portion of the total transmit power. The total transmission power mirrors that of any single-core transmission. Equation (3.1) represents the LDM superposition where $\mathbf{X}(\mathrm{k})$ denotes the LDM symbol of the kth sub-carrier, g is the power ratio between layers, and $\mathbf{X}_{cl}(k)$, $\mathbf{X}_{en}(k)$ represent the CL and EL symbols of the kth sub-carrier, respectively.

$$\mathbf{X}(k) = \mathbf{X_{cl}}(k) + g\,\mathbf{X_{en}}(k) \tag{3.1}$$

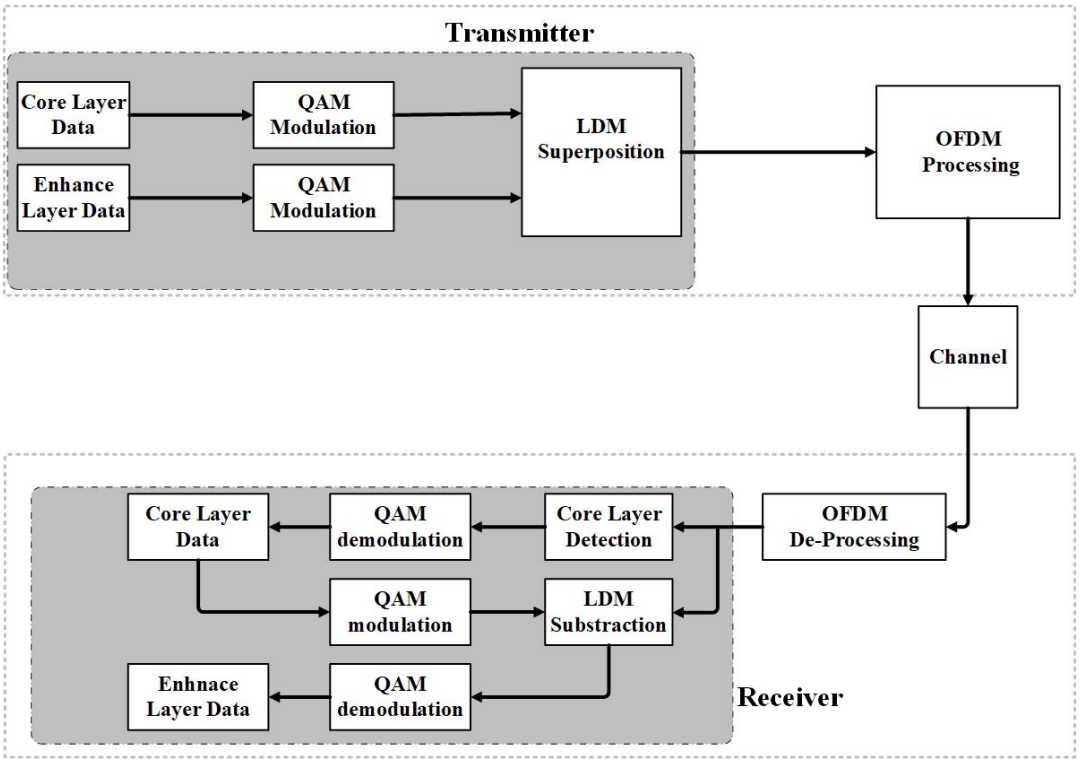

FIGURE 3.4: LDM-OFDM transmission framework

Channel Model

An AWGN channel model is considered where signals are transmitted to all receivers using a singular traffic channel. The IoT devices are presumed to be under varying channel conditions, ranging from high to low SNR. In contrast, the UE operates at high SNR as the CL is more noise-tolerant and can cater to IoT devices even under suboptimal channel conditions. The UE, given its EL requirements, needs to have a high SNR channel. Random noise is added to all transmitted symbols following AWGN distribution. Perfect CSI are assumed at all receiver, ensuring receivers possess all essential information for signal detection.

Receiver Framework for LDM Detection

The LDM signal at the receiver is expressed by

$$\mathbf{Y}(k) = \mathbf{X_{cl}}(k).\,\mathbf{H}(k) + g\,\mathbf{X_{en}}(k).\,\mathbf{H}(k) + \mathbf{N}_0(k) \tag{3.2}$$

where $\mathbf{Y}(k)$ is the received signal of kth sub-channel, $\mathbf{H}(k)$ is the channel matrix, and $\mathbf{N}_0(k)$ is the added noise. For a two-layer LDM, the signal detection at the receiver is realized in two stages, as shown in Figure 3.4. Initially, CL detection is carried out. The EL signal from (3.2) is considered as an added interference, and the detection is as simple as a standard OMA signal detection process. Equation (3.3) shows the total noise and interference for the CL detection. The signal at the receiver will have the originally transmitted signal with added noise as well as channel effects and is expressed as

$$\mathbf{N_{cl}}(k) = g\,\mathbf{X_{en}}(k)\,.\,\mathbf{H}(k) + \mathbf{N}_0(k) \tag{3.3}$$

One way to ensure high accuracy of CL data detection is to use Low QAM modulation. CL detection does not require more computing; hence this is suitable for low

power IoT devices. In contrast, the EL detection is done using SIC, which is more computationally intensive. The receiver needs to detect the CL data and reconstruct those data using the same technique used by the transmitter. The reconstructed CL data is subtracted from the received signal. Then the remaining signal is detected after power normalization. Equation (3.4) shows the subtracted signal for the EL detection.

$$\mathbf{Y_{en}}(k) = \mathbf{X_{cl}}(k).\,\mathbf{H}(k) + g\,\mathbf{X_{en}}(k)\,.\,\mathbf{H}(k) + \mathbf{N}_0(k) - \mathbf{X_{cl\ re}}(k) \tag{3.4}$$

Assuming a perfect CL detection with perfect channel estimation, EL signal is expressed as

$$\mathbf{Y_{en}}(k) = g\,\mathbf{X_{en}}(k)\,.\,\mathbf{H}(k) + \mathbf{N}_0(k) \tag{3.5}$$

The signal from (3.5) is amplified with a factor of $1/g$ before the detection of EL data. In this transmission framework, successful CL detection is essential for enhancing layer detection performance, so the CL needs to be reliable and robust in handling noise. Moreover, EL data detection is complex, so UE devices require higher computation capability.

3.3.2 System Model (Multipath Fading Channel)

The fading channel model is an extension of the AWGN channel model. It incorporates the effects of multipath fading, shadowing, and Doppler spread. The fading channel model is more realistic and provides a comprehensive understanding of the system performance in real-world scenarios as shown in Figure 3.5. This model demonstrate a LDM downlink transmission in multipath fading channel scenario. In this context, a Single-Input Single-Output (SISO) transmission model is considered, where both the transmitter and the receiver are equipped with a single antenna.

An LDM signal contains information for two different devices using a single traffic channel. The following equation can express the signal transmitted from the BS to both UE and IoT devices

$$\mathbf{x}(t) = \mathbf{x_{cl}}(t) + g\,\mathbf{x_{en}}(t) \tag{3.6}$$

Assuming an outdoor scenario with multiple paths, including a LoS path and other reflected paths. The receivers are placed in various locations under different channel conditions. Both receivers have multiple received signals coming from different reflecting objects around them, as shown in Figure 3.5. The number of paths for each receiver is different, with receiver 1 having a dominant path as it has a LoS transmission. Each path has a different path length; hence there are different delay elements, τ_l, $l = 0, \cdots, L_1$. Equation (3.7) represents the channel for UE where $\mathbf{h}_0\delta(t-\tau_0)$ represents the channel condition for the dominant path. This channel condition is simulated using Rician distribution as [148]

$$\sum_{l=0}^{L_1} \left(\mathbf{h}_l(t)\,\delta_l\left(t-\tau_l\right) + \mathbf{n_l}\right) \tag{3.7}$$

where L_1 is the total number of paths from the BS to the UE.

IoT devices are assumed to have NLoS transmission and has an L_2 number of reflected signals represented by (3.8). This model considers the existence of both static and dynamic reflector. The static reflectors are from a fixed obstacle, a permanent object such as building, trees, etc. The paths from static reflectors can be learned via feedback channel and past transmission. Moreover, time-varying objects such as moving vehicles can not be known or predicted as their position and behavior change. This channel is expressed as follows assuming a Rayleigh distribution [148]

$$\sum_{l=1}^{L_2} \left(\mathbf{h}'_l(t)\, \delta_l\,(t-\tau_l) + \mathbf{n}'_\mathbf{l} \right) \tag{3.8}$$

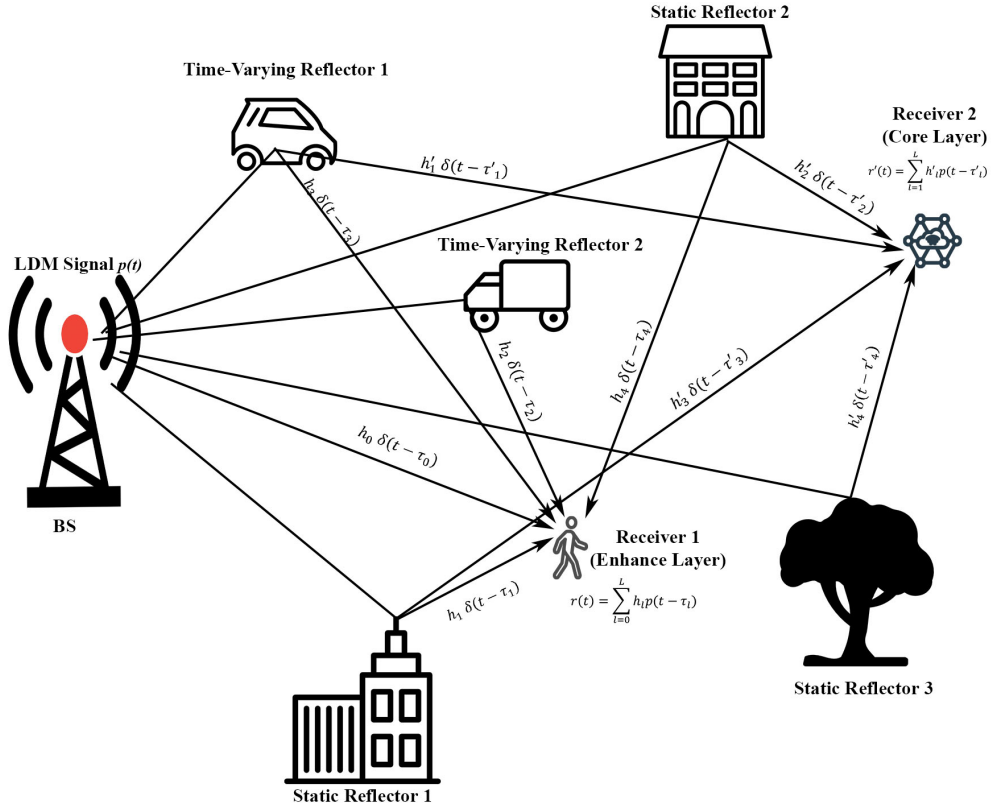

FIGURE 3.5: LDM transmission model in multi-path fading channel

The delay from different paths are assumed to be higher than the symbol duration and time-independent hence the fading experienced by UE is slow frequency selective fading. Using (3.1) and (3.7), the received signal $\mathbf{y_1}(t)$ is expressed by

$$\mathbf{y_1}(t) = \sum_{l=0}^{L_1} \left(\mathbf{x_{cl}}(t-\tau_l)\,.\,\mathbf{h_l}(t) + g\,\mathbf{x_{en}}(t-\tau_l)\,.\,\mathbf{h_l}(t) + \mathbf{n_l} \right) \tag{3.9}$$

Similar to UE, the IoT device also has multiple reflected signal paths with delay elements higher than the symbol duration and unchanged over the transmission time. Hence, receiver 2 has a slow frequency selective fading channel and the received

signal $\mathbf{y_2}$(t) is expressed from (3.1) and (3.8) as

$$\mathbf{y_2}(t) = \sum_{l=1}^{L_2} \left(\mathbf{x_{cl}}(t-\tau_l) \,.\, \mathbf{h'_l}(t) + g\, \mathbf{x_{en}}(t-\tau_l) \,.\, \mathbf{h'_l}(t) + \mathbf{n_l} \right) \tag{3.10}$$

This system model describes how LDM can take advantages of the different channel condition of UE and IoT devices. In next subsection, the impact of mMIMO mm-wave transmission is considered to on the LDM-OFDM framework.

3.3.3 System Model (Beamspace mMIMO mmWave Channel)

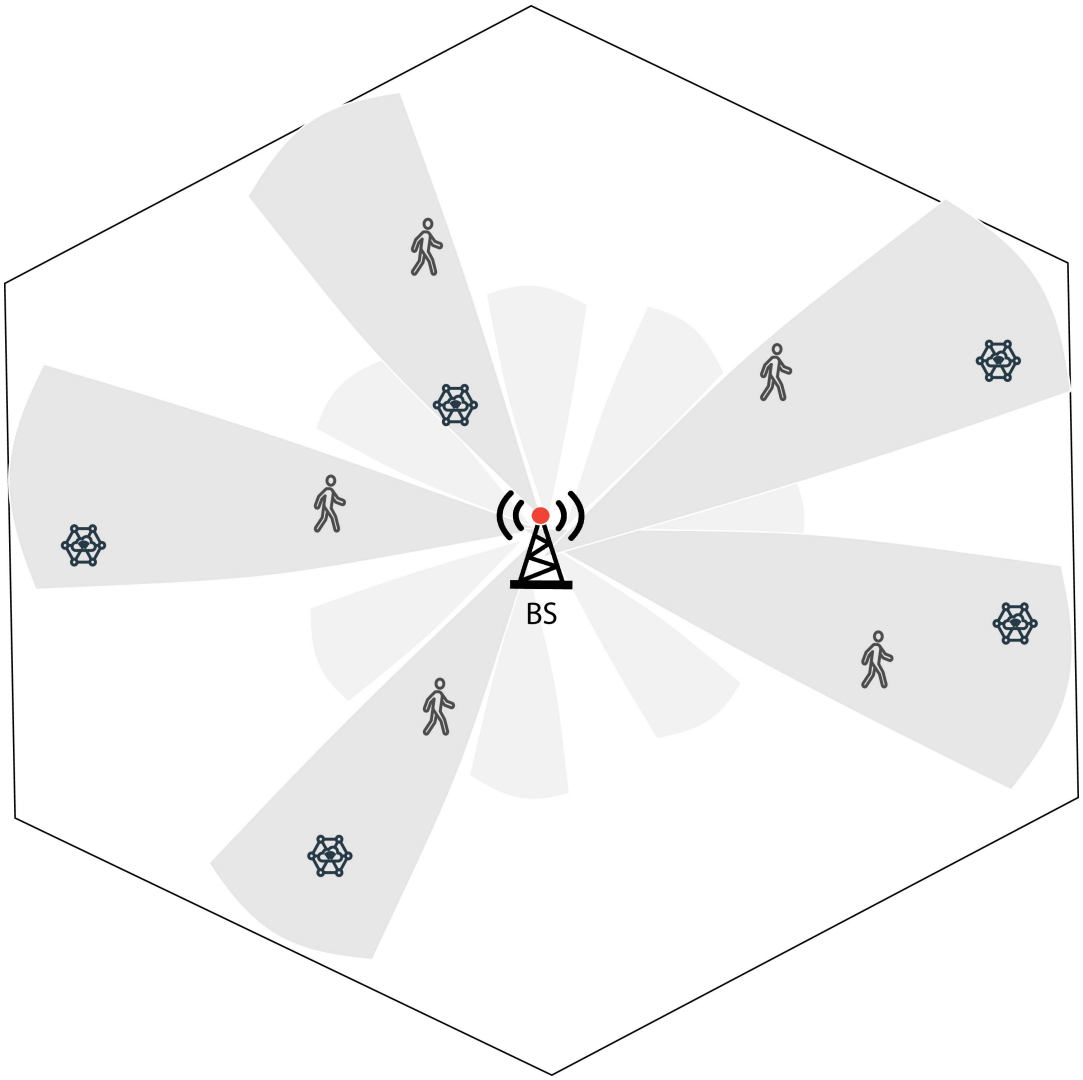

FIGURE 3.6: mMIMO beamforming transmission model for LDM-OFDM framework

A mmWave beamspace is considered for LDM-OFDM framework, as shown in Figure 3.6. The system consists of one BS and two types of users (UE and IoT devices), randomly and uniformly distributed in the cellular network. The BS is equipped with multiple antennas to generate multiple beams with the beamspace methods. Two receivers of different service requirement (UE and IoT devices) within the transmission area of one beam are paired for LDM transmission. Besides, to reduce the system complexity, inter beam interference is not considered by assuming perfect beamforming at the BS. The UE is located near the transmission, presenting a good channel condition, and the IoT device is at the edge of the transmission area, highlighting a poor channel condition. Equation (3.6) is the combined LDM signal transmitted from the transmitter. The LDM signal is transmitted into nth beamspace where CL data are for IoT devices, and EL data are for the UE. Both small and large scale fading are considered in this channel model due to their significance for mm-wave transmission. Equation (3.7) shows the small scale fading and (3.11) presents the large scale fading for mm-wave transmission assuming free space path loss [149].

$$L(r) = 32.4 + 20\log_{10}(f_c) + 20\log_{10}(r) \tag{3.11}$$

Here is for the nth beam where f_c is the carrier frequency in GHz, and r is the distance between transmitter and receiver in meters.

As the attenuation of mmWave is high, the high gain and high directional beam are generated by the BS to ensure high QoS. For simplicity, the antenna model are assumed as a sectorized antenna model, which means the array gain within the half-power beamwidth (main lobe gain) is the maximum power, and the first minor maximum replaces the side lobe gain. The total array gain $G(n)$ is denoted as [150,151],

$$G(n) = \begin{cases} \Psi, & \text{for main lobe} \\ \psi, & \text{for side lobe} \end{cases} \tag{3.12}$$

where $\Psi = N$, $\psi = \frac{1}{\sin^2(\frac{3\pi}{2\sqrt{N}})}$ and N is the main lobe gain.

The received signal for users is expressed as

$$y_{u1} = \frac{h_{u1}\, G(n)\, x_n}{L(d_1)} + n_{u1} \tag{3.13}$$

and the received signal for IoT devices is expressed as

$$y_{u2} = \frac{h_{u2}\, G(n)\, x_n}{L(d_2)} + n_{u2} \tag{3.14}$$

3.4 Theoretical Evaluation

The system models outlined in the previous section are analyzed to assess the performance of LDM in the proposed usage model. To provide a benchmark for this analysis and set a reference for subsequent studies, an empirical equation is formulated to scrutinize the performance limit of the LDM CL. Owing to the integration of EL data, the peak CL channel capacity is constrained by the g, as denoted in (3.23).

3.4.1 BER of LDM CL

The equation is based on the generic Symbol Error Rate (SER) expression of an uncoded OMA-OFDM system from [152, 153], which is

$$SER_k^{AWGN} = 4\left(1 - \frac{1}{\sqrt{M}}\right) Q\left(\sqrt{\frac{3\,\rho_k}{M-1}}\right) - 4\left(1 - \frac{1}{\sqrt{M}}\right)^2 Q\left(\sqrt{\frac{3\,\rho_k}{M-1}}\right)^2 \tag{3.15}$$

where

$$Q(x) = \frac{1}{\pi} \int_0^{\frac{\pi}{2}} \exp\left(-\frac{x^2}{2\sin^2\theta}\right) d\theta \tag{3.16}$$

and ρ_k is the SNR of the kth symbol.

Gray coding is assumed for the QAM constellation, leading to a single bit error for each symbol error. This relationship between BER and SER can be expressed as

$$\text{BER} = \frac{\text{SER}}{M}$$

An analytical model for the BER of the CL is derived from the above. For this evaluation, inter-symbol interference is not considered. Given that the EL has lower power compared to the CL, the value of g is consistently negative in dB. This configuration is applied across various QAMs. The relationship between the CL data rate and g in an uncoded OFDM system is observed as:

$$g = -4\, M_c \tag{3.17}$$

where M_c is the QAM order for the CL. Now the CL SNR is calculated from channel SNR as

$$\rho_{kcl} = \frac{2\,\rho_k}{-g} \tag{3.18}$$

Using the values of CL SNR from (3.18) in (3.15) the SER of the CL data is calculated as

$$SER_k^{AWGN} = 4\left(1-\frac{1}{\sqrt{M}}\right)Q\left(\sqrt{\frac{6\rho_k}{g(1-M)}}\right) - 4\left(1-\frac{1}{\sqrt{M}}\right)^2 Q\left(\sqrt{\frac{6\rho_k}{g(1-M)}}\right)^2 \tag{3.19}$$

3.4.2 Channel Capacity Distribution

The channel capacity of an AWGN channel is expressed in terms of bits/sec/Hz as [154]

$$C = \log_2\left(1+\frac{p_s}{p_n}\right) \tag{3.20}$$

where p_s is the signal power and p_n is the noise power. This shows the dependency between channel SNR and capacity, and is used to calculate the channel capacity for LDM layers as [84]

$$C_{cl} = \log_2\left(1+\frac{p_{cl}}{p_{el}+p_n}\right) \tag{3.21}$$

and

$$C_{el} = \log_2\left(1+\frac{p_{en}}{p_n}\right) \tag{3.22}$$

Given the known power ratio, g, the maximum system capacity of the CL can be assessed with a set value of g.

$$C_{cl} = \log_2\left(1 + \frac{1}{g}\right) \tag{3.23}$$

3.5 LDM Performance Evaluation

The OFDM framework integrated with LDM is employed as depicted in the proposed model. The model is created in Matlab, where it generates random data bits based on the transmission rate. These bits are processed as per the system model, illustrated in Figure 3.4. After transmission, BER is computed by comparing the received data bits for each layer against the originally transmitted data bits. Relevant parameters for this simulation can be found in Table 3.1. For the AWGN channel, both the analytical model presented in (3.19) and the simulated values are examined. Additionally, the channel capacity distribution among the LDM layers is assessed.

TABLE 3.1: OFDM parameters

Parameter	Values
No. of carriers	64
Single frame size	96 bits
Total no of frame	1000
No. of pilot bits	4
Cyclic extension	16 bits

Figure 3.7 illustrates the BER performance of the CL derived from both the simulation and the previously described analytical model. The SNR indicates the channel condition between the transmitter and receiver for the LDM signal. The power ratio g is adjusted based on the QAM modulation index M (comprising 16, 32, and 64) of the CL as referenced in (3.17). Observing Figure 3.7, there is a noticeable alignment between theoretical and simulated values, with curves from the same QAM often coinciding or deviating slightly. A diminishing BER performance is evident as the QAM modulation index increases, confirming the accuracy of the analytical model.

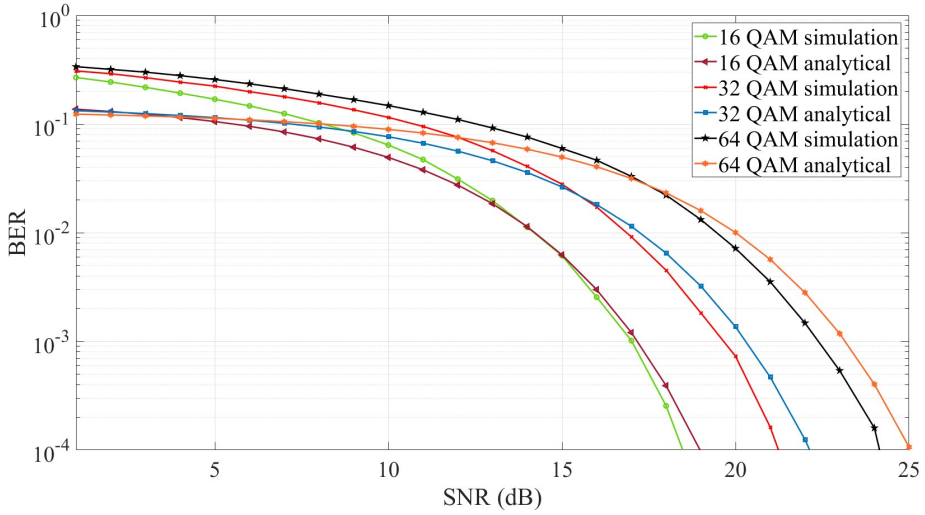

FIGURE 3.7: Performance comparison of LDM CL between simulation and analytical results for 16, 32 and 64 QAM modulation

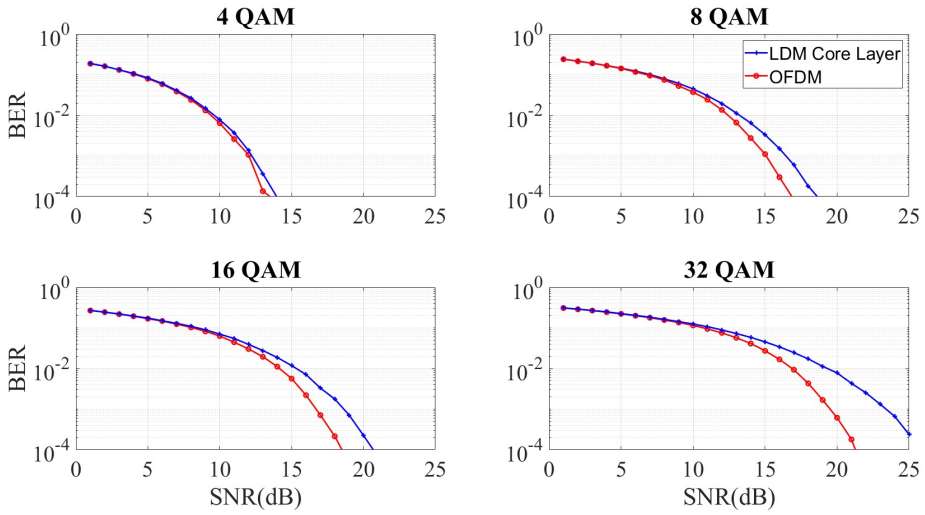

FIGURE 3.8: BER performance of LDM CL with OMA in same uncoded OFDM framework

Figures 3.8 and 3.9 examine the CL performance, contrasting its BER performance with that of an OMA system. In the simulations, both models utilize 4, 8, 16, and 32 QAM constellations. At reduced SNR levels, the performances of both OMA and LDM CL remain consistent. Yet, OMA transmission achieves same BER at a slightly lower SNR then LDM CL. Observing a 10^{-4} BER standard, the LDM CL mirrors the OMA performance but demands approximately 3 dB elevated SNR values across all QAM constellations. This differential in necessary SNR highlights the trade-off brought about by introducing EL to the CL. Meanwhile, Figure 3.9 depicts the influence of power ratio on the CL efficiency. The power ratio, symbolized by

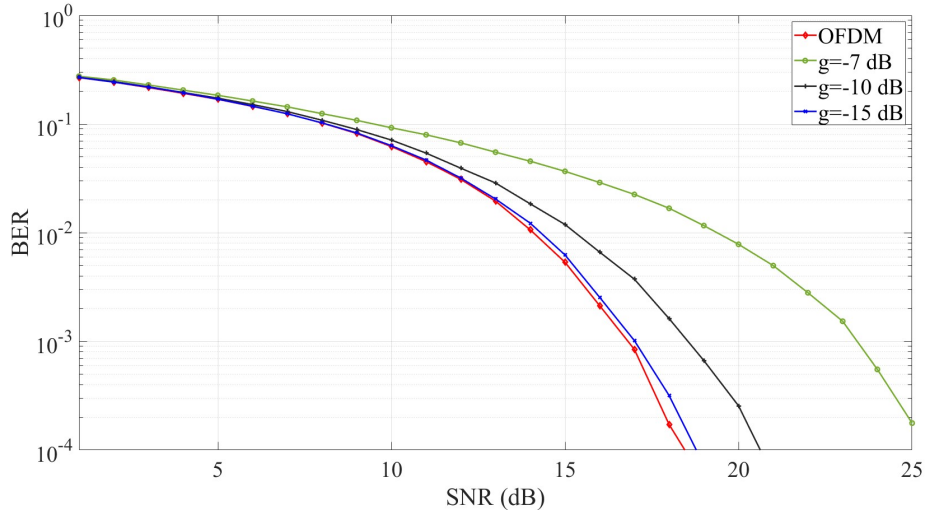

FIGURE 3.9: Impact of g on the BER of the CL transmission

g, critically affects the LDM CL function, suggesting system adjustments to g values based on service quality needs. The findings indicate that a power ratio range of -10 to $-15\ dB$ enables successful CL transmission.

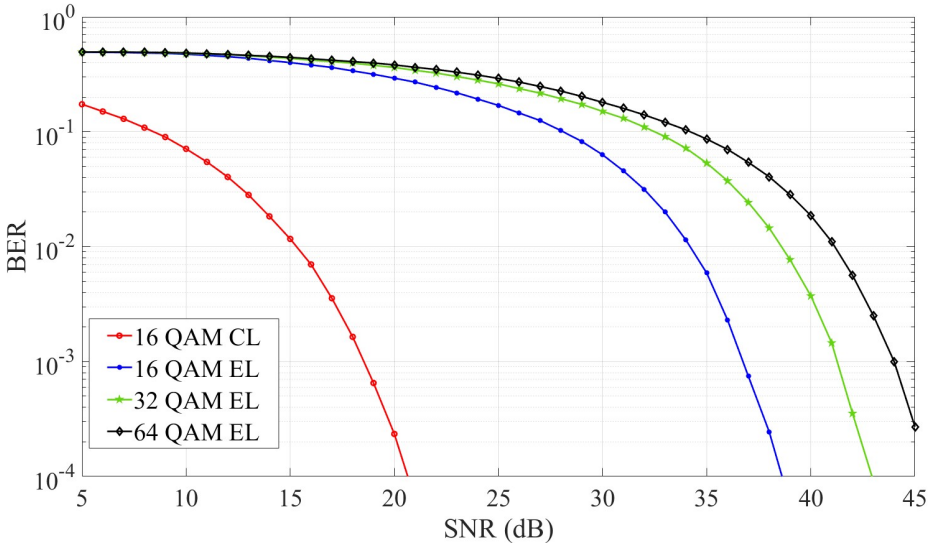

FIGURE 3.10: BER performance of LDM EL transmission for 16, 32 and 64 QAM constellation with a fixed CL data rate

In Figure 3.10, the simulated outcomes for both layers are presented. During this simulation, a constant power ratio g of $-10\ dB$ is employed, and the featured SNR characterizes the cumulative channel SNR. This encompasses the entirety of the LDM signal power paired with the channel AWGN noise power. Different data rate combinations for the CL and EL are tested. The CL data is stabilized at 192 bits

(16 QAM) per frame, with EL data varying between 192 bits (16 QAM), 240 bits (32 QAM), and 288 bits (64 QAM). Notably, CL performance remains consistent regardless of the EL data rate alteration. A BER of 10^{-4} is registered at an approximate 22 dB.

Reference [155] explored the CL performance for QPSK combined with robust LDPC coding of $4/15$, achieving this same BER at 7 dB. Their results for the EL performance for 64 QAM stood at 20 dB. Meanwhile, in [156], Binary Phase-Shift Keying (BPSK) was employed for the CL alongside $1/8$ Turbo coding for error rectification and QPSK for EL with $1/2$ turbo coding, culminating in comparable performances at 1 and 15 dB respectively. A parallel EL performance was observed at around 40 dB channel SNR for an uncoded OFDM system in the developed model. The demands for a much higher SNR are attributed to the absence of error rectification capacity, focusing primarily on gauging the inherent performance of LDM. There is also a consistent requirement of roughly 15 dB higher SNR for EL as compared to CL. Performance undergoes degradation as the data rate elevates. Figure 3.10 delineates the necessary channel conditions for different receivers, signifying that the CL receiver can withstand suboptimal transmission locales with low SNR. In contrast, the EL receiver necessitates an optimized coverage region to ensure successful data detection.

The BER performance of CL at lower SNR works well for small IoT devices as they will be distributed among different places with different channel condition. On the other hand, ELs needs higher SNR values, as seen in Figure 3.10, which is more suitable for UE. Therefore, this framework can take advantages of different requirements and conditions. Moreover, the theoretical BER values of CLs matches closely with simulation values as seen in Figure 3.7.

Channel capacity distribution between the LDM data layers is evaluated using (3.20), (3.21) and (3.22). Figure 3.11 shows the total channel capacity distribution between the LDM layers without any loss of total channel capacity. Another key point of this is a non-linear distribution of channel capacity between data layers. The distribution is controlled by the power ratio of the data layers. The CL capacity herein is higher than that in the EL. However, it gets saturated with an increase in SNR. This distribution works well for IoT devices in the usage model as the devices

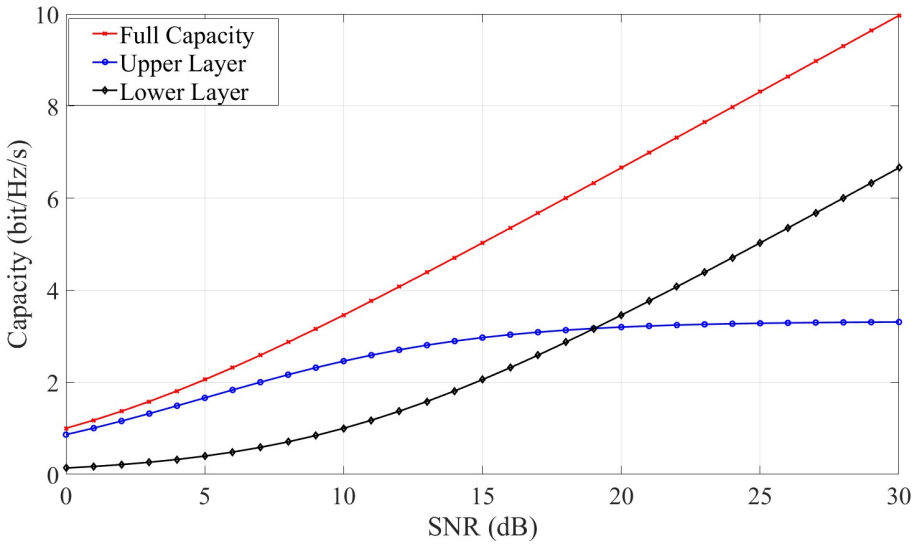

FIGURE 3.11: Channel capacity distribution between CL and EL

are assumed to be in different locations, which can cause bad channel conditions for some devices. Due to the robustness of the CL against the channel conditions, it can be used to serve all IoT devices. Moreover, the CL capacity is lower, which also fits with the IoT devices data requirements assumed in the usage model. On the other hand, the EL has a very low capacity at lower SNR. The capacity of EL increases significantly as the SNR values improve. EL has most of the available channel capacity in good channel conditions. The users can be served using EL as long as it meets both the network condition and requirement.

The LDM CL and EL data are simulated with Rayleigh fading channel expressed in (3.8). The number of paths affects the receiver performance significantly. The overall performance is worse in comparison to that of the AWGN channel as expected. Therefore, to achieve a better performance, transmitted data rate is lowered, using a lower QAM constellation of 4 QAM for CL transmission and up to 16 QAM for EL transmission.

Figure 3.12 presents the performance of CL and EL with different data rates for EL set against a backdrop of multi-path Rayleigh fading. This simulation contemplates 10 multi-path signals. The performance trajectory of both LDM layers mirrors observations from the prior AWGN channel simulation. Specifically, the EL demands a substantially elevated SNR to match the performance standards of the CL. Yet, the disparity in SNR between the CL and EL to achieve analogous BER metrics

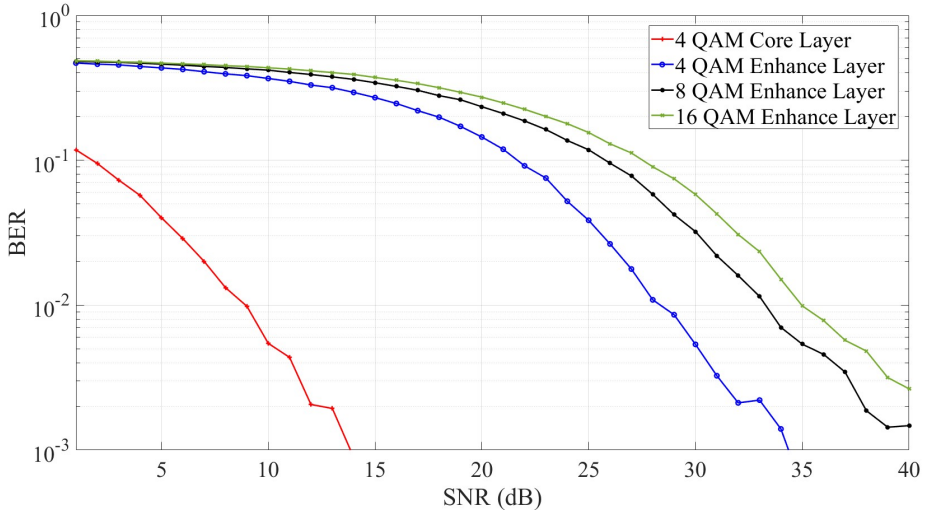

FIGURE 3.12: BER performance of *core* and EL for Rayleigh fading channel

is broader than in the context of the AWGN channel. Consequently, the inference drawn is that the fading channel exerts a more pronounced effect on the EL data.

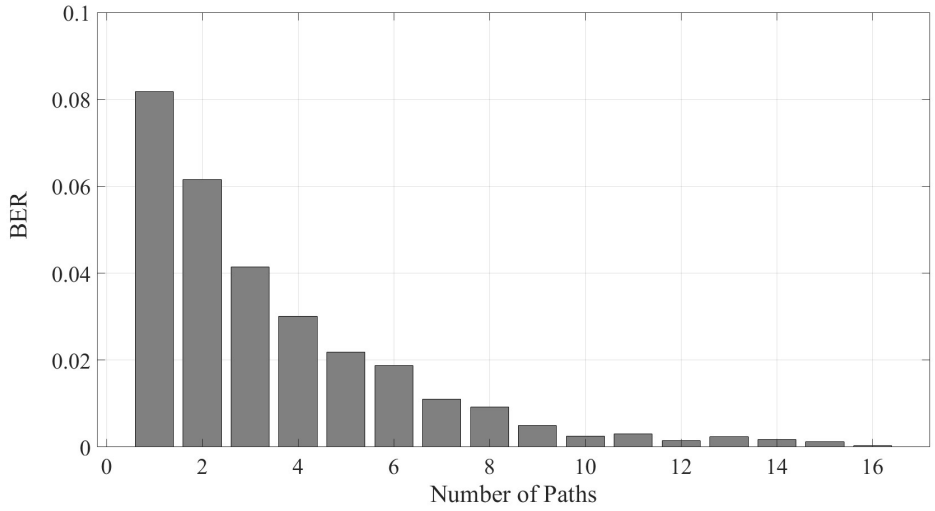

FIGURE 3.13: BER *vs* no. of fading paths for CL

Further insights are gleaned from Figure 3.13, which delineates the influence of path quantity on the CL performance. A fixed BER at 15 dB SNR for 4 QAM data transmission is utilized for this analysis. The data suggests that BER experiences enhancement as signals from a greater number of paths are introduced, as illustrated in Figure 3.13. Nonetheless, while initial increments in paths render a pronounced boost in performance, subsequent additions yield diminishing returns.

3.6 Impact of Receiver Mobility on Link Sustainability of LDM Pair

In this section, an initial mobility model for UE is introduced, under the assumption that IoT devices remain at a fixed location. An algorithm has been formulated to modify the PA, aiming to augment the UE-IoT pairing as the channel conditions for UE change due to mobility. Subsequently, this model is expanded to accommodate mobility of IoT devices. A corresponding analytical model is crafted to assess the repercussions on the sustainability of the LDM pair, particularly when the pair features varied mobility configurations.

3.6.1 User Mobility model

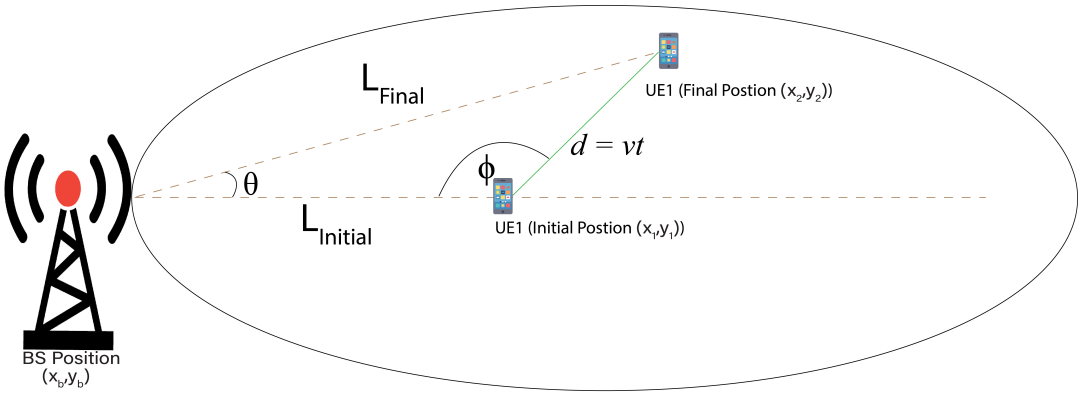

FIGURE 3.14: UE surface mobility model

The mobility of UE users (served by the EL) is taken into account, while IoT devices (which are catered to by the CL) are assumed to maintain a fixed position. Consequently, the channel condition for the IoT devices remains consistent, but that of the UE varies over time. Figure 3.14 illustrates the trajectory of UE, moving from its starting position to its endpoint, maintaining a LoS communication with the BS. The BS is positioned at the coordinates (x_b, y_b). The UE's starting point is set such that it forms a 0-degree angle with the outgoing signal, located at (x_1, y_1). Given that the UE relocates at a random velocity v over a duration t, the span d between the initial and concluding locations of UE can be articulated as:

$$d = v\,t \tag{3.24}$$

The UE is assumed to move at a random angle ϕ to the (x_2, t_2) after time t. Then the final position of UE is calculated using

$$x_2 = x_1 + d\cos(\phi) \tag{3.25}$$

and

$$y_2 = y_1 + d\sin(\phi) \tag{3.26}$$

The coordinates of BS and UE is now known. The distance between the initial and final location of UE and with BS is measured by

$$d = \sqrt{|(x_1 - x_2)|^2 + |(y_1 - y_2)|^2} \tag{3.27}$$

At the final position, the angle between BS and UE is taken as θ as shown in Figure 3.14. The distance between BS and UE initial and final position is calculated using (3.27) and from that, θ is measured as

$$\theta = \cos^{-1}\left(\frac{l_{\text{initial}}^2 + l_{\text{final}}^2 - d^2}{2l_{\text{initial}}\,l_{\text{final}}}\right) \tag{3.28}$$

Given that x_t represents the power dispatched from the BS, with n_p denoting the white noise power and h characterizing the channel fading. The path-loss, L_p, is determined using (3.11), factoring in the distance between the BS and the UE. Consequently, the SNR is computed as:

$$\rho = \frac{x_t \, h \cos\theta}{n_p \, L_p} \tag{3.29}$$

where h is the time selective fading coefficient.

$$h(t) = \sum_{i=0}^{L-1} a_i \, e^{-j\,2\,\pi\,f_c\,\tau_i} \, e^{j\,2\,\pi\,f_d t} \tag{3.30}$$

Given the established relationship, the channel fading parameter, h, can be determined from the carrier frequency f_c and the velocity of the devices, which gives rise to the Doppler frequency f_d. It is assumed that the initial SNR for the UE is ρ_1. The data for the UE is dispatched using the EL, and the PA is derived based on both ρ_1 and the network conditions of the IoT devices. As the UE begins to relocate from its initial position, its SNR begins to fluctuate. Every t time units, the BS recalibrates the PA based on the SNR observed at the UE. Algorithm 1 has been devised for the BS to execute this function.

As the UE moves through space, its channel condition changes. Algorithm 1 helps the system to decide a suitable action. It adjust the PA, as shown in the algorithm. If the UE's network condition does not meet the SNR values' minimum requirement, the system will break the LDM pair. After dissociating the LDM pair, the system can form a new LDM pair or use orthogonal multiplexing with a single traffic channel to serve that UE if the UE has better transmission from another BS or has a better channel condition. The system can then find another set of IoT devices in the new transmission range and form a new LDM pair. However, if these are not possible, the system will dedicate a traffic channel for users until such configuration

Algorithm 1: Adaptive PA to improve link sustainability of LDM pair

Data: x_t, h_{ue1} (from pilot data), n_p, ρ_{min} (Min required SNR for UE), ρ_1 (initial SNR of UE), BS location (x_b, y_b), UE trajectory from (x_1, y_1) to (x_2, y_2) with random angle ϕ and distance d_1, initial angle $\theta_0 = 0$ between BS and UE

Result: Adaptive configuration of LDM pair

`// Computations`

Compute Distance using (3.27);

Compute $L_{initial}$ (distance from BS to UE_1 initial position);

Compute L_{final} (distance from BS to UE_1 final position);

Compute d (distance from UE_1 initial to UE_1 final position);

Compute θ using (3.28) for UE final position;

Compute ρ_2 using (3.29) for UE final position;

`// Decision Process`

while $\rho_{min} < \rho_2$ **do**

  if $\rho_2 > \rho_1$ **then**

    Decrease the value of g;

  else if $\rho_2 = \rho_1$ **then**

    Maintain same PA;

  else

    Terminate the LDM pair;

is found.

The mobility of the UE and its effect on the SNR are critical factors in determining how long the UE can sustainably be served by the BS using LDM EL. The parameter ρ_{min} signifies the threshold, below which the quality of the link might not be sufficient for a reliable connection.

When the UE moves along a fixed trajectory, its distance from the BS changes, which in turn alters the SNR. Considering that the UE can move either vertically (along the y-axis) or horizontally (along the x-axis), it is essential to evaluate how long the SNR remains above the ρ_{min} threshold in each scenario.

UE moves vertically: Consider a UE traveling a distance d perpendicular to the beam direction, i.e., along the y-axis, at a constant speed v. The final position of the UE is given by $(x_1, y_1 + d)$. Given the assumption of knowledge regarding the initial position of the UE, both L_{final} (final distance from the BS) and θ_{final} (angle between the BS and the UE's final position) can be derived using (3.27) and (3.28), respectively, as functions of d.

By referring to the relationship outlined in (3.24) and factoring in the known velocity v, both L_{final} and θ_{final} can be described in terms of time, t. By utilizing the equation below for a given SNR_{min}, the duration t it takes for the UE to reach the threshold condition can be determined from (3.31). This time duration t indicates the minimum period the UE can be accommodated using LDM EL before the signal quality becomes untenable.

$$\frac{\cos\theta}{L_p} = \frac{\rho_{\text{min}}\, n_p}{x_t\, h} \tag{3.31}$$

UE moves horizontally: Consider a UE that moves d distance along with the beam direction (x-axis) at a fixed velocity v. Then, the final location of UE can be written as $(x1 + d, y_1)$. As in the previous condition the L_{final} and θ_{final} can be calculated using (3.27) and (3.28) as a function of time (t). With these values, similar to the minimum time calculation, the maximum time can be measured using (3.31).

3.6.2 IoT Mobility Model

IoT devices are assumed to be distributed randomly over the entire transmission area. Unlike users, IoT devices can start with any random angle θ_1 with transmission direction. Moreover, the relatively lower SNR requirement of CL is important as the IoT devices can be in a poor channel condition due to their position as well as smaller antenna gain. Figure 3.15 shows the mobility of IoT devices from an initial position to a final position with an LoS communication between the BS and IoT. The BS is assumed to be located at position (x_b, y_b).

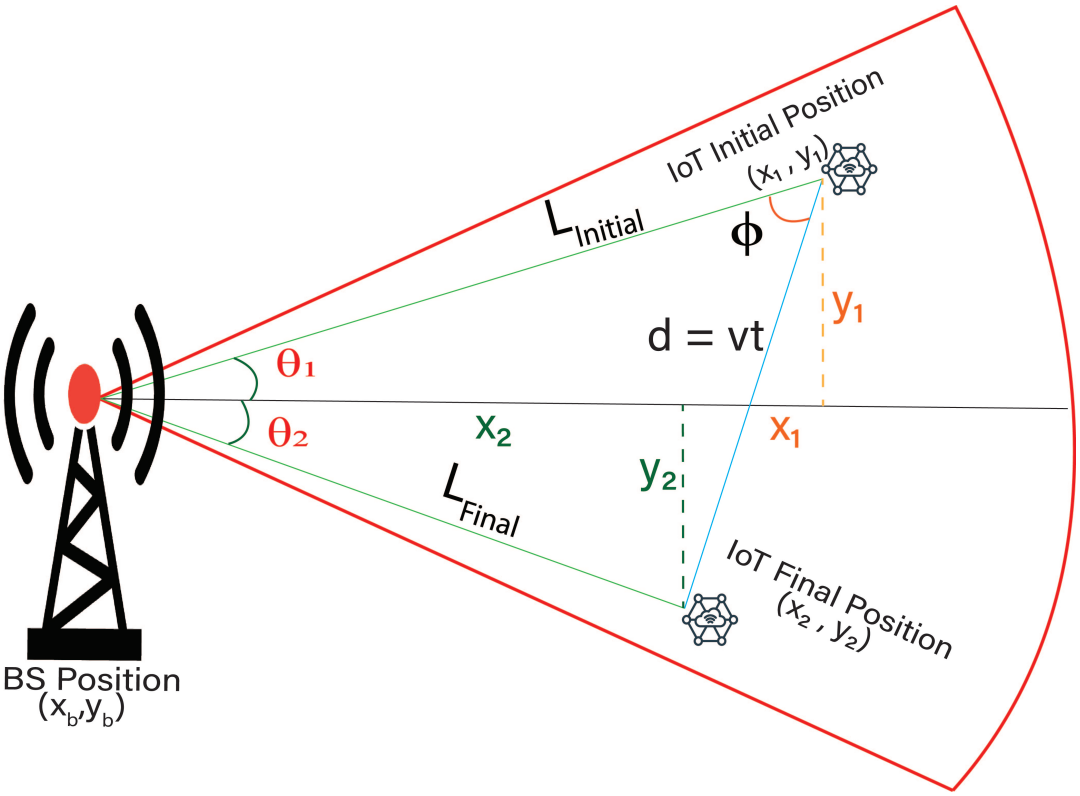

FIGURE 3.15: IoT surface mobility model

The initial IoT location is assumed to be at (x_1, y_1). Then the initial distance L_{initial} can be calculated using (3.27): And θ_1 is calculated as:

$$\theta_1 = \cos^{-1}\left(\frac{l_{\text{initial}}^2 + x_1^2 - y_1^2}{2l_{\text{initial}}\, x_1}\right) \tag{3.32}$$

If the device moves at a random speed v at a random angle ϕ for a time t to reach

its final position, then the distance between IoT's initial and final position d and the final coordinates can be calculated using equation (3.24), (3.25) and (3.26).

The coordinates of BS and IoT is now known. The distance between the initial and final location of IoT and with BS can be measured using (3.27). At the final position, the angle between BS and IoT is taken as θ_2 as shown in Figure 3.15 which is calculated as:

$$\theta_2 = \cos^{-1}\left(\frac{l_{\text{final}}^2 + x_2^2 - y^2}{2l_{\text{final}}\, x_2}\right) \tag{3.33}$$

The SNR at the IoT receiver can be calculated using the same (3.29) following the same steps of UE.

The range of IoT device's initial position

When forming an LDM pair, both UE and IoT devices must be within the coverage area. Since the transmission is directed towards the UE, it is essential to determine the boundary condition for the IoT device that will ensure its inclusion within the transmission angle. For simplification, assuming the BS location as (0,0), the initial distance between BS and IoT is described as:

$$\begin{aligned} L_{initial} &= \sqrt{(x_b - x_1)^2 + (y_b - y_1)^2} \\ &= \sqrt{x_1^2 + y_1^2} \end{aligned} \tag{3.34}$$

Using (3.32) and (3.34), the following relation is derived:

$$cos(\theta_1) = \frac{L_{initial}^2 + x_1^2 - y_1^2}{2\,L_{initial}\,x_1} \tag{3.35}$$

$$= \frac{x_1^2 + y_1^2 + x_1^2 - y_1^2}{2\,L_{initial}\,x_1}$$

$$= \frac{2\,x_1^2}{2\,L_{initial}\,x_1}$$

$$= \frac{x_1}{L_{initial}} \tag{3.36}$$

For the IoT device's initial position to be within the transmission area, the maximum value of θ_1 can be $\theta_{max} =$ Beamwidth/2. For this θ_{max} angle, the maximum value of the initial y position from a given x position using (3.36) is derived below.

$$\frac{cos(\theta_1)}{x_1} = \frac{1}{L_{initial}}$$

$$L_{initial} = \frac{x_1}{cos(\theta_1)}$$

$$x_1^2 + y_1^2 = \frac{x_1^2}{cos^2(\theta_1)}$$

$$y_1^2 = \frac{x_1^2}{cos^2(\theta_1)} - x_1^2$$

$$y_1 = \sqrt{\frac{x_1^2}{cos^2(\theta_1)} - x_1^2} \tag{3.37}$$

Equation (3.37) gives the maximum limit on the initial y position for IoT device for any given x value and transmission beamwidth.

3.6.3 Receiver Movement Patterns

The movement pattern of users can differ significantly depending on the area. Three distinct UE groups are considered, each representing a unique type of mobility. This movement is visualized on a 2D plane, where the X and Y axes mark the distance from a reference point. To identify the most suitable model for specific situations, various mobility models are explored. Three mobility models are evaluated for both UE and IoT devices, with their combined positions in the transmission scenario depicted in Figure 3.16

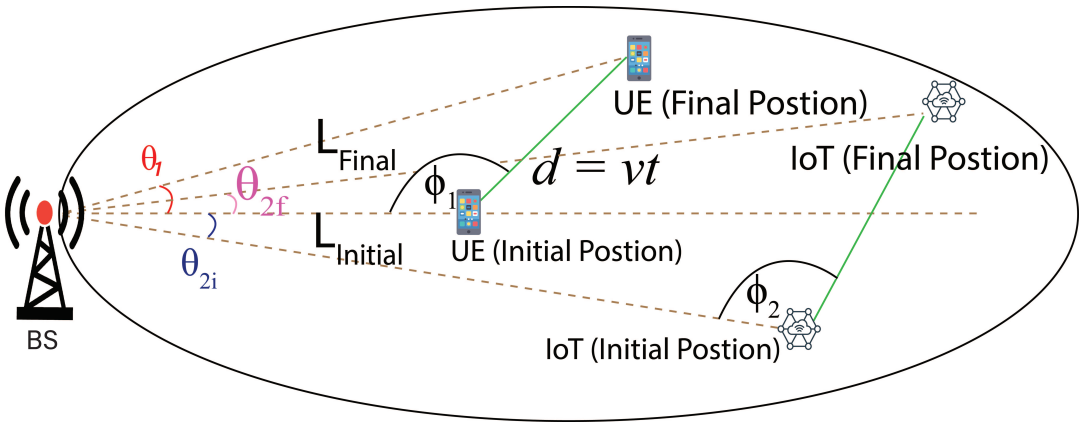

FIGURE 3.16: UE-IoT mobility model

Random Waypoint Mobility Model

This mobility model represents static to low movement in urban and rural areas, specifically tailored for non-motorized movements such as walking, running, and cycling. The speed of users in this model is assumed to fall within the range of 0 to 10 kph, with their directional angle spanning from 0 to 360°. The movement pattern is random in both speed and direction, as both can change unpredictably at any time [157]. The model assumes that devices adjust their speed after every t time interval and modify their direction after every 100 meters, as detailed in Appendix A-1. This assumption is based on the reasonable approximation of average distance a person covers before potentially changing direction. Choosing a shorter

distance for direction changes in the simulation could lead to scenarios where individuals appear to change directions too often, creating patterns of movement that seem random or without purpose. This does not align well with typical pedestrian behaviour, which usually shows more intentional and straight-line movement. The chosen distance of 100 meters offers a balanced approach, making sure that the simulated movement patterns are both realistic and accurately reflective of how people typically move in urban and rural environments.

Manhattan Mobility Model

This model refers to the urban street movement for motorised vehicles [157]. The roads are assumed to be in a grid design, and the change of direction can only be a multiple of 90°. The block lengths are assumed to be 200 meters for this work, which means the receiver can change direction every 200 meters with a speed range between 10 to 40 kph (Appendix A-2).

Freeway Mobility Model

This model represents motorised movement on the motorway. The UE speed is assumed to be between 40 to 100 kph. Moreover, as the motorway's vehicle does not take turns frequently and moves freely via a single road at a higher speed, the movement is assumed to be unidirectional for a short time frame. Therefore, a linear movement model is considered for these devices (Appendix A-3).

3.7 Evaluation of link Sustainability for Mobile Receivers

Section 3.5 outlined the transmission prerequisites for both IoT and UE. Using these benchmarks, the mobility model is assessed concerning sustainable link duration, a crucial Key Performance Indicator (KPI) for the proposed framework's effective transmission. In unicast transmission scenarios, brief link durations can lead to notable degradation in transmission quality, stemming from frequent LDM pair formations and terminations.

Initially, the influence of UE mobility on link time is examined, incorporating the PA Algorithm 1 to bolster link sustainability. Subsequent findings focus on the

interplay between PA, transmit beamwidth, and initial UE distances. Such insights pave the way for crafting optimal LDM pairs based on the UE mobility model and position. Lastly, a holistic system evaluation, considering combined mobility with a static PA, aims to discern the individual impacts of UE or IoT mobility from all mobility groups on link time. The simulation parameters are summarised in Table 3.2.

TABLE 3.2: Mobility simulation parameters

Parameter	**Values**
Carrier frequency, f_c	6 GHz
Transmit SNR	30 dB
Min required SNR at UE	25 dB
Random Waypoint	
Speed, s	$[0, 10]$ kph
Angle, ϕ	$[0, 360]^\circ$
Manhattan	
Speed, s	$[11, 40]$ kph
Angle, ϕ	$\{0, 90, 270, 360\}^\circ$
Freeway	
Speed, s	$[41, 100]$ kph

3.7.1 Impact of UE mobility on Link Time

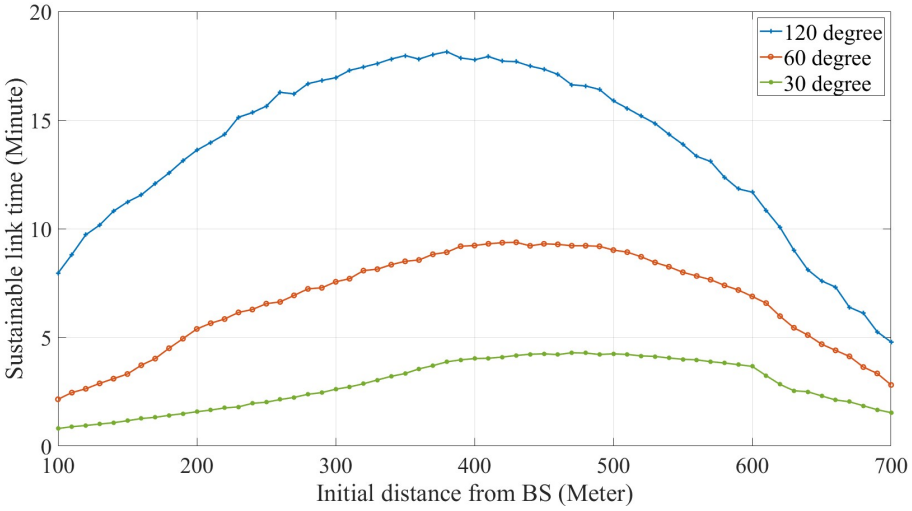

FIGURE 3.17: Impact of initial UE distance on link sustainability for random waypoint mobility model

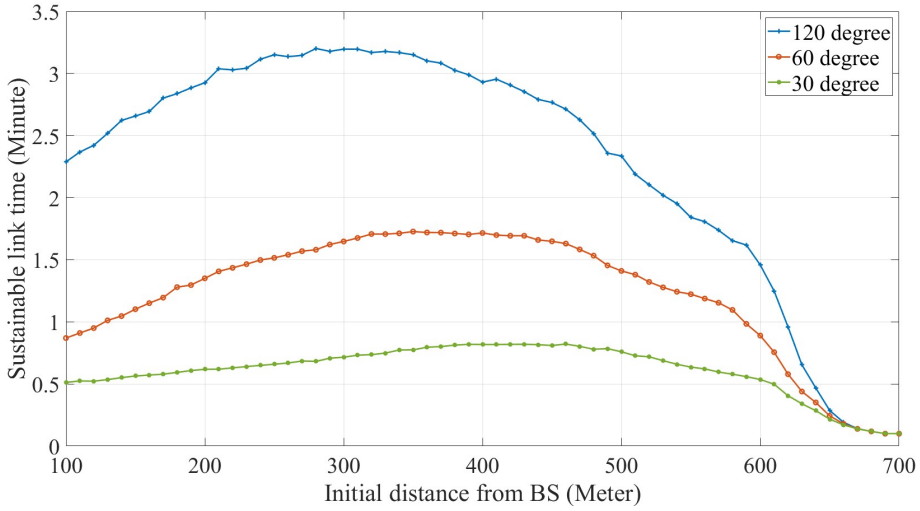

FIGURE 3.18: Impact of initial UE distance on link sustainability for Manhattan mobility model

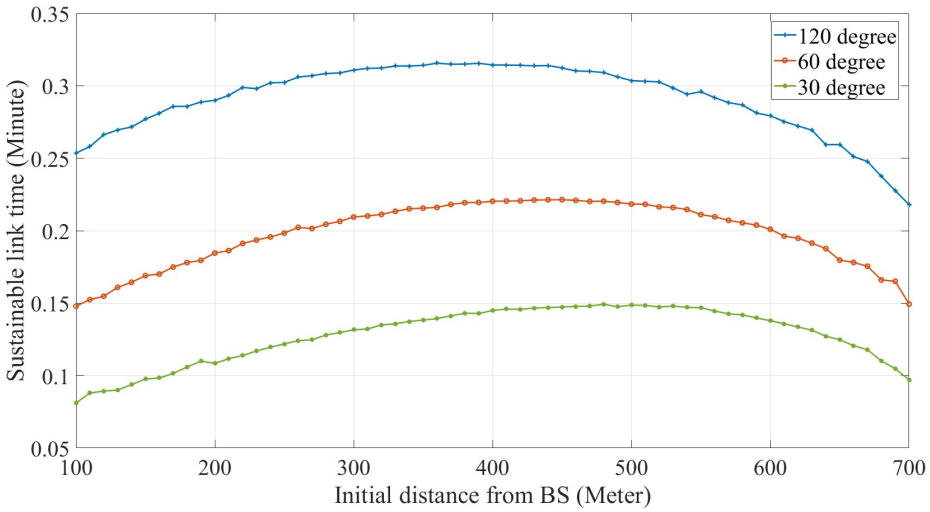

FIGURE 3.19: Impact of initial UE distance on link sustainability for Freeway mobility model

The sustainable link time for different initial positions of UE is illustrated in Figures 3.17, 3.18, and 3.19. The results underscore the significant influence of the mobility of the UE on these outcomes:

- **Low Mobility:** For users with limited movement, the sustainable link time can last up to 18 minutes before necessitating the termination of the LDM pair.
- **Medium Mobility (Urban Street Movement):** The link time in this scenario diminishes substantially, offering a maximum of 3 minutes.

- **High Mobility (Highway Users):** For these users, the sustainable link time dips even more drastically, affording a peak duration of 0.3 minutes.

This data highlights the suitability of LDM predominantly for users with low mobility. Additionally, the findings suggest the feasibility of creating a predictive model, grounded on the UE's initial distance and mobility pattern. This model could serve as a pivotal tool in prioritizing users during the initiation of a new LDM pair.

An intriguing pattern emerges from Figure 3.18, where there is consistent performance across varied beamwidths when the distance between UE and BS surpasses 620 meters. This consistency implies the potential for using a narrower beamwidth in such circumstances without compromising the sustainable link time.

Interestingly, for all three mobility categorizations, the sustainable link-time graph manifests a wave-like trend rather than a straightforward decline. An initial increase in sustainable link-time is observable as the UE drifts further from the BS. However, upon reaching an optimal range, the sustainable time initiates its descent. This optimal range, which yields the maximum sustainable link time, consistently hovers around an initial distance of 300-400 meters between UE and BS for all mobility models.

Equation (3.29) shows that the performance depends on two primary parameters, namely angle (θ) and path loss (lp), which depend on the UE's final distance from the BS. In order to find out the impact of the UE's initial distance from BS (l) on both these parameters, all other values are assumed to be fixed. Then from (3.25) and (3.26), the following equation is obtained:

$$x_2 = l + dc_1 \tag{3.38}$$

Assuming $x_1 = l$, cos(ϕ)=c_1 and l is the initial distance between the UE and BS y_2 is calculated as:

$$y_2 = \frac{d}{c_1} \tag{3.39}$$

Using (3.27), (3.38) and (3.39), the distance between UE's final location and BS is expressed as

$$L_{Final} = \sqrt{l^2 + \frac{d^2}{c_1^2} + d^2 c_1^2 + 2dc_1 l} \tag{3.40}$$

The free space path loss is then derived as

$$\begin{aligned} L_p &= \left(\frac{4\pi df}{c}\right)^2 \\ &= \left(\frac{4\pi f}{c}\right)^2 (L_{Final})^2 \\ &= k\left(l^2 + \frac{d^2}{c_1^2} + d^2 c_1^2 + 2dc_1 l\right) \end{aligned} \tag{3.41}$$

The change in the path loss with respect to the change in l can be derived from the derivative of (3.41) as

$$\frac{dL_p}{dl} = k(2l + 2cd) \tag{3.42}$$

Equation (3.42) shows that the path loss increases as the UE's initial distance increases. So, when the users are far from the BS, the path loss plays a more dominant role on the sustainable link time. Now, the angle between the final UE location and BS θ can be calculated using

$$\theta = \cos^{-1}\left(\frac{l^2 + L_{\text{Final}}^2 - d^2}{2lL_{\text{Final}}}\right)$$

$$= \cos^{-1}\left(\frac{2l^2 + \frac{d^2}{c_1^2} + d^2c_1^2 + 2dc_1l - d^2}{2l\sqrt{l^2 + \frac{d^2}{c_1^2} + d^2c_1^2 + 2dc_1l}}\right)$$

$$= \cos^{-1}\left(f(g)\right) \tag{3.43}$$

where,

$$f(g) \triangleq \frac{2l^2 + \frac{d^2}{c_1^2} + d^2c_1^2 + 2ldc_1 - d^2}{2l\sqrt{l^2 + \frac{d^2}{c_1^2} + d^2c_1^2 + 2ldc_1}} \tag{3.44}$$

Equation (3.45) is obtained by differentiating $f(g)$ with respect to l.

$$f'(g) = \frac{4l + 2dc_1}{2l\sqrt{l^2 + \frac{d^2}{c_1^2} + d^2c_1^2 + 2dc_1l}} - \frac{2l^2 - d^2 + \frac{d^2}{c_1^2} + d^2c_1^2 + 2dc_1l}{2l^2\sqrt{l^2 + \frac{d^2}{c_1^2} + d^2c_1^2 + 2dc_1l}}$$

$$- \frac{(2j + 2dc_1)\left(2l^2 - d^2 + \frac{d^2}{c_1^2} + d^2c_1^2 + 2dc_1l\right)}{4l\left(l^2 + \frac{d^2}{c_1^2} + d^2c^2 + 2dc_1l\right)^3/2} \tag{3.45}$$

Finally, differentiating θ with respect to l yields

$$\frac{d\theta}{dl} = \frac{-f'(g)}{\sqrt{1 - f(g)^2}} \tag{3.46}$$

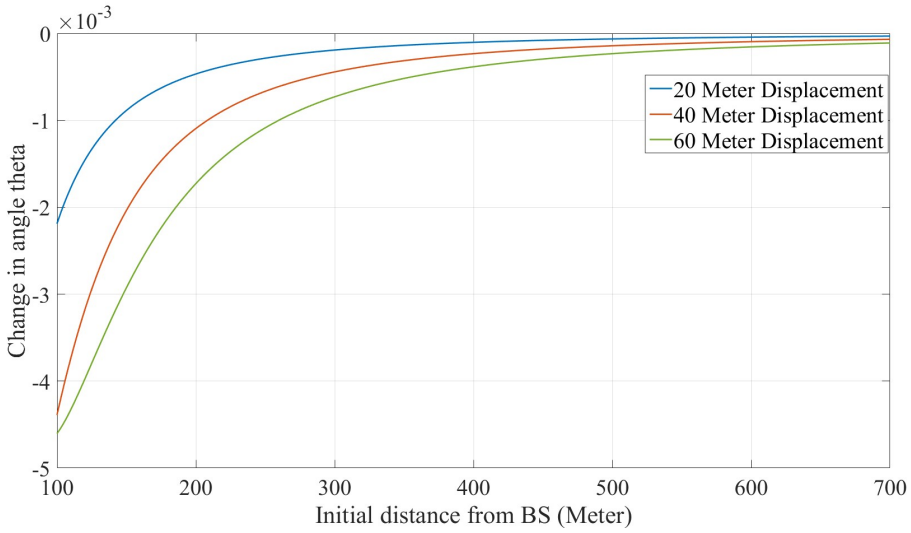

FIGURE 3.20: Initial distance *vs* rate of change in θ

Equation (3.46) presents the influence of l on the variation in θ. The simulation outcome of (3.46) is depicted in Figure 3.20. This figure indicates that the variation in θ is inversely proportional to l. As l continues to escalate, a diminished θ is observed for an identical user movement. Interestingly, for various displacement values, a consistent pattern emerges. In each of the three cases presented, the results seem to stabilize around a range of $300 - 400$ meters. Such a trend implies that when l is minimal, θ significantly impacts the UE received SNR. Conversely, as l grows, path loss becomes the overriding determinant. This phenomenon accounts for the wave-like performance observed in Figure 3.17, 3.18, and 3.19.

Figure 3.21, 3.22, and 3.23 illustrate the influence of transmission beamwidths on the sustainable link time for three distinct initial UE positions. Consistent with previous results, the optimal performance is achieved at 400 meters across all mobility groups. Furthermore, performance appears to enhance with increasing transmission beamwidth, offering an enlarged transmission area for users. Nevertheless, as the transmission beamwidth continues to grow, the increase in sustainable link time does not remain consistent across all scenarios. For an initial position of 200 meters, there is a more pronounced rise in sustainable link time at larger beamwidths, as evidenced by the steep ascent of the blue line after 40 degrees in Figure 3.21 and 3.22,

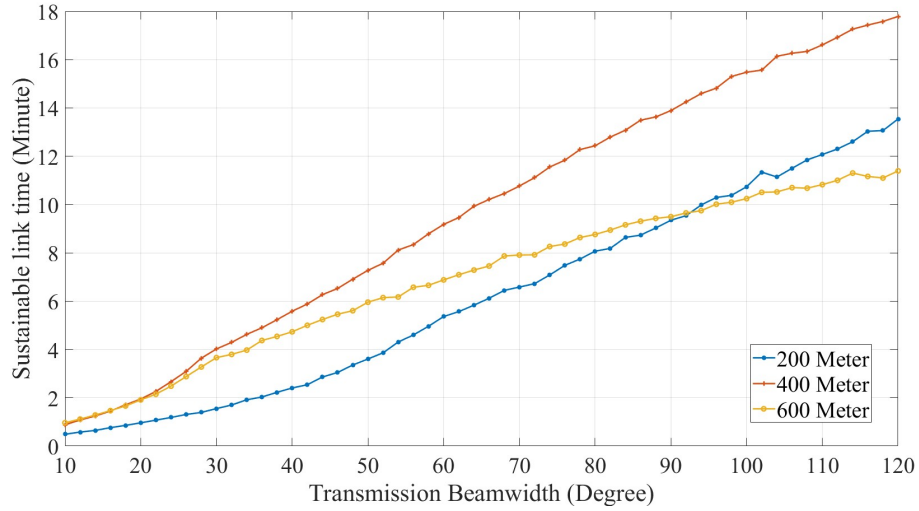

FIGURE 3.21: Impact of transmit beamwidth on link sustainability for Random waypoint mobility model

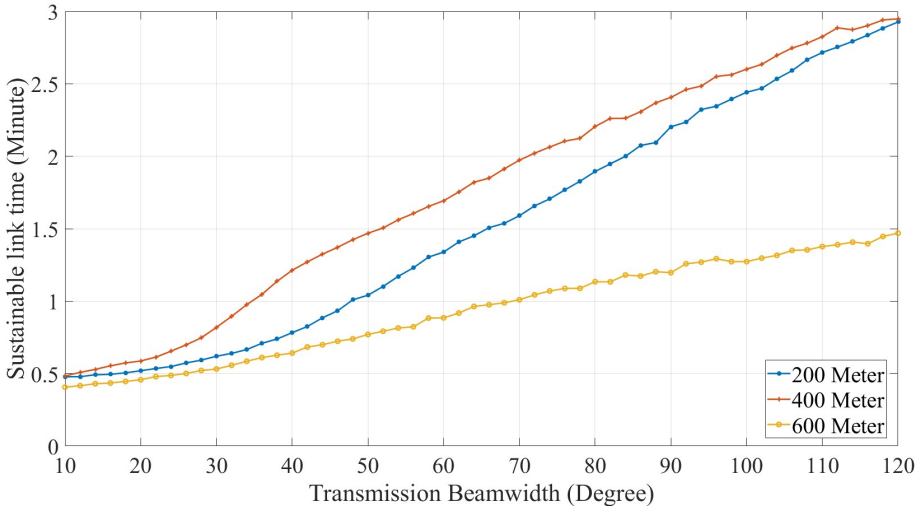

FIGURE 3.22: Impact of transmit beamwidth on link sustainability for Manhattan mobility model

and a lesser incline in Figure 3.23. Conversely, at a 600 meters starting point, an inverse trend is observed: the gain in performance diminishes with further widening of the beamwidth. This behavior results in intersections between the blue and yellow lines in Figure 3.21 and 3.23, while in other figures the blue line nearly matches the performance of the red line. These observations are consistent with the patterns identified in Figure 3.20, where minimal variation in θ is noticed beyond 400 meters, even with increasing l. Such insights are invaluable for designing MIMO beamforming for LDM transmission. Employing a broader beam transmission is more suitable when the UE is proximal to the BS. In contrast, as the UE recedes, a more narrow

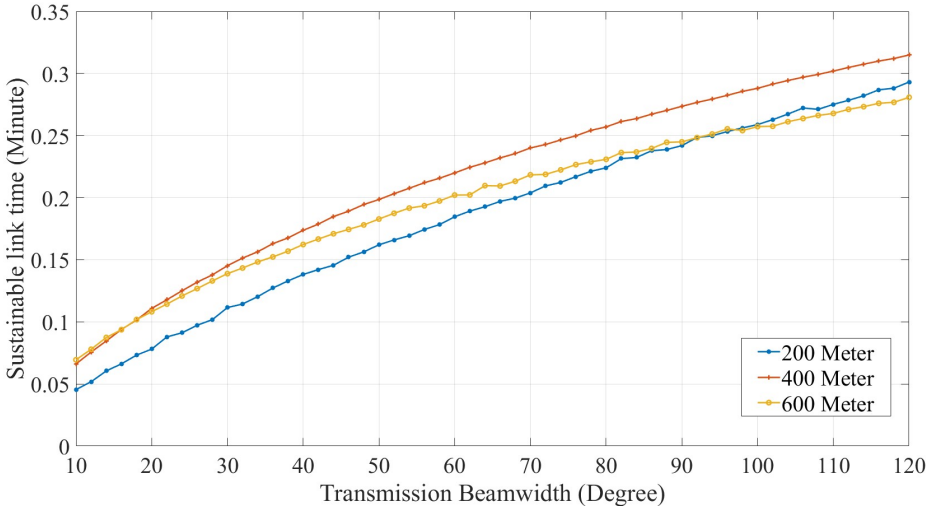

FIGURE 3.23: Impact of transmit beamwidth on link sustainability for Freeway mobility model

beam can be employed.

3.7.2 Impact of Singular & Combined Mobility on Link Time

The impact of both singular and combined mobility is evaluated from the developed model. The performance of the LDM pair was assessed in terms of link sustainability across various mobility models and transmission beamwidth combinations.

In the first scenario, the UE is assumed to remain static, while the IoT device exhibits mobility. The x position of the IoT devices spans from 0 to 500 meters and is selected randomly during each iteration. The range of the y position is computed using the given transmission beamwidth, the value of x, and the (3.37).

For the second scenario, a similar simulation is executed for the movement of the UE, under the assumption that the transmission angle is determined based on the initial position of the UE. Additionally, in the final setup, both the IoT and UE were concurrently moved to evaluate the sustainable link duration.

The random way-point and Manhattan models were also integrated to evaluate the link sustainability. Such comparisons will enable the system to form LDM pairs with greater efficiency, contingent upon the mobility category of the receivers. Notably, both models are indicative of urban environments, while the Freeway mobility model caters to motorway movement.

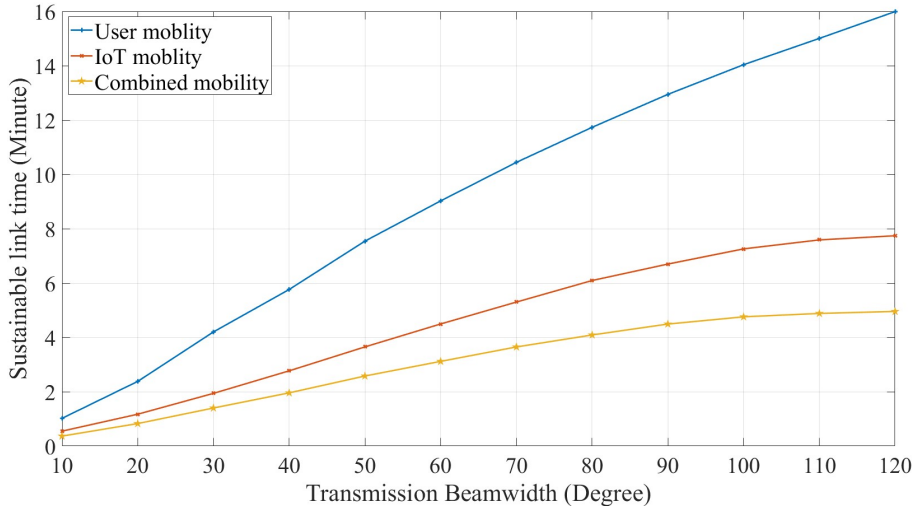

FIGURE 3.24: Singular and combined mobility *vs* link time for Random waypoint mobility model

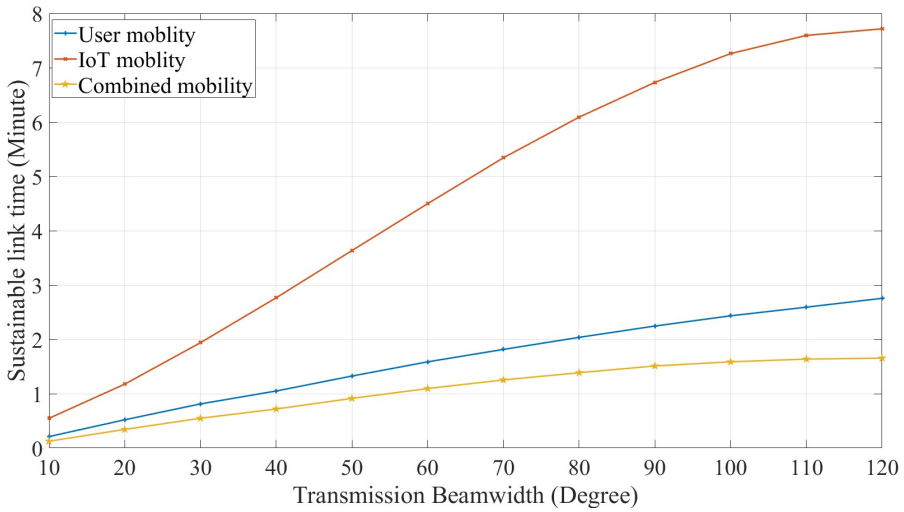

FIGURE 3.25: Singular and combined mobility *vs* link time for Random waypoint (IoT) and Manhattan (UE) mobility models

In both Figure 3.24 and 3.25, the IoT devices move according to the random waypoint mobility model, while the mobility model for users is varied. In Figure 3.24, both IoT and UE devices belong to the same mobility group. User mobility exerts a minimal impact on pair sustainability since UE initial position is at the centre of transmit beam. The IoT devices exit the transmission area more frequently. There exist scenarios where the initial position of the IoT devices is at the network's edge, leading to a quicker termination of the LDM pair. The cumulative results exhibit a trend akin to the IoT mobility, and as anticipated, the combined mobility yields a reduced sustainable link duration. In Figure 3.25, the UE operates on a more dynamic

mobility model and thus performs inferiorly to the IoT. A similar pattern emerges in this instance as well, where the combined mobility results in shorter durations than the UE mobility. Based on these findings, it is evident that optimum pairing would involve IoT devices and users from the same mobility group. If not, the system would need to identify a new device for pairing once one of the paired devices ventures out of the effective range.

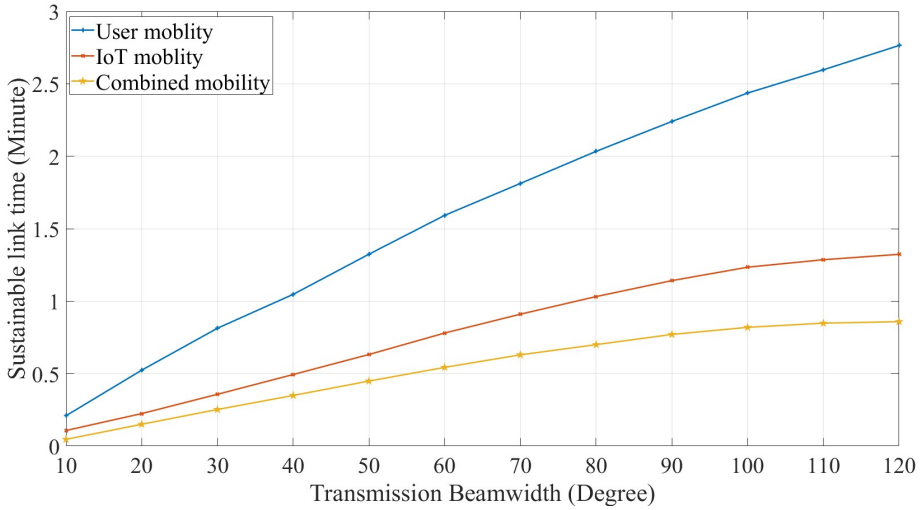

FIGURE 3.26: Singular and combined mobility *vs* link time for Manhattan mobility model

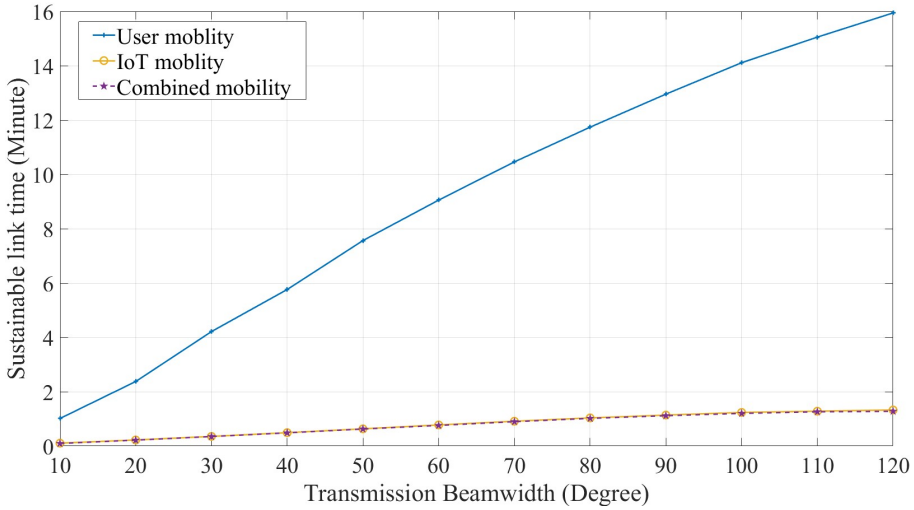

FIGURE 3.27: Singular and combined mobility *vs* link time for Manhattan (IoT) and Random waypoint (UE) mobility models

In both Figure 3.26 and 3.27, the Manhattan mobility model governs the movement of the IoT devices, while different mobility models dictate the motion of the

UE. In Figure 3.26, akin to the scenario involving the random way-point mobility model, the UE remains within the transmission area for a notably extended duration. With a 120 degree transmission angle, the UE mobility yields nearly double the link sustainability time compared to the IoT mobility. Figure 3.27, however, presents a similar set of outcomes with a notable exception. Contrary to the other results, the combined mobility closely matches the IoT mobility in this case. This pattern emerges due to the discrepancy in the link sustainability time between UE and IoT mobility. Given that the UE mobility offers a much lengthier sustainable link duration, the pairing typically needs termination owing to the IoT device's network constraints. Such observations can guide the BS to monitor the condition of one device more frequently, depending on their mobility model, thereby reducing computational burdens and enhancing overall efficiency.

TABLE 3.3: Summary of link sustainability for all mobility models

Mobility Model	IoT	User	Both	Ratio IoT	Ratio User
Random Waypoint	4.49	9.02	3.1	0.69	0.34
Random Waypoint-Manhattan	4.49	1.58	1.09	0.24	0.68
Manhattan	0.78	1.59	0.54	0.7	0.34
Manhattan-Random Waypoint	0.77	9.05	0.76	0.98	0.08
Freeway	0.15	0.21	0.1	0.64	0.46

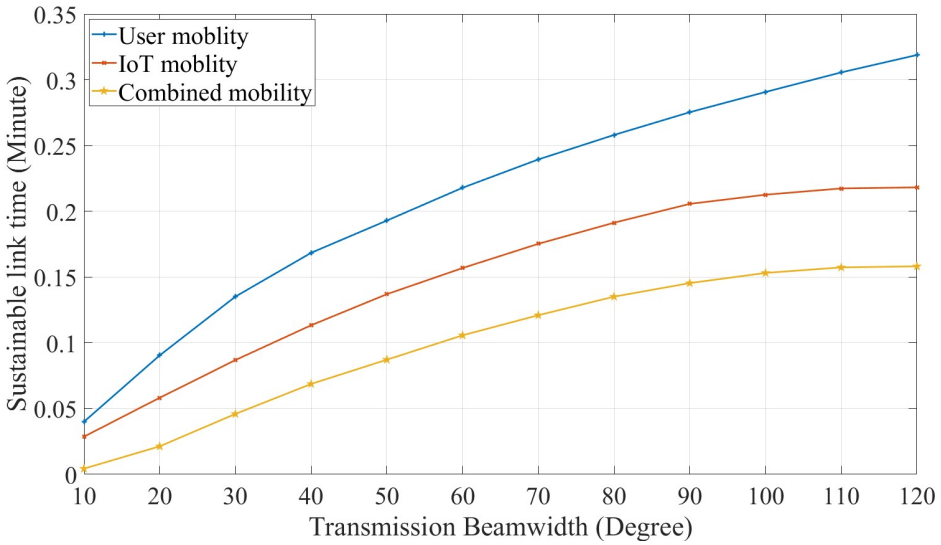

FIGURE 3.28: Singular and combined mobility *vs* link time for Freeway mobility model

In Figure 3.28, both the IoT device and UE follow the freeway mobility model.

With both devices moving at higher speeds, the sustainable time is significantly reduced compared to the urban scenarios. However, the disparity in performance between IoT and UE devices is narrower in this context. For future work, other technologies like beam-following might be employed to enhance performance, especially since the movement is unidirectional and predictable. Table 3.3 presents a comparison of link sustainability at a 60 degree transmission angle across all five transmission scenarios. When both devices belong to the same mobility group, IoT devices tend to exit the range before the UE. The table indicates that, if the disparity between UE and IoT sustainability becomes too vast, the gap between IoT and combined mobility performance narrows. This understanding of established patterns can guide the BS during LDM pairing, leading to the formation of more efficient IoT-UE LDM pairs, potentially enhancing LDM performance in upcoming wireless networks.

3.8 Summary

3.8.1 Contributions

The chapter provides a thorough analysis of the LDM-OFDM system model, demonstrating its effectiveness for IoT and UE. Key highlights include the alignment of analytical models with simulations across different QAM orders, validating the model's reliability in evaluating the LDM CL's performance. The chapter also delves into the surface positioning model for tracking receiver movement and optimizing performance based on QAM orders and SNR values. An adaptive PA algorithm is introduced, enhancing unicast service delivery and enabling the BS to make informed decisions about the LDM pair termination. The model's adaptability is further showcased in capturing essential parameters for IoT mobility.

3.8.2 Limitations

Despite its strengths, the model has several limitations. The analytical model primarily focuses on the CL and its interference with the LL, with a fixed PA for the LL,

suggesting the need for a more versatile approach. The model's current channel representation is basic and does not include specific environments like urban or rural settings, nor does it account for multi-antenna propagation. Additionally, the mobility model does not align with the latest 3GPP guidelines, lacking considerations for LoS/NLoS and multipath count in various environments. The PA algorithm, mainly centred on the EL layer channel condition, indicates a requirement for a broader approach, especially for multi-layer deployments.

3.8.3 Future Work

The subsequent chapter, Chapter 4, will address these limitations and explore enhancements. It will focus on developing a comprehensive N-NOMA aided 5G physical model, coupled with a more robust BER analytical model for N-NOMA that incorporates interference from both ULs and LLs. Future investigations will also consider advanced physical layer techniques like channel coding and MIMO precoding. Moreover, the next chapter, Chapter 5, aims to integrate feedback-driven PA and adapt the model to encompass various environmental conditions, enhancing the model's robustness and applicability to diverse scenarios.

Chapter 4

Design & Evaluation of N-NOMA on NR Physical Layer for 5G & Beyond

4.1 Introduction

This chapter delves into the integration of N-NOMA into a 5G NR compliant transceiver model, aiming to reveal the full potential of the NOMA technology in practical scenarios. An N-NOMA-aided 5G NR physical layer design is proposed, where a simplified N-NOMA multiplexer with a one-shot multiplexing technique is developed to reduce transmitter complexity and potential delay for processing the additional NOMA layers. This design offers a new perspective for the NOMA technology to address various challenging use cases, such as mMTC and Enhanced Mobile Broadband (eMBB) under low SNR regimes. Then, in order to provide a comprehensive error performance evaluation of the proposed N-NOMA physical layer design, various system configurations, e.g., different Modulation and Coding Schemes (MCSs) with LDPC code and different MIMO settings are taken into account. During the evaluation of the proposed design, some key factors missing from the existing BER analytical models in the literature is identified, e.g., the imperfect SIC. The derived BER expressions capture the effect of the SIC errors, which is consistent in the developed analytical and simulation performance comparison. Through the simulation, the link-level performance of the proposed physical layer design is comprehensively evaluated and discussed.

Over time, extensive literature [14–17, 158, 159] has developed on exploring the intricate nature of the NOMA-based transmitter and the effect of variable channel conditions on system performance, which motivates to consider a new transceiver design, incorporating a series of NOMA functionalities to a 5G NR-complaint physical layer to enable heterogeneous services over a common channel. The authors of [160] combined spatial modulation with MIMO and LDM, suggesting that increasing the MIMO order could potentially enhance the delivery of broadcast/multicast services. However, the model does not incorporate key elements such as LDPC forward error correction and practical MIMO channel modelling. In [83] it suggested that using low-rate LDPC codes in the UL improves the overall performance and achieves higher transmission efficiency. Motivated by these research gaps, this study consider a practically novel transceiver model, incorporating a series of NOMA functionalities for heterogeneous services to a 5G NR-complaint physical layer, including MIMO precoding and LDPC coding, with TDL or CDL channel model. The proposed NOMA physical layer processing chain follows the structure of LDM, extracted from the 2 layer LDM-OFDM structure from Chapter 3. Critical NOMA techniques for incorporation and integration is also considered, including symbol rate synchronisation by aligning signals and optimal placement of NOMA physical layer processing functions in the 5G transceiver chain, to reduce latency and complexity.

While the two data layers LDM or NOMA structure remains limited capacity to support services such as mMTC and eMBB with massive concurrent users, (N-NOMA) (> 2) can play a significant role here to enhance system capacity [83]. In recent work, Kim *et al.* [83] explored the potential of a time-shared 3-layer LDM system for ATSC 3.0, and tested various multi-layer systems and investigated their capacity enhancement potential. The time-shared 3-layer NOMA is a way to provide 3 services using a 2-layer LDM design where the LL is shared between two services due to the performance degradation and complexity associated with vertical integration. However, the integration of N-NOMA, e.g., more than 2 layers, will introduce severe challenges to the practical system, e.g., the requirement of high transmission power and the increased complexity of the transceiver design. As demonstrated in [30, 82], adding more NOMA layers, while possible, the minimum

SNR requirement increases, which is challenging in practical scenarios, particularly if the microWave/mmWave spectrum is used. Compared to previous generations, 5G NR physical layer performance at low SNR regimes offers a higher QoS owed to the inclusion of technical enablers such as LDPC and MIMO. It is of great interests to see if a combination of NOMA and NR technologies can reduce the minimum SNR requirements when adding new layers. On the other hand, the work in [12] showed that the complexity at the transmitter side arises from data processing, NOMA multiplexing, PA, and user grouping. The main issues at the receiver side are the multiple SIC operations $(n-1)$ SIC operation for the nth data layer) and maintaining the minimum SNR levels for successful signal detection [161]. Resource allocation in N-NOMA transmission is a complex problem concerning PA and user pairing as data layers increase [59, 162, 163].

The motivation is not only to explore the feasibility of N-NOMA in conjunction with 5G NR technical enablers, but also potentially address some key implementation issues of the N-NOMA-aided physical layer. For example, one of the drawbacks of including more NOMA layers in a standard sequential combiner is the added complexity of the additional signal processing functions [83]. This chapter presents the design of a one-shot technique that multiplexes all NOMA layers using a single function. Another example is that, during the SIC operation, an imperfect detection of higher layer data can add interference to the LL signal. This important parameter has not been considered in the previous BER analytical models, leading to an overoptimistic estimation of error. As the scale of the NOMA order increase, the estimation becomes even more deflated with the SIC operation in the system. An accurate BER analysis, essential for validating NOMA architectures in practice, should incorporate the impact of SIC into the error modelling, e.g., considering both residual and non-residual errors in case of the perfect or imperfect SIC, respectively. In [164], a closed form BER was derived for NOMA with receiver diversity for several modulation orders. However, the authors did not capture the impact of SIC in their proposed solution, and they assumed a single antenna transmission which has certain limitations in 5G. The authors in [162] derived a theoretical BER expression for N-NOMA-QAM with equal power distribution between data layers. However,

they did not considered OFDM or MIMO processing in their expression. Furthermore, although they explored SIC operation for the BER performance, they did not quantify the additional interference caused by the imperfect SIC, or as defined in this study, non residual errors. With the above in perspective, the aim is to derive a closed-form BER analytical expression by accounting for both residual and non-residual errors from SIC at the receiver, incorporating MIMO gain, using TDL/CDL model and thus expanding its scope. The method used to determine the error probability is based on the Q function estimation. In this context, an uncoded OFDM system is assumed, along with Gaussian distributed interference for both residual and non-residual errors.

The structure of the remainder of this chapter is as follows: Section 4.2 proposes a system model incorporating a 2-layer NOMA-aided 5G physical layer and a transceiver model. This model is extended in Section 4.3 into an N-NOMA transceiver model, allowing the transmission of over 2 data layers using a single traffic channel. This model is further simplified to reduce latency and complexity. Section 4.4 presents a closed-form BER expression to determine the maximum error for any layer of data in N-NOMA transmission. The results of the proposed system and analytical models are presented and evaluated in Section 4.5. Finally, Section 4.6 summarizes findings and future works.

4.2 5G Transceiver Framework Incorporating 2-Layer NOMA

A 2-layer NOMA system, demonstrating the proposed modular physical layer design, has been developed. This design integrates NOMA-aided transceiver blocks into the standard 5G NR-compliant downlink data transmission model, as outlined in 3GPP TR 38.901 [138]. As illustrated in Figure 4.1, besides the standardized transceiver blocks such as LDPC-based encoding and OFDM modulation, the model also combines NOMA multiplexing and SIC, MIMO precoding and CDL/TDL channel models, among other functions.

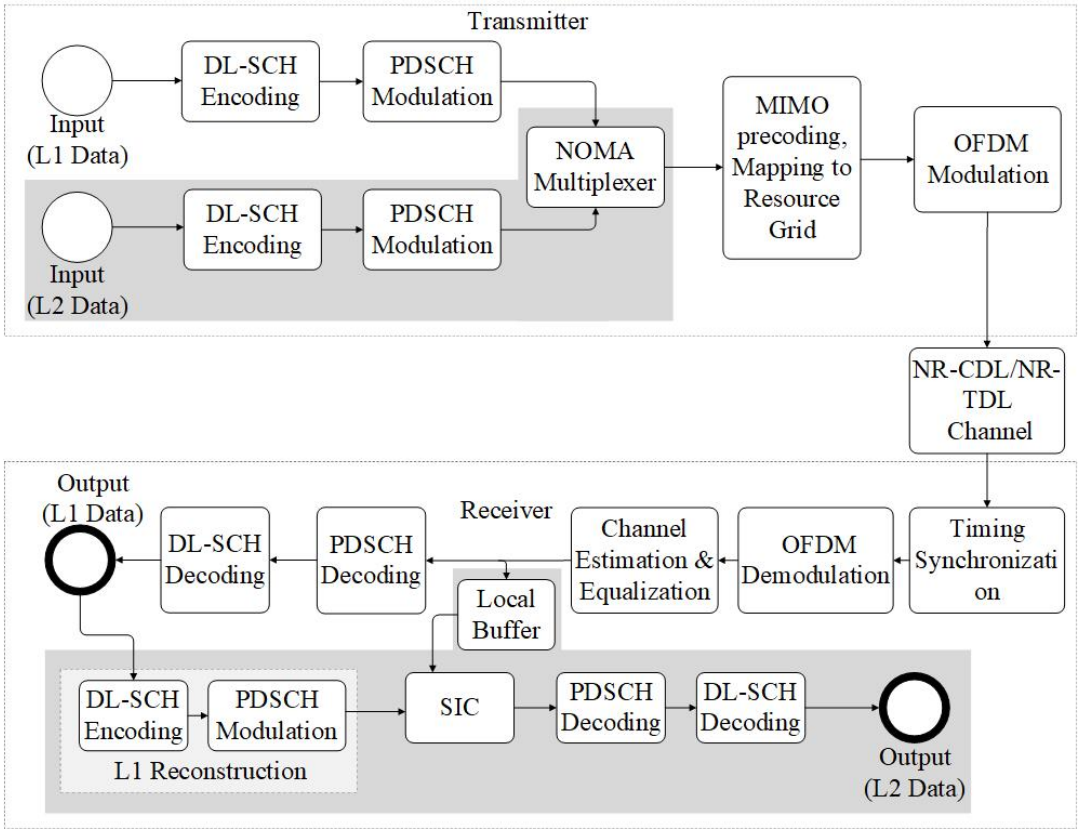

FIGURE 4.1: Illustrates a 5G transceiver model integrating a 2-layer NOMA scheme. The shaded areas denote proposed modifications for NOMA integration, while the remaining components adhere to the standard 3GPP 5G transceiver model.

4.2.1 Transmitter Design

5G NR downlink transmitter commonly has the data input (in binary bits) in the physical layer intended for single-user cases. The design considers multi-user cases, e.g., with the data streams for two users separated into two data layers (e.g., L1 and L2) using NOMA multiplexing, which is merged with the standard data processing chain to combine and transmit data blocks for two independent users using a single traffic channel.

Since the processing of individual data blocks can be parallelly executed before multiplexing, the only added latency in the transmitter side is the time required for NOMA integration. The multiplexing can be achieved on a bit or symbol level, while for both data layers the length of the processed bit/symbol needs to be identical to carry out this operation. As such, the challenges of this design are: 1) synchronizing the bit/symbol rate of both layers before multiplexing and 2) determining the

optimum position of the NOMA multiplexer in the transmitter chain.

Recall in our system description that two input sources defined as L1 data and L2 data, which can be expressed as:

$$\mathbf{x}_{l1} = (x_{l1,1}, \cdots, x_{l1,n_{l1}}) \tag{4.1}$$

$$\mathbf{x}_{l2} = (x_{l2,1}, \cdots, x_{l2,n_{l2}}) \tag{4.2}$$

where $x_{l1,i}, x_{l2,i} \in \{0,1\}, \forall i$, and n_{l1}, n_{l2} represent the total number of L1 and L2 bits to be transmitted, respectively. To effectively synchronize the symbol rate for transmission, n_{l1} and n_{l2} are derived based on the OFDM transmission symbol rate n_s, which is the number of data symbols in each frame, and the respective coding rates ρ_{l1}, ρ_{l2}, and bits per modulated symbol, m_{l1}, m_{l2}, determined by the modulation order (M) by $m = \log_2 M$. The bit rate of both layers is calculated using the following expressions:

$$n_{l1} = n_s \cdot \rho_{l1} \cdot m_{l1} \tag{4.3}$$

$$n_{l2} = n_s \cdot \rho_{l2} \cdot m_{l2} \tag{4.4}$$

Both layers of data are first processed through the DL-SCH Encoding block, where $\mathbf{x}_{l1}$ and $\mathbf{x}_{l2}$ are encoded according to the coding rates, ρ_{l1} and ρ_{l2}. The DL-SCH block uses LDPC error-correcting encoding, in line with 3GPP TR 38.901 Release 16 [138]. The output of the DL-SCH block can be expressed as follows:

$$\mathbf{x}_{dl1} = (x_{dl1,1}, \cdots, x_{dl1,n_{dl1}}) \tag{4.5}$$

$$\mathbf{x}_{dl2} = (x_{dl2,1}, \cdots, x_{dl2,n_{dl2}}) \tag{4.6}$$

where the size $n_d = (n/\rho)$ for both UL and LL. Next, $\mathbf{x}_{dl1}$ and $\mathbf{x}_{dl2}$ are modulated into QPSK or QAM symbols as per PDSCH block. The output is in the following

format:

$$\mathbf{s}_{l1} = (s_{l1,1}, \cdots, s_{l1,n_s}) \tag{4.7}$$

$$\mathbf{s}_{l2} = (s_{l2,1}, \cdots, s_{l2,n_s}) \tag{4.8}$$

where $s_{l1,i}, s_{l2,i} \in \{s_1, s_2, \cdots, s_M\}$, $\forall$ M_{l1} and M_{l2}.

Data integration into the NOMA signal could occur at multiple stages within the 5G transmitter framework, leading to varying degrees of complexity and latency. As both data layers undergo simultaneous processing until they reach the point of multiplexing, implementing a bit-level NOMA multiplexer reduces the total count of operational blocks within the transmitter, decreasing the overall computational complexity. Conversely, symbol-level NOMA multiplexing allows the system to assign different bit rates to each layer, where symbols are synchronized using varying code rates ρ and modulation orders M. Furthermore, the placement of the NOMA integration block within the transmitter also determines the location of SIC at the receiver and the number of additional blocks required for L1 reconstruction. This factor is crucial in determining the overall latency at the L2 signal detection.

In [15], a symbol level 2-Layer NOMA integration was implemented within a simplified 5G transceiver model, incorporating a HARQ. Similarly, [165] designed a low complexity LDM-enabled transceiver model for ATSC 3.0, also applying symbol level integration. In line with these studies, the NOMA integration block is positioned after the PDSCH block, representing the earliest data symbol form in the 5G physical layer as per 3GPP TR 38.901 [138]. This design approach offers the benefit of individual coding rates ρ and modulation orders M to perform synchronised symbol rates, enabling transmission of different bit rates for each layer while minimizing latency. In a sense, this is the optimum position for NOMA multiplexer block.

The symbols from both layers are multiplexed together using the following relation:

$$s_{NOMA,i} = s_{l1,i} + g \cdot s_{l2,i} \tag{4.9}$$

$s_{l1,i}$ and $s_{l2,i}$ are ith L1, L2 QAM symbols, and $s_{NOMA,i}$ is the ith NOMA multiplexed symbol. The combined data $\mathbf{x}_{NOMA}$ can be expressed as:

$$\mathbf{x}_{NOMA} = (s_{NOMA,1}, \cdots, s_{NOMA,n_s}) \tag{4.10}$$

Assuming the transmitter is equipped with a uniform linear array pattern of n_t antennas each have 0 dBi gain, and its precoding vector is in the form of:

$$\mathbf{p}_w = (w_1, \cdots, w_{n_t}) \tag{4.11}$$

$\mathbf{x}_{NOMA}$ is then multiplied with $\mathbf{p}_w$ to spread the data according to the precoding weight as:

$$\mathbf{X}_{pre} = \mathbf{x}_{NOMA}^T \times \mathbf{p}_w \tag{4.12}$$

The matrix that represents the preceded signal from (4.12) can be expressed as follows:

$$\mathbf{X}_{pre} = \begin{bmatrix} s_{p,11} & s_{p,12} & \dots & s_{p,1n_s} \\ s_{p,21} & s_{p,22} & \dots & s_{p,2n_s} \\ \vdots & \vdots & \ddots & \vdots \\ s_{p,n_t1} & s_{p,n_t2} & \dots & s_{p,n_tn_s} \end{bmatrix} \tag{4.13}$$

These signals are then mapped into the resource grid and converted to OFDM-modulated signals using a series of signal processing blocks (e.g., IFFT, DAC), ready for radio transmission. The OFDM symbol matrix $\mathbf{X}$ can be expressed as:

$$\mathbf{X} = \begin{bmatrix} s_{o,11} & s_{o,12} & \cdots & s_{o,1n_o} \\ s_{o,21} & s_{o,22} & \cdots & s_{o,2n_o} \\ \vdots & \vdots & \ddots & \vdots \\ s_{o,n_t1} & s_{o,n_t2} & \cdots & s_{o,n_tn_o} \end{bmatrix} \tag{4.14}$$

where the index

$$n_o = \frac{\text{Sampling Rate}}{\text{Non-Uniform Fast Fourier Transform (NFFT) size}} \tag{4.15}$$

is the frequency resolution in Hz.

4.2.2 Channel Model

The most accepted 5G channel models between a transmitter and a receiver with MIMO and mMIMO transmissions are TDL and CDL models, respectively, as set by the ETSI TR 138 900 V14.2.0. Both of these channel models are considered in the system model.

TDL Channel Model

The TDL channel models are defined for a total frequency range from 0.5 to 100 GHz with a maximum bandwidth of 2 GHz. TDL model is useful in MIMO systems because it captures the effects of multipath propagation, and these channel models are categorized into TDL-A, TDL-B, and TDL-C to represent different NLoS channel profiles and TDL-D and TDL-E for LoS channel profile. The channel impulse response of a TDL channel, $h(t, \tau) \in \mathbb{C}$, for N_{tap} number of taps is given by [166]

$$h(t,\tau) = \sum_{k=1}^{N_{tap}} a_k(t) \;\; \delta(\tau - \tau_k) \tag{4.16}$$

where $a_k(t)$ is $\alpha(t)e^{(-j2\pi f_c t)}$ with τ_k delay and $\delta(\tau - \tau_k)$ is the Dirac delta function representing all signals with τ_k delay [166].

CDL Channel Model

The CDL models are defined for the same frequency range and maximum bandwidth and are more suitable for representing MIMO transmission with beamforming. Similarly, CDL-A, CDL-B and CDL-C represent the NLoS channel models, whereas CDL-D and CDL-E are used to represent the LoS channel models. Each CDL model can be scaled in delay and angles to achieve the desired RMS delay spread and angle spreads. The channel impulse response of the CDL channel is described in [167]

$$H_{u,s}(t,\tau) = \sum_{n=1}^{N} \sum_{m=1}^{M} \left(a_{u,s,n,m} \sqrt{\frac{P_n}{M}} \, \delta(\tau - \tau_n) \right) \tag{4.17}$$

where u is the antenna element index of the receiver, s is the antenna element index of the transmitter, N is the number of clusters between BS and UE, and M is the number of rays within each cluster. The gain coefficient $a_{u,s,n,m}$ is calculated as:

$$a_{u,s,n,m} = \mathbf{f_{UE}}_{,u,n,m} \; \mathbf{f_{BS}}_{,s,n,m} \tag{4.18}$$

where $\mathbf{f_{UE}}_{,u,n,m}$ and $\mathbf{f_{BS}}_{,s,n,m}$ denote the antenna gains of the antenna elements u and s in the UE and BS, respectively.

The channel correlation matrix $\mathbf{H}$ between n_o transmission paths and n_r received antenna can be written as:

$$\mathbf{H} = \begin{bmatrix} h_{11} & h_{12} & \dots & h_{1n_o} \\ h_{21} & h_{22} & \dots & h_{2n_o} \\ \vdots & \vdots & \ddots & \vdots \\ h_{n_r1} & h_{n_r2} & \dots & h_{n_rn_o} \end{bmatrix} \tag{4.19}$$

Each element of **H** combines signals of transmit antenna element using (4.16), indicating how related the signals received at different antennas.

4.2.3 Receiver Design

The radio signal is received by n_r antenna elements, and the linear channel model **Y** can be defined as:

$$\mathbf{Y} = \mathbf{H} \times \mathbf{X} + \mathbf{N} \tag{4.20}$$

where **N** is the zero-mean variance-σ^2 AWGN. The observation matrix **Y** is expressed as

$$\mathbf{Y} = \begin{bmatrix} s_{r,11} & s_{r,12} & \dots & s_{r,1n_o} \\ s_{r,21} & s_{r,22} & \dots & s_{r,2n_o} \\ \vdots & \vdots & \ddots & \vdots \\ s_{r,n_r1} & s_{r,n_r2} & \dots & s_{r,n_rn_0} \end{bmatrix} \tag{4.21}$$

The receiver first applies a path filter to the received signal **Y**, synchronizing the time and mitigating the effects of varying path delays of **H**. Following channel equalization, the signal then proceeds to OFDM demodulation, passing through a channel filter to reduce noise and path gain. To extract NOMA symbols $\mathbf{y}_{NOMA}$ as a vector from **Y**, the received signal is processed through timing synchronization, OFDM demodulation, channel estimation and equalization blocks, sequentially. The output

from the channel estimation and equalization blocks $\mathbf{y}_{NOMA}$, is given by:

$$\mathbf{y}_{NOMA} = (s_{r,1}, \cdots, s_{r,n_s}) \tag{4.22}$$

The L1 and L2 data are required to be extracted from the received NOMA symbols $\mathbf{y}_{NOMA}$. Unlike the transmitter chain, the receiver can not process both data layers in parallel due to the SIC operation, which requires the L1 data to be detected first. To perform the SIC, the L1 data is detected from $\mathbf{y}_{NOMA}$, with the L2 data being treated as residual interference during this detection phase. Concurrently, $\mathbf{y}_{NOMA}$ is stored in a local buffer for L2 layer detection, which will subsequently be utilized for SIC during NOMA subtraction.

For the detection of L1, the $\mathbf{y}_{NOMA}$ undergoes processing via PDSCH demodulation (L1 layer) and produces encoded L1 bits as:

$$\mathbf{y}_{l1e} = (y_{l1e,1}, \cdots, y_{l1e,n_{dl1}}) \tag{4.23}$$

where $y_{l1e,i} \in \{0, 1\}\ \forall i$. The signal is then passed through the L1-DL-SCH decoder $(g_{e,l1})$, to remove channel coding and the received L1 data bits $\mathbf{y}_{l1}$ can be expressed as:

$$\begin{aligned} \mathbf{y}_{l1} &\leftarrow g_{e,l1}(\mathbf{y}l1e) \\ \mathbf{y}_{l1} &= (y_{l1,1}, \cdots, y_{l1,n_{l1}}) \end{aligned} \tag{4.24}$$

The received $\mathbf{y}_{l1}$ will be processed using the same DL-SCH and PDSCH encoding module used for L1 encoding at the transmitter. The reconstructed L1 layer symbols

$\mathbf{y}_{rl1}$ can be expressed as:

$$\mathbf{y}_{rl1} = (s_{rl1,1}, \cdots, s_{rl1,n_s}) \tag{4.25}$$

At this stage, both $\mathbf{y}_{NOMA}$ and $\mathbf{y}_{rl1}$ are input into the NOMA subtraction, which executes SIC by eliminating $\mathbf{y}_{rl1}$ from $\mathbf{y}_{NOMA}$. If the reconstructed symbol $s_{rl1,i}$ is different from the original L1 transmit symbol, then the SIC operation adds additional interference in the L2 symbols, which is defined as non-residual interference. The result of this SIC operation is subsequently multiplied by $(1/g)$ to compensate for the L2 power reduction implemented at the transmitter and given by:

$$\mathbf{y}_{l2s} = \frac{\mathbf{y}_{NOMA} - \mathbf{y}_{rl1}}{g} \tag{4.26}$$

The retrieved L2 symbols can be expressed as:

$$\mathbf{y}_{l2s} = (sl2_1, \cdots, sl2_{n_s}) \tag{4.27}$$

Now, $\mathbf{y}_{l2s}$ is demodulated using L2 PDSCH demodulation to extract encoded L2 bits, as

$$\mathbf{y}_{l2e} = (y_{l2e,1}, \cdots, y_{l2e,n_{dl2}}) \tag{4.28}$$

which will be processed by L2 DL-SCH decoder $(g_{e,l2})$, to remove channel coding bits and retrieve L2 data. The L2 received bits can be expressed as:

$$\mathbf{y}_{l2} \leftarrow g_{e,l2}(\mathbf{y}l2e)$$
$$\mathbf{y}_{l2} = (y_{l2,1}, \cdots, y_{l2,n_{l2}}) \tag{4.29}$$

4.3 5G Transceiver Framework Incorporating Multilayer NOMA

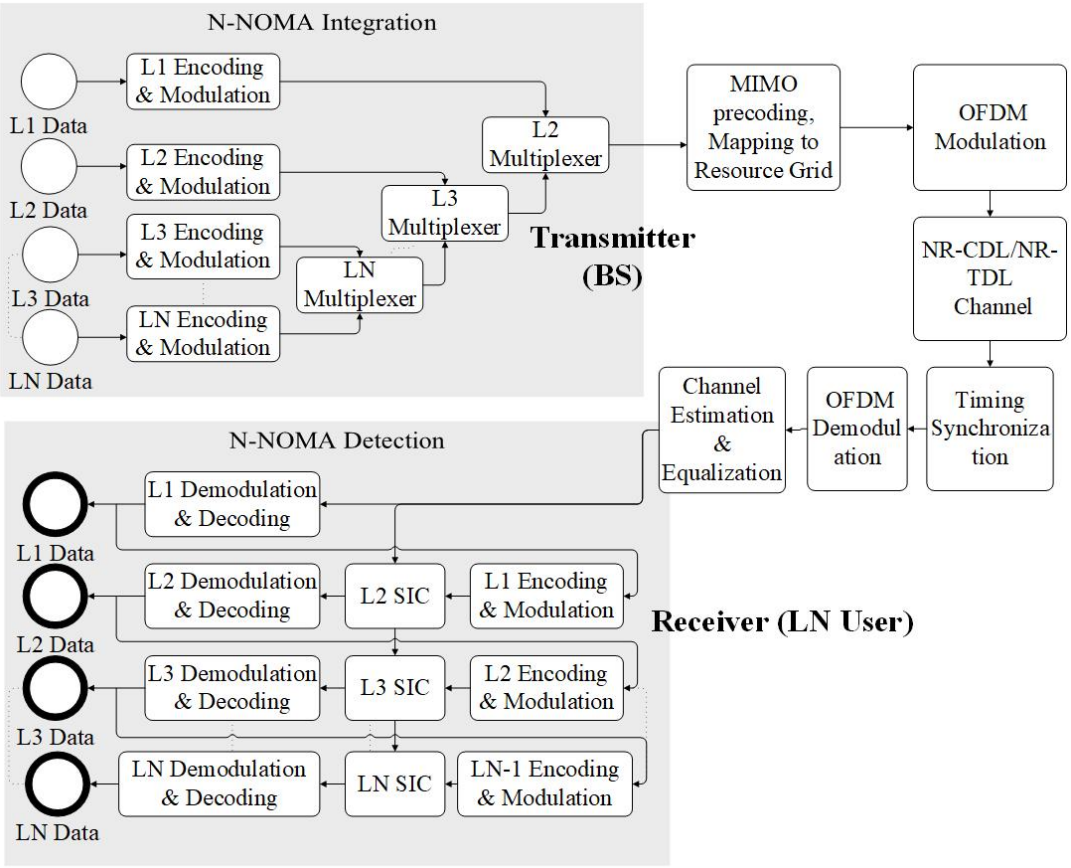

FIGURE 4.2: An extended 5G transceiver model, incorporating an N-NOMA scheme. The shaded areas denote the proposed modifications for N-NOMA integration, allowing for the multiplexing of N data layers. The remaining components adhere to the standard high-level 3GPP 5G transceiver model.

In this section, the system model is extend as shown in Figure 4.1 to incorporate N-NOMA as shown in Figure 4.2. In this design, the N-NOMA multiplexing uses the same sequential combiner used in [83]. The proposed system model integrates N data layers into a single channel using NOMA multiplexing. Therefore, the total

input for the system can be defined as a vector of size n_i for the uth data layer, represented as:

$$\mathbf{x}_u = (x_{u,1}, \cdots, x_{u,n_u}) \tag{4.30}$$

Each data layer is then processed according to its own DL-SCH and PDSCH configuration, as explained in Section 4.2. The processed data symbols for the uth data layer can be expressed as:

$$\mathbf{x}_{su} = (s_{u,1}, \ldots, s_{u,n_{su}}) \tag{4.31}$$

Figure 4.2 shows NOMA multiplexing using a sequential combiner technique, which multiplexes 2 lowest data layers, and then the combined signal is multiplexed with a third data layer, and so on. An N-NOMA transmission must execute $n-1$ multiplexing blocks following this technique. If the the power ratio between uth and $(u-1)$th data layer is g_u, then the combined NOMA symbols $\mathbf{x}_{NOMA}$ is expressed as:

$$\begin{aligned} \mathbf{x}_{NOMA} &= g_1(\mathbf{x}_{s1} + \ldots + g_{n-1}(\mathbf{x}_{sN-1} + g_n \mathbf{s}_N)) \\ &= \sum_{i=1}^{N} \left[\prod_{j=1}^{i} g_j \right] \mathbf{x}_{si} \end{aligned} \tag{4.32}$$

The NOMA signal can now be processed for transmission according to the 5G physical layer as described in the previous section.

Using a one-shot multiplexing technique, data symbols from all N layers can be seamlessly multiplexed, following (4.32). This one-shot multiplexer for N-NOMA

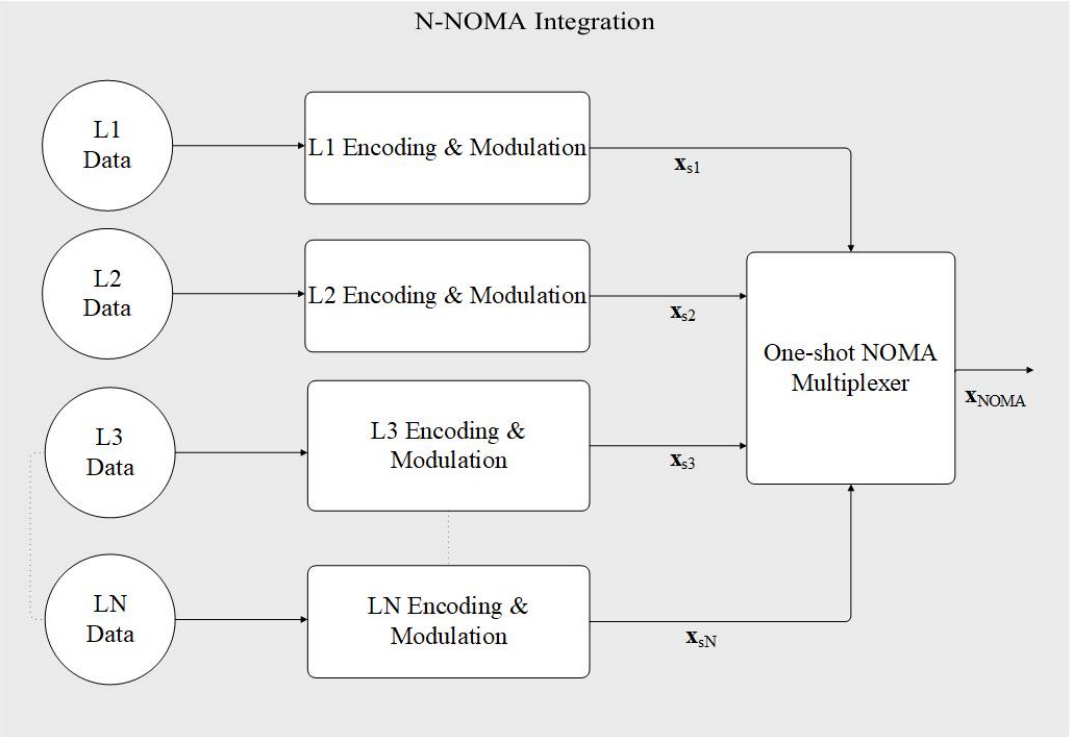

FIGURE 4.3: Depicts the one-shot N-NOMA integration in the 5G NR physical layer, demonstrating the multiplexing of all data layers in a single block

transmission is shown in Figure 4.3. To test the efficiency of this new multiplexer, the latency of both system is evaluated and compared in Figure 4.4. These findings indicate a substantial reduction in latency as additional data layers are incorporated into the system. For a 2-Layer system, the latency remains the same, as the process of 2-layer integration is identical in both systems. However, from three to higher layer multiplexing, the latency from the one-shot multiplexer is significantly lower than the sequential combiner multiplexer, as shown in Figure 4.4. The implemented code for the one-shot multiplexer is available in the GitHub repository (Appendix A-4).

From (4.32), the total power of the transmitted signal is the sum of powers from each data layer, as:

$$P_{total} = \sum_{u=1}^{N} \left[P_t \prod_{i=1}^{u} g_i \right] \tag{4.33}$$

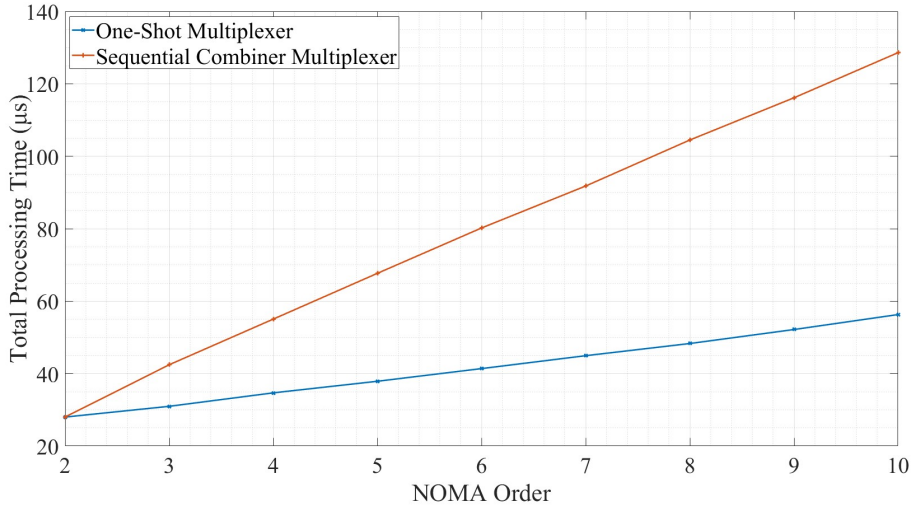

FIGURE 4.4: Latency comparison between the sequential combiner NOMA multiplexing and one-shot NOMA multiplexing, emphasizing the efficiency of the latter approach. (Simulation device: Intel core i7-13700K, 32 GB DDR5 (5600 MHz) RAM, NVIDIA RTX 4090)

The data is transmitted using a single traffic channel following the transmitter model in Figure 4.2 with the same principle of a 2-NOMA system. The received signal is initially synchronised and then demodulated to remove the OFDM components and corrected based on channel estimation while the NOMA symbols are as in (4.22). The data of the first layer is detected using standard NR PD-SCH demodulation and DL-SCH decoding blocks, as shown in Figure 4.2. During this signal detection, no prior knowledge of NOMA data layers is required, and the sum power of all subsequent layers is treated as noise.

Detecting any uth data layer where $u > 1$ requires SIC to remove $u-1$ layer symbols from the received NOMA symbols. Therefore the L_N data can not be detected before the L_{N-1} data is detected, and so on. This operation can be explained for uth data layer using (4.26). The generalised equation for uth layer SIC is written as:

$$\mathbf{y}_{su} = \frac{\mathbf{y}_{s(u-1)} - \mathbf{y}_{r(u-1)}}{g_u}, \ \forall \ 2 \leq u \leq N \tag{4.34}$$

4.4 BER Analysis for N-NOMA

This section presents a closed-form error probability expression, incorporating MIMO gain, using the TDL model and accounting for residual and non-residual errors from SIC.

4.4.1 Error Probability for M-QAM Transmission

The SER expression for a QAM-OFDM system with AWGN channel can be expressed as [168]:

$$P_{rs} \leq 4\, Q\left[\sqrt{\frac{3\,\gamma_s}{M-1}}\right] \tag{4.35}$$

where $Q[\cdot]$ denotes the Gaussian Q-function, and γ_s represents the SNR of the transmitted symbol, s. In the context of an M-QAM OFDM system over an AWGN channel with transmit power P_t, the upper bound of error probability is expressed as:

$$\widehat{P}_{rs} = 4\left[\sqrt{\frac{3\,P_t}{N_0(M-1)}}\right] \tag{4.36}$$

where N_0 denotes the noise spectral density.

4.4.2 Derivation of the Effective Channel Gain for MIMO Channel

Factoring in the effects of MIMO transmission, the effective channel gain for a physical layer MIMO system is denoted as G_u. The MIMO transmission channel uses n_t transmit antennas and n_r receive antennas. The TDL channel model, as referenced in (4.16), is employed to compute the spatial channel gain. Initially, the channel matrix $\mathbf{H}$ for $n_t \times n_r$ transmission is formulated. Subsequently, Singular Value Decomposition (SVD) is applied to determine the total channel gain, G_{total}, at receiver u_i.

Channel Matrix Formation

The process begins with constructing a $n_r \times n_t$ channel matrix $\mathbf{H}$, where the element $h_{i,j}(t,\tau)$ represents channel response at time t with delay τ, expressed as:

$$h_{i,j}(t,\tau) = \sum_{k=1}^{N_{tap}} a_{i,j,k}(t)\ e^{-j2\pi f_c \tau_k} \tag{4.37}$$

where f_c is the carrier center frequency, and $a_{i,j,k}(t)$ is the complex gain of the kth tap between the ith receive antenna and the jth transmit antenna at time t, τ_k is delay of the kth tap and N_{tap} is the total number of taps. The channel matrix $\mathbf{H}$ is expressed as:

$$\mathbf{H} = \begin{bmatrix} h_{1,1}(t) & h_{1,2}(t) & \cdots & h_{1,n_t}(t) \\ h_{2,1}(t) & h_{2,2}(t) & \cdots & h_{2,n_t}(t) \\ \vdots & \vdots & \ddots & \vdots \\ h_{n_r,1}(t) & h_{n_r,2}(t) & \cdots & h_{n_r,n_t}(t) \end{bmatrix} \tag{4.38}$$

Total MIMO Channel Gain using SVD

To derive the effective channel gain from $\mathbf{H}$, SVD is used to approximate the eigen-decomposition as follows [169]:

$$\mathbf{H} = \mathbf{U} \cdot \mathbf{\Sigma} \cdot \mathbf{V}^H \tag{4.39}$$

where $\mathbf{U}$ is an $n_r \times n_r$ unitary matrix, $\mathbf{\Sigma}$ is an $n_r \times n_t$ matrix with non-negative real numbers on the diagonal, and $\mathbf{V}$ is an $n_t \times n_t$ unitary matrix. $diag(\mathbf{\Sigma}) = \sigma_1, \sigma_2, \ldots, \sigma_{\min(n_r,n_t)}$,

are the singular values of **H** and represent the effective channel gains for each spatial mode in the MIMO system.

The effective channel gains for all spatial modes in the MIMO system is obtained as follows:

$$G_k = |\sigma_k|^2, \quad k = 1, 2, \ldots, \min(n_r, n_t) \tag{4.40}$$

Assuming transmit diversity, the coefficient gains are combined as follows [170]:

$$G_{\text{total}} = \sum_{k=1}^{\min(n_r, n_t)} G_k \tag{4.41}$$

G_{total} is incorporated into (4.36) to obtain the impact of MIMO transmission with transmit diversity as:

$$\widehat{P}_{rs} = 4\ Q\left[\sqrt{\frac{3\ G_{\text{total}}\ P_t}{N_0\ (M-1)}}\ \right] \tag{4.42}$$

4.4.3 N-NOMA Interference from UL & LL

In an N-NOMA system that utilizes SIC, the total error probability for a layer is a function of both non-residual and residual errors that arise from the SIC. Let E_u be the decoding error event at the uth layer and C_u as the successful decoding event at the uth layer. Using Bayes theorem, the symbol error probability for the uth layer is therefore defined using the weighted sum of non-residual and residual error probability, which can be expressed mathematically as

$$P_{rs;u} = \underbrace{\Pr\{E_u|C_{u-1}\}}_{\text{Non-residual error}} \Pr\{C_{u-1}\} + \underbrace{\Pr\{E_u|E_{u-1}\}}_{\text{Residual error}} \Pr\{E_{u-1}\} \tag{4.43}$$

Non-Residual Error Probability

The impact of non-residual noise on NOMA layers can be measured as the conditional error probability that the uth layer symbol is incorrectly decoded, given that the previous layer, $(u-1)$, has been successfully decoded. The probability of a correctly decoded symbol in $(u-1)$ layer as $\left(1-\widehat{P}_{rs;(u-1)}\right)$, and the interference from the non-residual error as the sum power of the subsequent NOMA layer is calculated. The non-residual symbol error probability for uth layer is derived in (4.45) by considering the transmit power of the uth layer power,

$$P_u = P_t \prod_{i=1}^{u} g_i \tag{4.44}$$

extracted from (4.33), and the total interference (N_0+ non-residual interference).

$$\Pr\{E_u|C_{u-1}\} \Pr\{C_{u-1}\} = 4\, Q\left[\sqrt{\frac{3\, G_u P_t \prod_{i=1}^{u} g_i}{\left(N_0 + \sum_{i=u+1}^{N} P_t \prod_{j=1}^{i} g_j\right)(M_u - 1)}}\right]\left(1 - P_{rs;(u-1)}\right) \tag{4.45}$$

When $u = 1$, the first layer detection does not have any dependency on the SIC performance, $\left[1-\widehat{P}_{rs;(u-1)} = 1\right]$ calculates the SER for layer 1. In (4.52), interference from other layers is accounted for in the denominator of the expression inside the $Q[\cdot]$ by assuming the interference from subsequent data layers to follow a Gaussian distribution. The interference term

$$\sum_{i=u+1}^{N} P_t \prod_{j=1}^{i} g_j \tag{4.46}$$

defines the cumulative interference from all other NOMA layers with an index greater than u. This term is added to the noise spectral density N_0 in the denominator, which improves the quality of symbol error probability estimation.

Residual Error Probability

$[\Pr\{E_u|E_{u-1}\}]$ is defined as the residual error probability for uth layer $\forall\ u > 1$ when the $(u-1)$ layer symbol is decoded incorrectly. To determine the maximum impact of the residual error, the maximum pair-wise distance between the transmitted and detected $(u-1)$ layer QAM symbol is considered. Assuming a Square QAM (SQAM) constellation for $(u-1)$ layer with transmit power P_{u-1}, the average symbol power P_{avg} is expressed as:

$$P_{avg} = \frac{2\ P_t \prod_{i=1}^{u-1} g_i}{3\ (M_{u-1}-1)} \tag{4.47}$$

The minimum pairwise distance, which is the distance between two adjacent symbols along the axis, denoted as d_{min}, is calculated from P_{avg} as follows:

$$d_{min} = \frac{2\ \sqrt{P_{avg}}}{\sqrt{M_{u-1}}-1} \tag{4.48}$$

Figure 4.5 illustrates an SQAM constellation of order M. The maximum pairwise distance is the Euclidean distance between diagonally opposite QAM symbols(as represented by points A and B in Figure 4.5). The figure also shows the distance between two edge points on the axis, denoted as d_{axis}, and given by $d_{axis} =$

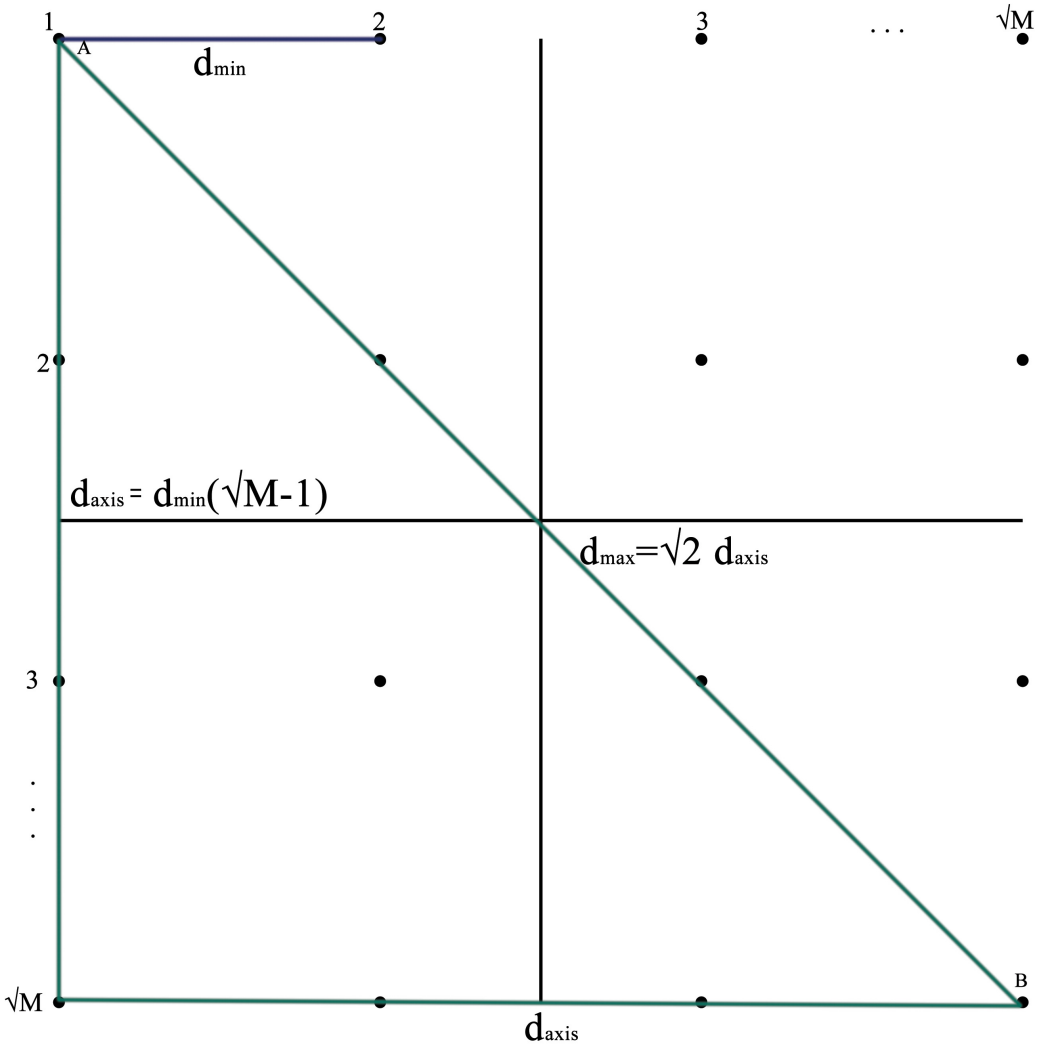

FIGURE 4.5: Maximum and minimum pairwise distance for SQAM constellation in Cartesian coordinates.

$d_{min}(\sqrt{M}-1)$ as there are $\sqrt{M}$ points along each axis, and the distance between adjacent points is d_{min}. Then the maximum pairwise distance, d_{max} is derived, as follows:

$$d_{max} = \sqrt{2}\ \left(\sqrt{M_{u-1}} - 1\right)\ d_{min} \tag{4.49}$$

Then, the revised right term of (4.49) is

$$2\sqrt{2P_{avg}} \tag{4.50}$$

Substituting the value of P_{avg} from (4.47) in (4.50), the maximum pairwise distance for $u-1$ layer symbols is derived as:

$$d_{max_{u-1}} = 4\sqrt{\frac{P_t \prod_{i=1}^{u-1} g_i}{3\,(M_{u-1}-1)}} \tag{4.51}$$

$d_{max_{u-1}}$ in (4.51) is the interference from the residual error for the uth NOMA layer. Assuming a Gaussian distribution for $d_{max_{u-1}}$, this term is added to the denominator with N_0 and residual interference in (4.52) leading to (4.45).

$$\Pr\{E_u|E_{u-1}\}\Pr\{E_{u-1}\} = 4Q\left[\sqrt{\frac{3G_u P_t \prod_{i=1}^{u} g_i}{\left(N_0 + 4\sqrt{\frac{P_t \prod_{i=1}^{u-1} g_i}{3\,(M_{u-1}-1)}} + \sum_{i=u+1}^{N} P_t \prod_{j=1}^{i} g_j\right)(M_u-1)}}\right] P_{rs;(u-1)} \tag{4.52}$$

The symbol error probability for the uth NOMA layer is obtained from (4.43), incorporating both residual and non-residual error probabilities from (4.52) and (4.45), respectively. The first NOMA layer, independent of SIC, does not exhibit residual error. So the generalised expression for the SER for any NOMA layer in a QAM-MIMO-OFDM transmission in an AWGN channel is derived in (4.53), enhancing error estimation by accounting for interference from adjacent NOMA layers.

$$\widehat{P}_{s;u} = \begin{cases} 4Q\left[\sqrt{\frac{3G_u P_t \prod_{i=1}^{u} g_i}{\left(N_0+\sum_{i=u+1}^{N} P_t \prod_{j=1}^{i} g_j\right)(M_u-1)}}\ \right], & \text{if } u\text{=1} \\ 4Q\left[\sqrt{\frac{3G_u P_t \prod_{i=1}^{u} g_i}{\left(N_0+\sum_{i=u+1}^{N} P_t \prod_{j=1}^{i} g_j\right)(M_u-1)}}\ \right]\left(1-P_{s;(u-1)}\right) & \\ \quad +4Q\left[\sqrt{\frac{3G_u P_t \prod_{i=1}^{u} g_i}{\left(N_0+4\sqrt{\frac{P_t \prod_{i=1}^{u-1} g_i}{3\,(M_{u-1}-1)}}+\sum_{i=u+1}^{N} P_t \prod_{j=1}^{i} g_j\right)(M_u-1)}}\ \right] P_{s;(u-1)}, & \text{otherwise} \end{cases} \tag{4.53}$$

Assuming a Grey coding, the BER upper bound is derived from (4.53) as follows:

$$P_{b;u} = \frac{\widehat{P}_{s;u}}{\log_2 M_u} \tag{4.54}$$

The total probability of error from all NOMA layers is then expressed as:

$$P_{bNOMA} = \sum_{i=1}^{N} P_{b;u} \tag{4.55}$$

4.5 Results & Analysis

The outcomes of a comprehensive analysis and link-level simulations of 2-NOMA and N-NOMA system models using MATLAB are presented. The simulation model uses standard 5G NR physical layer technologies, such as DL-SCH, PDSCH, LDPC, and MIMO precoding, in line with 3GPP TR 38.901 [138]. The incorporation of 2- and multi-layer NOMA within the standard 5G transceiver framework for end-to-end

link-level simulation was done to obtain specific KPIs (e.g., BER and throughput). The results of these simulations correlate the KPIs with transmission configuration metrics such as NOMA power ratio, modulation schemes, MIMO order, and LDPC coding rate with various code lengths. The OFDM carrier parameters are fixed as per Table 4.1. The performance of the NOMA-MIMO-OFDM system is analyzed according to the developed BER model in (4.54) and its performance is compared with the simulation model, cementing the hypothesis that high-performance operation may be achieved by 5G physical layer under low-SNR.

TABLE 4.1: Fixed carrier parameters

Carrier Information	**Value**
Sub-carrier spacing	15 Hz
# resource blocks	52
# symbols per slots	14
# slots per frame	10
# slots per sub-frame	1

4.5.1 NOMA L1 *vs* OMA

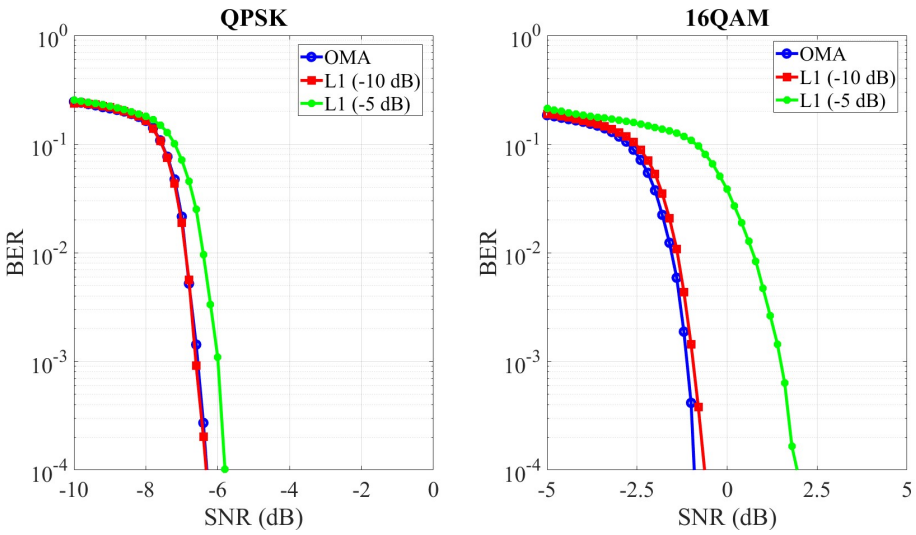

FIGURE 4.6: Comparison of BER between OMA and L1 NOMA transmission under QPSK and 16 QAM modulation, utilizing an $[8 \times 1]$ MIMO order and $(490/1024)$ LDPC code rate in a TDL-D channel model.

The comparison of BER performance between L1 of a 2-NOMA and OMA transmission, as depicted in Figure 4.6, shows the performance degradation in L1 compared to a single-user OMA transmission. At $-10\ dB$ power ratio, the performance of L1 is almost the same as that of OMA transmission for both QPSK and 16QAM transmission. However, allocating higher power for L2 ($-5\ dB$) causes significant performance degradation in L1 16QAM transmission as it achieves the same BER at a $3\ dB$ higher SNR channel.

Although NOMA requires a higher SNR to attain the same BER, additional data layers can be transmitted using the same traffic channel. Figure 4.6 shows that a low rate L1 is more robust and provides a higher degree of freedom in NOMA power distribution without significant performance degradation. This means L1 is more suited for low data rate PTM mMTC transmission, where the devices are distributed over large geographical areas with low or poor signal quality.

4.5.2 NOMA Performance Analysis

This section delves into the performance of NOMA layers and the services that individual layers can achieve. Simulations for both 2-layer and 3-layer NOMA transmissions are conducted to examine the relationship between NOMA layer performance and various configuration parameters. These parameters include the NOMA power ratio, modulation order, MIMO, and channel coding.

Given that the complexity grows with each added NOMA layer, the focus is primarily on evaluating the effects of power ratio, modulation, and MIMO order for a 2-NOMA transmission. This approach helps in establishing clear relationships observed in the results. Insights derived from these findings can be generalized to multi-layer transmissions that follow similar foundational principles. Moreover, the results highlight the flexibility in transceiver configuration necessary to satisfy the specified QoS criteria.

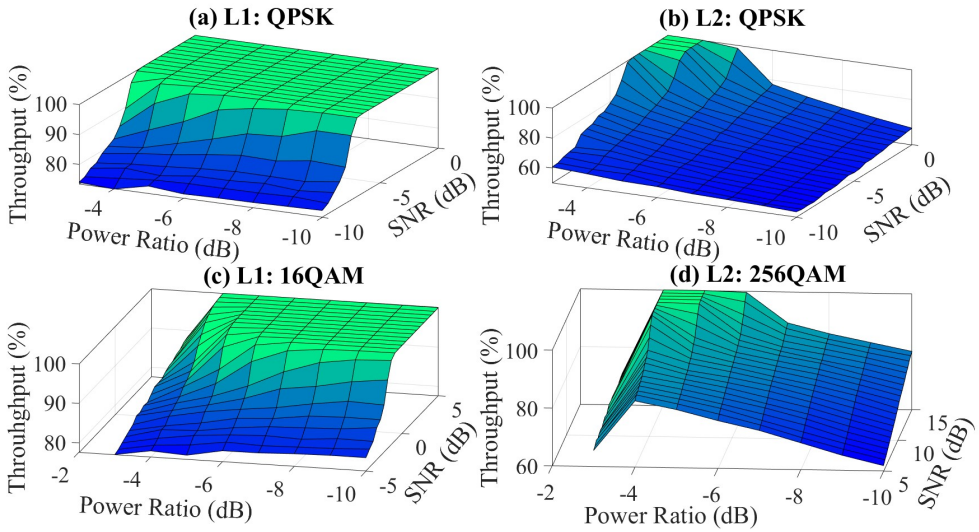

FIGURE 4.7: Impact of power ratio on the throughput of L1: $[8 \times 1]$ and L2: $[8 \times 2]$ transmission with $(490/1024)$ LDPC code rate and TDL-D channel model for two different data rate combinations (a-b) and (c-d): (a) L1-QPSK (-10 to 0 dB) (b) L2-QPSK (-10 to 0 dB) (c) L1-16QAM (-5 to 5 dB) (d) L2-256QAM (5 to 15 dB)

NOMA Power Ratio

Figure 4.7 compares the throughput of NOMA layers for different power ratios in different L1 and L2 receivers' channel conditions. The throughput is calculated according to [171] as follows:

$$\text{Throughput (\%)} = \frac{N_{Rx} - N_{eRx}}{N_{Tx}} \times 100 \tag{4.56}$$

where N_{Rx} is the number of received bits, N_{eRx} is the number of erroneously received bits and N_{Tx} is the number of transmitted bits. Figure 4.7 present a surface graph highlighting the impact of different power ratio on L1 and L2 throughput within the channel SNR range.

The first NOMA pair, depicted in Figure 4.7(a,b), employs QPSK for both L1 and L2 with both receivers having the same channel SNR range of -10 to 0 dB. Figure 4.7(a) demonstrates that L1 achieves the same throughput at a power ratio of -3 dB, compared to -10 dB, with nearly the same channel SNR. Specifically, L1 only requires a 1 dB higher SNR at the -3 dB power ratio to achieve the same throughput.

Figure 4.7 (b) shows improvement in L2 throughput as the power of L2 increases, and in this SNR range, L2 achieves 100% throughput when the power ratio is higher than $-5\ dB$. The first two subplots, Figure 4.7-(a), (b), show a minimum power limit in L2 to achieve 100% throughput on a given SNR range. This minimum power requirement for successful data detection comes from the modulation power and order, which determines the Euclidean distance between modulation symbols.

The second NOMA pair, depicted in Figure 4.7(c,d), employs 16 and 256 QAM for L1 and L2 with both receivers having a different channel SNR range of -5 to 5 and 5 to 15 dB. Both L1 simulation shown in Figure 4.7 (a,c) shows that L1 achieves higher throughput as the power of L2 is decreased in NOMA multiplexing. This is because reducing the power ratio allocated to L2 relative to L1 improves the performance of L1 at a given SNR value, as L1 detection is independent of L2 detection and does not involve SIC. Figure 4.7 (c) shows that at a power ratio over $-4\ dB$, the L1 fails to detect its symbol even in high channel SNR. This failure to detect L1 also results in a drop in L2 throughput in the same power ratio, as shown in Figure 4.7(d). This shows the maximum power that can be allocated to L2 as L1 and L2 fails to achieve high throughput at $-3\ dB$ power ratio. This is because if the interference from L2 to L1 is more than the maximum noise tolerance of L1 modulation, then L1 symbols can not be detected correctly, irrespective of the user's channel condition. As the L2 symbol detection depends on SIC, the L2 performance decreases despite a higher power allocated to the symbols.

Figure 4.7 demonstrates the impact of power ratio on each layer's throughput, emphasizing the need for local optimization that considers the specific channel conditions, modulation, and MIMO order of individual NOMA layers to maximize the overall system performance.The result also shows that at a $-5\ dB$ power ratio, both layers achieved maximum throughput for all four different data rate combinations. Building on this result, the $-5\ dB$ power ratio is used in the following analysis.

Channel Models

Figure 4.8 presents a comprehensive analysis of the BER performance across different layers of NOMA under various channel conditions. Simulations utilized four

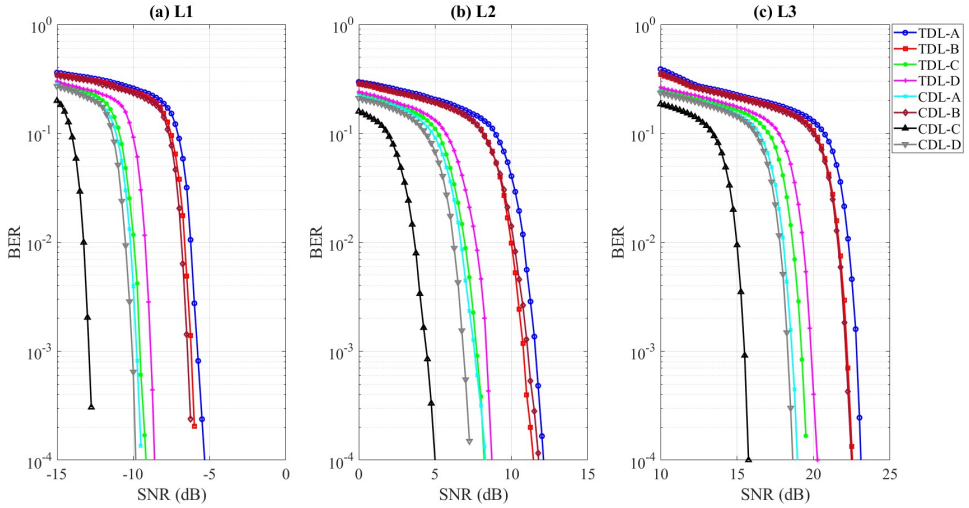

FIGURE 4.8: BER for 3-layer NOMA in TDL and CDL channels. Transceiver: $[8 \times 2]$ MIMO, $(490/1024)$ LDPC. Modulations: QPSK (L1), 16QAM (L2), 64QAM (L3).

distinct TDL and CDL channel models, capturing the intricacies of both urban and rural transmission landscapes. Delving into the technical aspects, TDL channel models emphasize their unique delay spread characteristics, enabling an effective representation of multipath propagation. On the other hand, CDL models, with their rich multi-dimensional spatial characteristics, leverage MIMO arrays to portray realistic channel conditions, especially in dense urban environments.

Within this framework, a noteworthy consistency was observed: all three NOMA layers displayed uniform BER outcomes across the evaluated channels. For instance, the TDL-A model, with its inherent delay profile, demanded the highest SNR. In contrast, the spatially diverse CDL-C model emerged as the most efficient, necessitating the lowest SNR. Overall, the CDL channels showcased superior performance at diminished SNR levels, underscoring their proficiency in mirroring advanced MIMO channel dynamics.

Modulation Order of NOMA Layers

Various data rate transmissions are analyzed, including QPSK, 16, 64, and 256 QAM for L2, and QPSK and 16QAM for L1, with MIMO configurations of $[8 \times 1]$ for L1 and $[8 \times 2]$ for L2. Figure 4.9 shows that the BER of L1 remains consistent for both

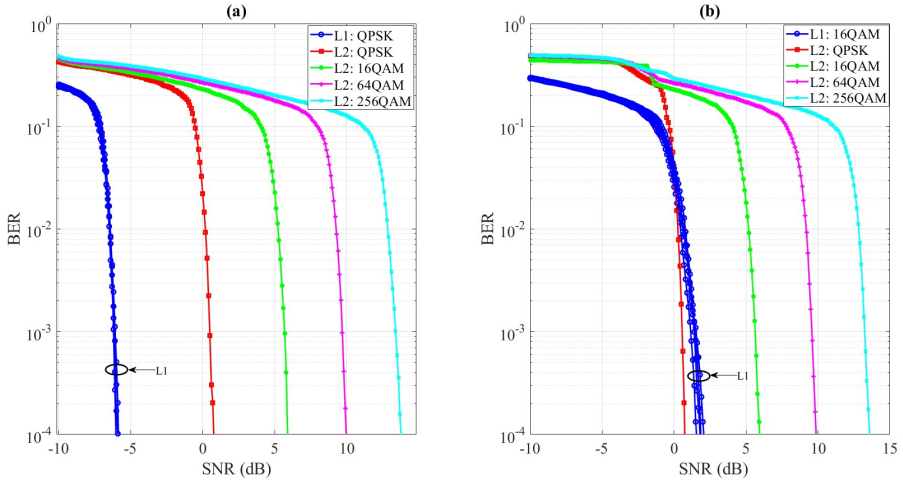

FIGURE 4.9: Comparsion of BER across various data rates in a 2-NOMA layer utilizing (490/1024) LDPC code rate, examined in a TDL-D channel

QPSK and 16 QAM, irrespective of the L2 modulation order. Similarly, the performance of L2 remains unaffected for QPSK and 16 QAM L1 transmissions. The performance of L1 and L2 has no dependency on each other's modulation order. This characteristic allows leveraging any layer's improved channel condition by providing a high data rate service, making NOMA highly resilient in fulfilling diverse user requirements of mMTC and eMBB transmissions.

Figure 4.9-(b) also reveals that for 16 QAM L1 and QPSK L2 transmissions, L2 performs better under low-SNR conditions due to higher MIMO order and lower data rate. The detection of L1 data SIC at L2 requires a lower SNR than at L1. This means that even when L2 is in worse channel conditions than L1, low data rate transmission of L2 is still feasible.

MIMO Order

Figure 4.10 showcases the influence of MIMO order on the BER performance of L1 and L2. Considering the resource limitations of mobile receivers, one receiver antenna is assumed for L1 (symbolizing mMTC devices) and two receiver antennas for L2 (representing eMBB devices). The simulation employs $1, 2, 4$, and 8 transmit antennas to represent various MIMO orders.

The findings from Figure 4.9, highlight the performance enhancement of L2 due to an additional receive antenna. These results echo the same potential for varying

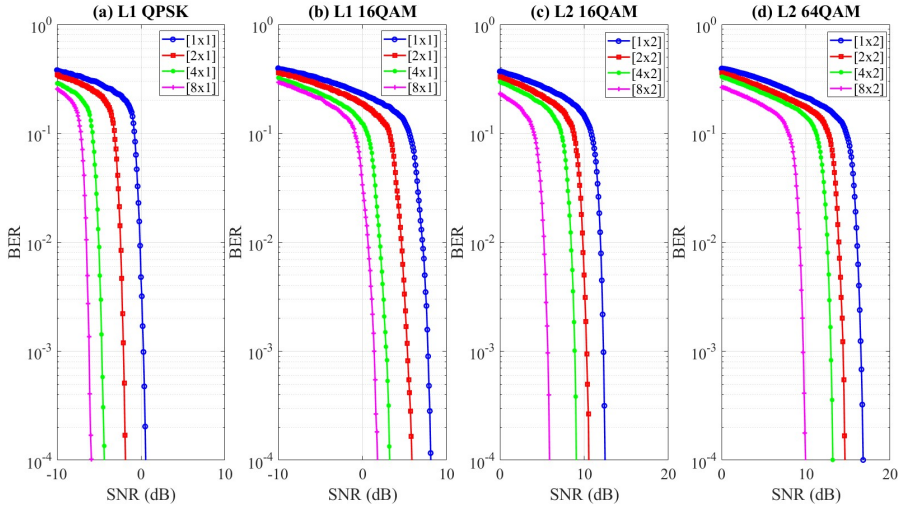

FIGURE 4.10: Impact of MIMO configuration on BER performance of L1 and L2 for different data rate transmission with $(490/1024)$ LDPC coding and -5dB NOMA power ratio

MIMO orders. In all four transmission scenarios depicted in Figure 4.10-(a,b,c,d), the BER improves as the MIMO order increases. The BER of L1 improves by 6 dB for an $[8 \times 1]$ configuration from a $[1 \times 1]$ configuration for both data rate transmissions. Meanwhile, the BER of L2 improves by 8 dB, indicating that a higher MIMO order can significantly enhance the performance of lower orders. The higher MIMO order makes NOMA PTM transmission promising in downlink scenarios.

LDPC Coding Length

LDPC codes have been proven to be asymptotically optimal for wireless channels. However, practical issues of code rates across different NOMA layers should be examined closely. To quantify the impact of LDPC channel coding on the BER performance of NOMA, six different coding rates: $(150/1024)$, $(320/1024)$, $(490/1024)$, $(680/1024)$, $(850/1024)$ and $(950/1024)$ are used. These are referred to as CR(1-6) in Figure 4.11. The BER of NOMA layers L1, L2, and L3, altering only the coding rate of the respective layer while maintaining the other two at CR3 is simulated. The code length impacts the BER of all three layers significantly, but the impact is more vivid in LLs with higher-order modulation.

Figure 4.11-(a,b,c) illustrates that the BER line follows the same curve for all code lengths, with shorter code lengths reducing the BER at lower SNR. The findings

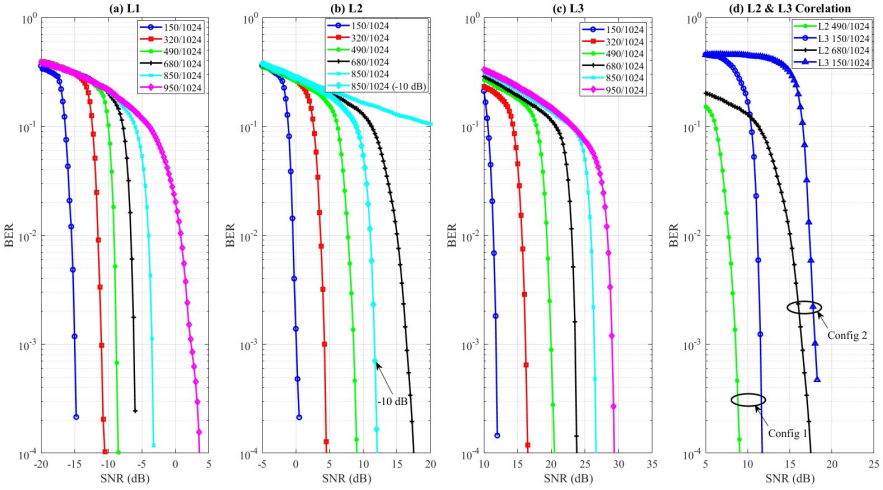

FIGURE 4.11: Impact of LDPC coding rate on the BER of 3 NOMA $[8 \times 2]$ transmission with $-5\ dB$ power ratio between L1-L2 and L2-l3 using TDL-D channel: (a) L1-QPSK (b) L2-16QAM (c) L3-64QAM (d) L2-16QAM, L3-64QAM

suggest that a shorter coding rate can enhance the noise tolerance margin, which can be used to offset additional interference from NOMA layers.

From Figure 4.11-(b), it is noted that L2 fails to detect its signal when CR5 coding rate is used, while both L1 and L3 successfully detect signals under all coding rates. The inability to detect a signal even at high SNR points can be attributed to the events when the interference residual noise surpasses the maximum noise tolerance. In such cases, NOMA transmission of that layer and any subsequent LLs will fail.

This hypothesis is validated by simulating a different setup in (b), where the power ratio is reduced between L2 and L3 to $-10\ dB$. The resulting BER performance with CR5 is 4 dB lower than with CR4 at a $-5\ dB$ NOMA power ratio. Based on these findings, one can optimize the performance to offset the residual error's impact, potentially leading to a successful multi-layer NOMA configuration.

Figure 4.11-(b,c) illustrates that L3 with CR1 coding rate attains an acceptable BER at a lower SNR compared to L2 with CR4 coding rate. This observation facilitates the exploration of the impact of SIC and a higher layer coding rate on the performance of the LL, as highlighted in Figure 4.11-(d). In this figure, CR3 and CR4 are employed for L2, while CR1 is used for L3. The results indicate that the L3 receiver struggles to detect signals at a lower SNR when paired with the L2 CR4 coding rate. Under this configuration, the L3 BER line starts to descend subsequent

to the dip of the L2 BER line. It is also evident that the necessary SNR to reach a consistent BER increases incrementally with the rise in modulation order for each code rate.

In the study conducted by Iradier et al. [15], a 3-layered NOMA transmission was designed for 5G networks, accomplishing a BER of 10^{-4} at SNR of 11, 15, and 17 dB for layers L1, L2, and L3, respectively. The results presented in this section show that the transceiver model presented in this chapter achieves 10^{-4} BER at a lower SNR. The enhanced performance can be attributed to the inclusion of MIMO and LDPC.

4.5.3 Theoretical BER Evaluation of N-NOMA

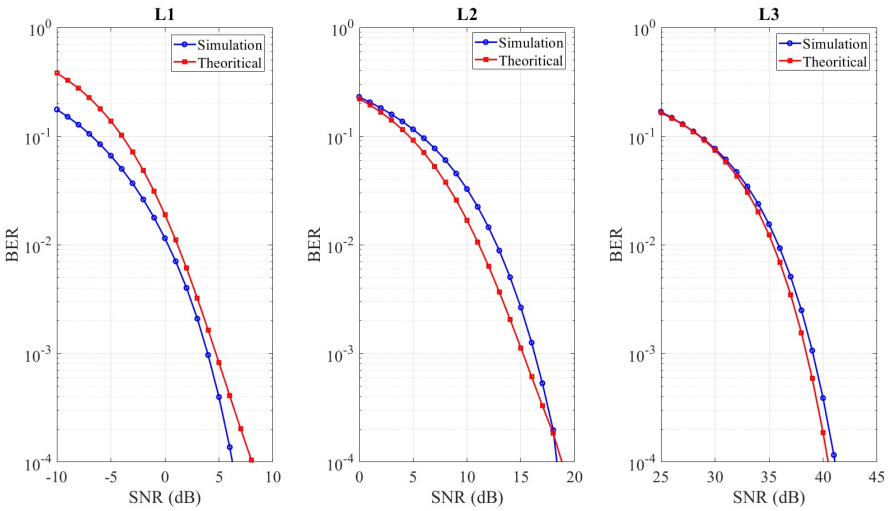

FIGURE 4.12: BER analysis illustrating the theoretical performance of a 3-layer NOMA system using (4.54). The comparison is obtained using an end-to-end simulation model of the same system. The transmission layers are as follows: Layer 1 (L1) comprises an $[8 \times 2]$ QPSK, Layer 2 (L2) utilizes an $[8 \times 4]$ 16QAM, and Layer 3 (L3) deploys an $[8 \times 8]$ 64QAM.

Figure 4.12 provides a comparative analysis between the BER of a 3-NOMA system, as defined by (4.54), and results obtained from a complete end-to-end simulation model, which incorporates an uncoded OFDM with MIMO AWGN channels designed for a 3-layer NOMA transmission. In this model, QPSK, 16QAM, and 64QAM are employed for L1, L2, and L3 layers, with 2, 4, and 8 receive antenna elements respectively. Power ratios for L2 and L3 are set at $-5\ dB$ and $-10\ dB$.

As demonstrated in Figure 4.12, the theoretical BER closely aligns with the simulated results, indicating the validity of the derived equation. While the simulation results for the BER of L1 exhibit minor improvements, the BER performance of L2 and L3 show a substantial alignment between theoretical predictions and simulation outcomes.

4.6 Summary

4.6.1 Contributions:

In the realm of wireless communications, the introduction of a novel 5G NR-compliant NOMA design stands out as a significant milestone. This design, marked by its integration of optimally positioned NOMA-aided transceiver functions, promises to push the boundaries of current communication standards. The intrinsic beauty of this design is its comprehensive performance assessment, allowing for the consideration of multifaceted parameters. From forward error correction to MIMO precoding and from modulation schemes to coding rate, every facet has been meticulously studied. Furthermore, this exploration provides a renewed vision for non-orthogonal access technology. It shows new areas to explore, potentially leading to future discoveries and filling current knowledge gaps. As part of this innovative journey, the research has dared to replace the traditional multi-layer sequential combiners with a more streamlined one-shot N-NOMA multiplexing method. This critical decision stems from a need to address the nagging issues of transmission latency and transceiver complexity. And to crown it all, an analytical BER expression has been developed, one that stands out in its precision, especially in determining the effects of residual and non-residual errors on N-NOMA layers. Validating these findings, simulations conducted on a 5G NR-compliant link level simulator have not only affirmed the proposed physical layer design but also highlighted N-NOMA's promise to cater to a broader user base.

4.6.2 Limitations:

However, like all pioneering works, this chapter does have its constraints. The analytical model, while robust, hints at areas for refinement, especially in integrating the subtleties of channel coding and fine-tuning its interaction with TDL/CDL channels. There is also the consideration of residual interference. The model, in its current form, leaned on the maximum residual interference to set the uppermost error threshold. Adopting a more precise model for residual error would elevate the model's accuracy. Additionally, while the multiplexing procedure has been reimagined to reduce latency, the detection process, with its extensive nature, remains a formidable challenge.

4.6.3 Future Work:

This chapter lays a foundation that calls for deeper investigation. At its core, the analytical model is rooted in the Q function, encompassing an uncoded OFDM system within an AWGN channel. The findings spotlight the alignment of the multi-layer system with the uncoded N-NOMA-OFDM setup, emphasizing the model's adeptness at capturing both types of errors: residual and non-residual. Such insights point towards opportunities for enhancements, particularly integrating channel coding and TDL/CDL parameters into a richer analytical model. Additionally, the adoption of a probabilistic model for more accurate residual interference could better align the analytical model with real-world 5G and B5G scenarios. There is growing agreement on the importance of refining the detection process. Consider a clustering-based method as an alternative to the traditional SIC operation, designed to cancel ULs interference from the received NOMA signal. This strategy could drastically cut down receiver complexity and latency, while also eliminating the current buffer requirement tied to SIC.

Chapter 5

Adaptive Power Allocation to Enhance N-NOMA Link Time

5.1 Introduction

Building on the 2 layer LDM PA presented in Chapter 3, the idea is further developed for the N-NOMA system from Chapter 4. This chapter delves into the design and application of an adaptive PA algorithm tailored for downlink N-NOMA transmission. The model is tested based on the proposed 5G transciver model as shown in Figure 4.2. At the heart of this exploration lies the algorithm's greedy strategy, which harnesses transmission feedback as a guide for the dynamic distribution of power across NOMA layers. The overarching objective remains twofold: optimizing the system's overall throughput and maximise the sustainable link time for mobile N-NOMA cluster.

The intricacies of NOMA layer detection are heightened with the addition of each data layer. Any power designated to a particular layer inadvertently influences the performance of all NOMA layers. This intertwined relationship demands a holistic approach to the PA process to ensure peak system performance. The scenario becomes even more multifaceted when each data layer targets distinct users, each bringing their unique channel conditions and QoS expectations. Such dynamics highlight the need for a dynamic PA, tailored to the specifications of each N-NOMA cluster, rather than a one-size-fits-all static PA.

Furthermore, the intricate nature of this challenge suggests that systems may not

always realize optimal outcomes. There may be instances where continued optimization endeavors yield marginal benefits. In response to these challenges, three distinct algorithms are introduced, detailed in Section 5.2. The inaugural algorithm, employing a greedy tactic, aims to bolster the overall system throughput, all the while respecting the QoS benchmarks set for each receiver. The subsequent algorithm is crafted to discern the pinnacle of PA efficiency, recognizing instances where continued adjustments only cycle through redundant values. These two pioneering algorithms provide the foundation for the third, which is adept at pinpointing the optimal PA in static channel conditions.

In Section 5.3, the 2D mobility model from Section 3.6 is expanded to a 3D format, encompassing RMa and UMa scenarios as per 3GPP standards. This model calculates the SNR for any receiver, adhering to the standard 3GPP approach which includes both LoS and NLoS connections. To bolster the link sustainability for multi-user N-NOMA clusters, an adaptive PA is introduced.

In Section 5.4, the performance of the newly introduced algorithms is evaluated, examining its efficacy for both stationary and mobile receivers. Lastly Section 5.5 summarises chapter's contributions and future work.

5.2 N-NOMA Dynamic PA in Static Channel

In this section, the details of dynamic PA for N-NOMA in static channel conditions are explored. The main goals are to cut down on total error and optimize the performance of the N-NOMA cluster. The first three algorithms designed to meet these challenges are introduced and discussed.

5.2.1 Optimise PA Algorithm

The world of N-NOMA systems has its own set of hurdles when it comes to distributing power, especially when trying to keep the BER in check for every user. Algorithm 2 lays out a flexible PA method made just for these systems. Using a greedy method, it aims to quickly find the best way to balance power among users (Appendix A-5). If every user achieves a successful transmission with the established PA settings, the system will maintain the current configuration until there is

a change in conditions. Conversely, if the system does not meet the required BER for all users after a predetermined number of iterations, it will deem the cluster as unsustainable and consequently disband the NOMA cluster.

Process Overview

1. **Start**: Begin with each user's BER difference, the total user count, and starting power ratios.
2. **Find Users with Big BER Differences**: Check if any user's BER difference goes beyond a set limit. If yes, pick the user with the biggest difference.
3. **Change Power Based on User Spot**:
    - For the top user with the biggest difference, take power from the next user.
    - On the other hand, for the last user, give power to the user with the smallest difference.
    - For users in between, look at the differences of users close by and change the power based on those differences.
4. **Share New Power Ratios**: After changes, share the new power ratios for everyone.

Mathematical Formulations

The deviation in BER for a user u can be represented as:

$$\Delta\epsilon_u = \epsilon_u - \epsilon_{maxU} \tag{5.1}$$

where ϵ_u denotes the BER for user u and ϵ_{maxU} signifies the upper threshold for acceptable BER.

The recalibration in power ratio is contingent on the following conditions:

$$g_u = \begin{cases} g_u - 1, & \text{if } \Delta\epsilon_u > 0 \text{ and } u = 1 \\ g_u + 1, & \text{if } \Delta\epsilon_u > 0 \text{ and } u = N \\ g_u \pm 1, & \text{predicated on deviations of neighboring users} \end{cases} \tag{5.2}$$

Algorithm 2: PA for N-NOMA layers using a greedy approach

Require: BER Deviation for each user: $\Delta\epsilon_u$, Number of users: N, Power ratios: $\mathbf{g}_u$.

Process: **if** $\Delta\epsilon_u > 0 \; \exists \; (1 \leq u \leq N)$ **then**

- $u = \max(\Delta\epsilon_u)$
- **if** $u == 1$ **then**
  - $g_{u+1} \leftarrow g_{u+1} - 1$
- **else if** $u == N$ **then**
  - $u_{min} = \min(\Delta\epsilon_u)$
  - $g_{u_{min}+1} \leftarrow g_{u_{min}+1} + 1$
- **else**
  - **if** $\Delta\epsilon_{u-1} > 0$ *and* $\Delta\epsilon_u < 0$ **then**
    - $g_u \leftarrow g_u - 1$
    - $g_{u+1} \leftarrow g_{u+1} + 1$
  - **else if** $\Delta\epsilon_{u-1} < 0$ *and* $\Delta\epsilon_u > 0$ **then**
    - $g_u \leftarrow g_u + 1$
    - $g_{u+1} \leftarrow g_{u+1} - 1$
  - **else if** $\Delta\epsilon_{u-1} > 0$ *and* $\Delta\epsilon_u > 0$ **then**
    - **if** $\Delta\epsilon_{u+1} < 0$ **then**
      - $g_{u+1} \leftarrow g_{u+1} - 1$
- **Return** $\mathbf{g}_u$

5.2.2 Power Optimization Oscillation Monitoring Algorithm

In the context of N-NOMA systems, achieving optimal power distribution is paramount. However, continual adjustments to PA can lead to oscillations, where the system continually toggles between states without settling on an optimal configuration. Such oscillations can be detrimental, leading to increased power consumption and reduced system stability. To address this, an oscillation detection mechanism is introduced, as illustrated in Algorithm 3. This mechanism monitors the BER history and employs variance as a metric to ascertain if the system is oscillating.

Process Overview

1. **Initialization**: The algorithm is initialized with the BER history, denoted as H_ϵ, the current total BER, represented as ϵ_{total}, and a predefined threshold for variance, θ.

2. **Variance Computation**: The variance of the BER history, H_ϵ, is computed. This variance, σ^2, provides insights into the fluctuations in the BER over time.

3. **Oscillation Detection**: If the computed variance, σ^2, is less than the threshold, θ, the system is deemed to be oscillating. Otherwise, it is considered stable.

Mathematical Formulation

Given the BER history H_ϵ with n values, the variance σ^2 is computed as:

$$\sigma^2 = \frac{1}{n}\sum_{i=1}^{n}(\epsilon_i - \bar{\epsilon})^2 \tag{5.3}$$

Where:

- ϵ_i is the BER at the i^{th} instance.
- $\bar{\epsilon}$ is the mean BER, given by $\bar{\epsilon} = \frac{1}{n}\sum_{i=1}^{n}\epsilon_i$.

Algorithm 3: Oscillation detection during power optimization

Require: BER history: H_ϵ, Current total BER: ϵ_{total}, Threshold for variance: θ.

Output: Boolean indicating if oscillation is detected.

Process: Compute the variance of H_ϵ: $\sigma^2 = \text{Variance}(H_\epsilon)$.

if $\sigma^2 < \theta$ **then**
  Return True

else
  Return False

5.2.3 PA Algorithm: Maximise Throughput

The algorithm presented in Algorithm 4 is devised to optimize the performance of a N-NOMA cluster. By leveraging dynamic PA in a fixed channel environment, the algorithm ensures that the system operates within optimal conditions. If the conditions are breached, the system can either optimize the existing cluster or break into a new cluster to maintain performance.

Process Overview

The algorithm operates in a loop while the NOMA user group is active. Within each iteration, the algorithm:

- Computes the BER for each user and the total system.
- Checks for oscillations using the Oscillation Detection algorithm.
- If oscillations are detected, it verifies if all individual BER values are within the maximum tolerance. If not, the current cluster is terminated, and a new cluster is initialized by replacing the problematic user.
- Updates the BER history and invokes Algorithm 2 for power ratio optimization.
- Checks for stability in power ratios. If stable values are observed, the loop is terminated.

Mathematical Formulation

Given the BER for user u, ϵ_u, the total BER for the system is computed as:

$$\epsilon_{total} = \sum_{u=1}^{N} \epsilon_u \tag{5.4}$$

Where N is the total number of users in the NOMA user group.

The individual BER for user u is given by:

$$\epsilon_u = \frac{1}{n_u} \sum_{i=1}^{n_u} x_{ui} \oplus y_{ui} \tag{5.5}$$

Where x_{ui} and y_{ui} are the input and output signals, respectively, for user u at the i^{th} instance.

5.3 Adaptive PA for Mobile N-NOMA Clusters

In this section, the focus is on ensuring stable connections for users in N-NOMA groups, for receivers operating under dynamic channel conditions. Recognizing the inherent volatility of mobile environments, a 3D positioning and mobility model tailored for the receiver is proposed. This model serves as a foundation for subsequent in-depth exploration of the SNR calculation model, which has been meticulously designed in accordance with the 3GPP mobility framework for Pathloss (PL), catering to both RMa and UMa scenarios. Using these basic models, this section concludes with the introduction of a targeted algorithm. This algorithm is designed to strengthen the stability and longevity of N-NOMA connections, ensuring they perform at their best, even with dynamic channel conditions.

Algorithm 4: Static PA for N-NOMA in static channel

Input: for $u = 1$ *to* N **do**

$x_u \leftarrow \{x_1, x_2, ...x_{nu}\} \mid x_i \in \{0, 1\}$,

Initial SNR values: $\rho_u, init$,

Predefined power ratio: $g_u \leftarrow g_{u;init}$,

Maximum BER tolerance: ϵ_{maxU}.

Initialize: BER history: $H_\epsilon \leftarrow$ empty list

Output: Optimized power ratios g_u for the NOMA user group.

Procedure: while *NOMA user group is active* **do**

for $u = 1$ *to* N **do**

$y_u \leftarrow f_{5G}(x_{NOMA}, \rho_u)$,

$\epsilon_u \leftarrow \frac{1}{n_u} \sum_{i=1}^{n_u} x_{ui} \oplus y_{ui}$.

Compute total BER: $\epsilon_{total} \leftarrow \sum_{u=1}^{N} \epsilon_u$

if *OscillationDetection*$(H_\epsilon, \epsilon_{total})$ **then**

if *All individual* $\epsilon_u \leq \epsilon_{maxU}$ **then**

Break

else

Terminate Current Cluster

Reinitialize with working users and replace problematic user

Continue with new cluster

Update H_ϵ with ϵ_{total} and remove the oldest value if the length of H_ϵ exceeds a predefined threshold.

Invoke Algorithm 2 for power ratio optimization.

Return Optimized power ratios g_u.

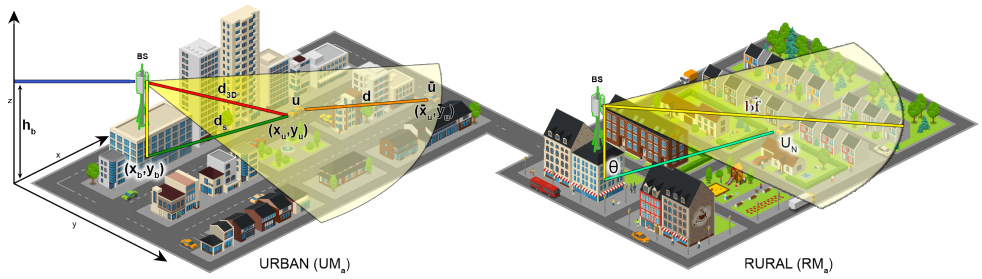

FIGURE 5.1: Downlink mobile N-NOMA transmission in urban and rural areas with MIMO beamforming and 3D mobility model.

5.3.1 3D User Positioning Model

As illustrated in Figure 5.1, the user transitions from the starting location to the concluding location over a specified time span t. Adopting a planar model (2D) from Section 3.6, the positions of the BS and the user at the outset are denoted as (x_b, y_b) and (x_u, y_u), respectively. Consequently, the distance between the BS and the user's initial location is defined as:

$$d_s = \sqrt{|(x_u - x_b)|^2 + |(y_u - y_b)|^2} \tag{5.6}$$

The starting coordinates of N users can be represented as

$$[(x_{u1}, y_{u1}), \ldots, (x_{ui}, y_{ui}), \ldots, (x_{uN}, y_{uN}), \forall\, 1 \leq i \leq N]$$

Given that the LL of NOMA users necessitates superior signal conditions, assumption is that the primary transmission beam targets the location of the N-th user initially; $\left[\vec{\mathbf{bf}} = (x_{uN} - x_b, y_{uN} - y_b)\right]$. Consequently, the angle, denoted as θ, in degrees, between the location of the i-th user and $\vec{\mathbf{bf}}$ is articulated as:

$$\theta = \frac{180}{\pi} \arccos\left(\frac{(x_{ui}-x_b)(x_{un}-x_b)+(y_{ui}-y_b)(y_{un}-y_b)}{\sqrt{(x_{ui}-x_b)^2+(y_{ui}-y_b)^2}\sqrt{(x_{un}-x_b)^2+(y_{un}-y_b)^2}} \right) \tag{5.7}$$

Equation (5.7) is used to determine both the starting and concluding angles of the transmission direction for the location of the i-th user, represented as θ_i and $\hat{\theta}_i$, respectively. Given that the user traverses at a velocity of v over a duration of t, the span between the user's commencement point and the terminal location is expressed as:

$$d = v\,t \tag{5.8}$$

The user moves d distance from the position of (x_u, y_u) with a random angle ϕ to the final position $(\hat{x}_u, \hat{y}_u)$, which is expressed as:

$$\hat{x}_u = x_u + d\cos(\phi) \text{ and} \tag{5.9}$$

$$\hat{y}_u = y_u + d\sin(\phi) \tag{5.10}$$

The 3D distance between the user's current location and BS is calculated from d_s as [138]:

$$d_{3D} = \sqrt{d_s^2 + (h_t - h_u)^2} \tag{5.11}$$

where h_t & h_u are the height of BS and user, respectively.

5.3.2 PL & SNR

Both the RMa and the UMa, as described in the 3GPP documents [138], have been taken into account for the PL model, and these are presented in Table 5.1. This table illustrates a condensed PL equation, accompanied by a set of assumptions.

Subsequently, Pr_{LOS} and PL are determined utilizing the surface distance d_s and the 3D distance d_{3D}. This involves a probabilistic random designation between LoS and NLoS connections. The SNR, symbolized by the notation ρ, derived from PL, x_t, and n_p, is articulated as:

$$\rho = \frac{x_t \cdot \left| \cos\left(\frac{\pi\theta}{\theta_{3\mathrm{dB}}}\right) \right|^n}{PL \cdot n_p} \tag{5.12}$$

where $\theta_{3\mathrm{dB}}$ is the half-power beamwidth and n is the beam shaping parameter.

5.3.3 Adaptive PA Algorithm: Maximise Cluster Link Time

An algorithm is developed to enhance the sustainable link time for N-NOMA cluster for mobile receivers. This algorithm utilises both Algorithm 2, 3 to adjust the power allocated to each NOMA layers based on the receiver feedback.

Process Overview

The Adaptive PA algorithm for N-NOMA mobile receiver cluster operates iteratively until the NOMA cluster is unsustainable. During each cycle of its execution, the algorithm:

- Determines the SNR for each user and computes their respective received signals.
- Calculates the BER for each user and computes the deviation from the maximum allowed BER.

TABLE 5.1: PL Models and LoS Probability for RM_a and UM_a [138]

Scenario	LoS/NLoS	LoS probability ($\Pr_{LOS}$)	PL [dB], f_c in GHz and d in meters	Assumptions
RM_a	LOS	$\exp\left(-\frac{d_s-10}{1000}\right)$	$PL_{RM_a-LOS} = \begin{cases} PL_1 \; 10m \le d_s \le d_{BP} \\ PL_2 \; d_{BP} \le d_s \le 10km \end{cases}$ $PL_1 = 20\log_{10}(40\pi d_{3D} f_c/3)$ $+ min(0.03h^{1.72}, 10)\log_{10}(d_{3D}) - min(0.044h^{1.72}, 14.77)$ $+ 0.002\log_{10}(h)d_{3D}$ $PL_2 = PL_1(d_{BP}) + 40\log_{10}(d_{3D}/d_{BP})$	$h_b = 35m$ $d_{BP} = 2\pi h_b h_u f_c/c$ $10m \le d_s \le 10km$ $W = 20m_{(\text{avg. street width})}$ $h = 5m_{(\text{avg. building height})}$
	NLOS		$PL_{RM_a-NLOS} = max(PL_{RM_a-LOS}, PL'_{RM_a-NLOS})$ $PL'_{RM_a-NLOS} = 161.04 - 7.1\log_{10}(W) + 7.5\log_{10}(h)$ $-(24.37 - 3.7(h/h_b)^2)\log_{10}(h_b)$ $+(43.42 - 3.1\log_{10}(h_b))(\log_{10}(d_{3D}) - 3)$ $+20\log_{10}(f_c) - (3.2(\log_{10}(11.75h_u))^2 - 4.97)$	
UM_a	LOS	$\frac{18}{d_s} + \exp\left(-\frac{d_s}{63}\right)\left(1 - \frac{18}{d_s}\right)$	$PL_{UM_a-LOS} = \begin{cases} PL_1 \; 10m \le d_s \le d'_{BP} \\ PL_2 \; d'_{BP} \le d_s \le 5km \end{cases}$ $PL_1 = 28.0 + 22\log_{10}(d_{3D}) + 20\log_{10}(f_c)$ $PL_2 = 28.0 + 40\log_{10}(d_{3D}) + 20\log_{10}(f_c)$ $-9\log_{10}(d'^2_{BP} + (h_b - h_u)^2)$	$10m < d_s$ $h_b = 25m$ $h_u \le 13m$ $d'_{BP} = 4h_b h_u f_c/c$ $1.5m \le h_u \le 13m$ $10m \le d_s \le 5km$
	NLOS		$PL_{UM_a-NLOS} = max(PL_{UM_a-LOS}, PL'_{UM_a-NLOS})$ $PL'_{UM_a-NLOS} = 13.54 + 39.08\log_{10}(d_{3D})$ $+20\log_{10}(f_c) - 0.6(h_u - 1.5)$	

- Checks whether each user's BER deviation is within permissible limits. If the BER for any user surpasses the threshold, it invokes the Algorithm 2 to optimize power ratios.
- Keeps track of iterations to ensure that the algorithm does not run indefinitely, thereby ensuring computational efficiency.
- Periodically updates each user's position and SNR to reflect real-time mobility and channel conditions.
- Monitors the iteration count against a pre-set threshold to determine whether to terminate the NOMA user cluster, which acts as a fail-safe against potential endless loops or in situations where optimal conditions can not be met.

Mathematical Formulation

The core of the algorithm revolves around the adaptive PA strategy. Three distinct functions are employed to depict the transmission process:

1. Mobility Function:

$$P'_u = f_m(m_m, t, P_u)$$

Where P'_u is the updated position of the user, m_m represents the mobility model, t is the time, and P_u is the current position of the user. Two previous discussed mobility models (Random Waypoint, Manhattan) are used in this chapter evaluate the proposed algorithm.

2. SNR Function:

$$\rho_u = f_\rho(p_t, n_p, P_{bs}, P'_u)$$

Where ρ_u is the SNR for the user, p_t is the transmit power, n_p is the noise power, P_{bs} is the BS position, and P'_u is the updated position of the user.

3. BER Function:

$$\epsilon_u = \frac{1}{n_u} \sum_{i=1}^{n_u} x_{ui} \oplus y_{ui}$$

where ϵ_u is the BER for user u, x_{ui} is the transmitted bit, and y_{ui} is the received bit.

The algorithm aims to minimize the deviation $\Delta\epsilon_u$ which is given by:

$$\Delta\epsilon_u = \epsilon_u - \epsilon_{maxU}$$

Where ϵ_{maxU} is the maximum BER tolerance for user u.

The adaptive PA strategy is then applied to ensure that $\Delta\epsilon_u \leq 0$ for all users, ensuring optimal link sustainability.

5.4 Results

The results of a detailed analysis and link-level simulations for N-NOMA system models (Appendix A-7), conducted using MATLAB, are presented. This simulation model incorporates standard 5G NR physical layer technologies such as DL-SCH, PDSCH, LDPC, and MIMO precoding, consistent with 3GPP TR 38.901 [138]. A mobility model has been developed to determine the channel condition for each NOMA receiver. This information is then processed by the 5G transceiver, which utilizes Algorithm 4 (for static receiver) and Algorithm 5 (for mobile receiver). Abstraction of this link level simulation shown in Figure 5.2, highlighting the iterative feedback from both the mobility and PA blocks. Key parameters for the 5G transceiver and mobility model are outlined in Table 5.2.

Algorithm 5: Adaptive PA for N-NOMA mobile receiver cluster

Input: Transmit power(p_t), Noise power (n_p), BS position($P_{bs} \leftarrow (x_b, y_b)$),

QoeMaxIterationThreshold

for $u = 1$ *to* N **do**

User data: $x_u \leftarrow \{x_1, x_2, ...x_{nu}\} \mid x_i \in \{0, 1\}$,

User position: $P_u \leftarrow (x_u, y_u)$,

Initial power ratio: g_u,

Maximum BER tolerance: ϵ_{maxU}.

Initialize: for $u = 1$ *to* N **do**

SNR: $\rho_u \leftarrow f_\rho(p_t, n_p, P_{bs}, P_u)$,

Received signal: $y_u \leftarrow f_{5G}(x_{NOMA}, \rho_u)$.

Procedure: iterationCount $\leftarrow 0$,

while *NOMA user group is active* **do**

conditionMet $\leftarrow$ false,

for $u = 1$ *to* N **do**

BER for user u: $\epsilon_u \leftarrow \frac{1}{n_u} \sum_{i=1}^{n_u} x_{ui} \oplus y_{ui}$,

BER deviation: $\Delta\epsilon_u = \epsilon_u - \epsilon_{maxU}$,

if $\Delta\epsilon_u \leq 0$ **then**

conditionMet $\leftarrow$ true

if *conditionMet* **then**

iterationCount $\leftarrow 0$

if $\Delta\epsilon_u > 0 \; \exists \; (1 \leq u \leq N)$ **then**

Invoke Algorithm 2 for power ratio optimization,

iterationCount $\leftarrow$ iterationCount + 1

for $u = 1$ *to* N **do**

Update user position: $P_u \leftarrow f_m(m_m, t, P_u)$,

Update SNR: $\rho_u \leftarrow f_\rho(p_t, n_p, P_{bs}, P_u)$,

Receive signal: $y_u \leftarrow f_{5G}(x_{NOMA}, \rho_u)$.

if *iterationCount* $\geq$ *QoeMaxIterationThreshold* **then**

Terminate the NOMA user cluster,

Break

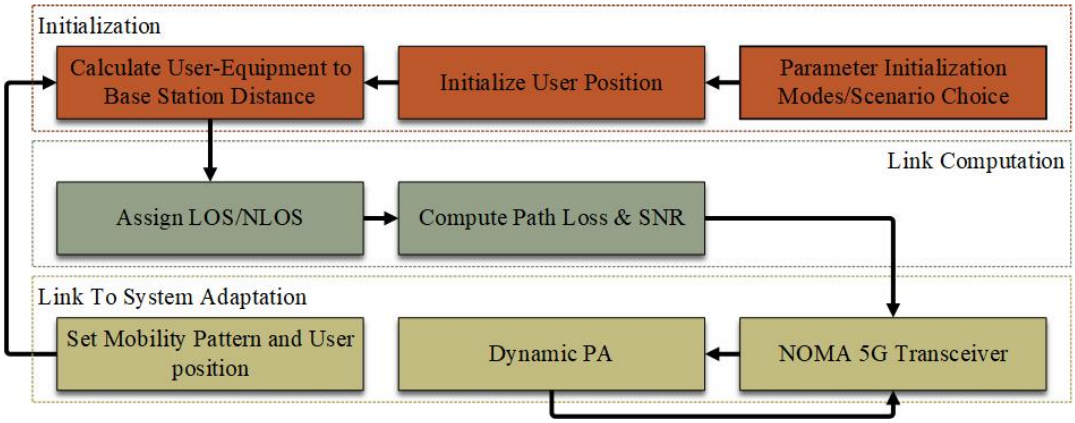

FIGURE 5.2: Mobility abstraction model

TABLE 5.2: 5G simulation parameters and user mobility model

Parameter	**Value**
Communication Parameters	
Transmission frequency	2.4 GHz
Sub-carrier spacing	15 Hz
# resource blocks	52
# symbols per slots	14
# slots per frame	10
# slots per sub-frame	1
LDPC coding length	490/1024
Modulation order	QPSK, 16QAM, 64QAM
MIMO configuration	8×2
Channel model	TDL-A(NLoS), TDL-D(LoS)
Mobility Parameters	
Manhattan mobility model	11-40 kph
Random waypoint mobility model	0-10 kph
Height Parameters	
BS height	35 m (RMa), 25 m (UMa)
Receiver height	1.5 m

The results illustrated in Figure 5.3 showcase the refined PA derived from diverse initial PA settings under specific static channel conditions. These outcomes were simulated using three unique sets of channel SNRs combined with initial PA. It becomes evident from the data that the introduced algorithm successfully attains the optimal system throughput in a range of 6-14 iterations.

As depicted in Figure 5.3 (a, b), the optimal PA distribution appears to be influenced by the user channel. This observation holds true even when all other parameters remain consistent, with the only variation being the channel condition. This emphasizes the importance of localised PA based on the channel conditions of all

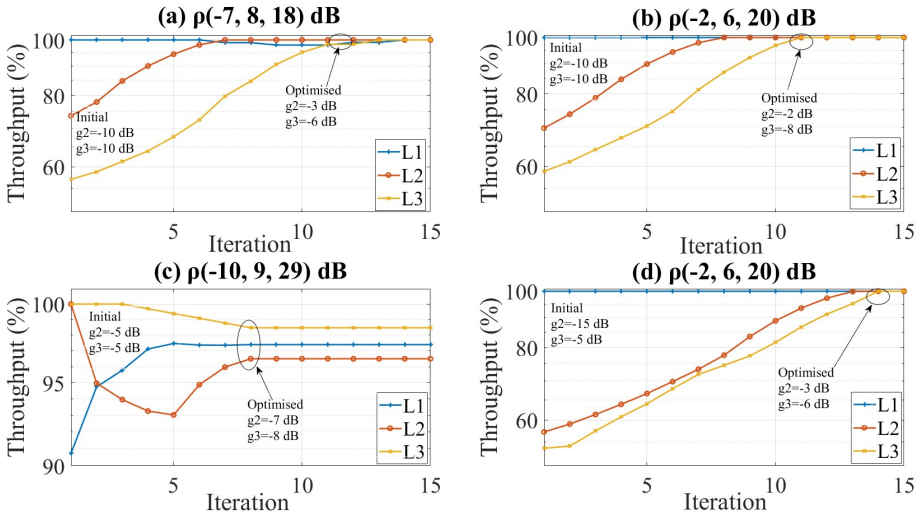

FIGURE 5.3: Iterative optimum PA for 3-NOMA transmission to achieve maximum system throughput. (L1:QPSK, L2:16QAM, L3:64QAM)

receiver in a NOMA cluster to enhance transmission efficiency.

A comparison between Figure 5.3 (b, d) reveals the effects of varying initial PA settings on users in identical channel conditions QoS requirement. In Figure 5.3 (b), the system achieves its best PA $(-2, -8)\ dB$, starting from an initial PA of $(-10, -10)$ dB, in 11 iterations. Conversely, Figure 5.3 (d) reaches its ideal PA $(-3, -6)\ dB$ from a starting point of $(-15, -5)\ dB$ in 14 iterations. These observations underscore the proficiency of the proposed PA technique.

Additionally, Figure 5.3 (c) delves into the impact of power distribution on the performance of individual layers. Here, the y-axis is specifically focused on a throughput range of $(90 - 100)$ %. In this context, the process began with a pronounced power ratio for layers 2 (L2) and 3 (L3), leading to a diminished throughput for layer 1 (L1) initially. To enhance throughput, the algorithm's first step was to curtail the power for L2, which boosted L1's throughput but drastically reduced that of L2 and slightly affected L3. Subsequent iterations opted to decrease the power for L3 rather than augmenting L2's power. This strategy improved the throughput for L2 and culminated in the attainment of the optimal PA within 8 iterations.

Figure 5.4 illustrates the sustainable link duration for a user cluster during a downlink 3-NOMA transmission. Each user within the cluster adheres to either the Manhattan (Appendix A-2) or Random Waypoint (Appendix A-1) mobility model.

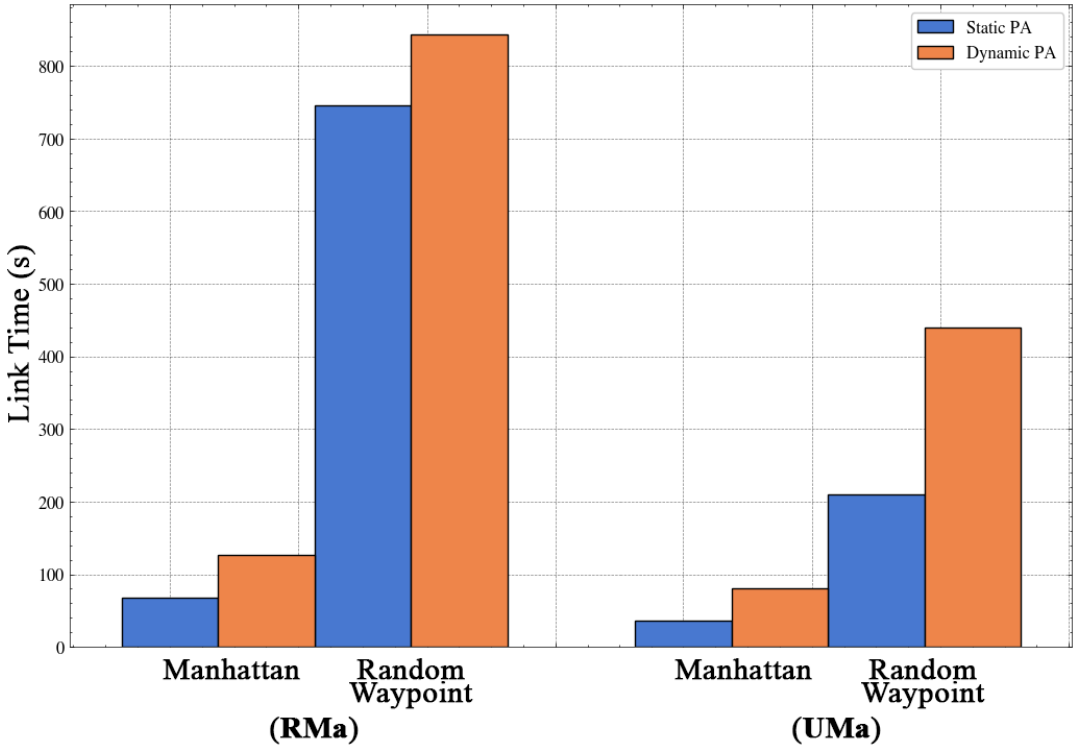

FIGURE 5.4: Comparison of downlink NOMA user pair link sustainability between fixed and proposed dynamic PA in rural and urban scenarios.

Simulations were performed considering both static and adaptive PA. All users in the cluster begin from their preset positions, distanced at (500, 300, 200) meters for u_1, u_2, u_3 respectively, and move at consistent time intervals ranging from 5 to 20 seconds, determined by their speed. Subsequent computations deduce both the surface and 3D distances between each user's location and the BS. These distances act as the bedrock to evaluate the channel SNR under specific LoS/NLoS conditions. The LoS assignment relies on a devised function, which is provided in the GitHub repository linked in Appendix A-6. The data underscores a marked improvement in link sustainability duration across both mobility models in urban and rural environments, underscoring the importance of adaptive PA in accentuating the efficacy of NOMA as a Next Generation Multiple Access (NGMA) technique.

Figure 5.5 showcases the duration of sustainable link for a 3-user NOMA cluster across varying transmission beamwidths, spanning from 10° to 120°. The beamforming initially targets the starting position of U3. For beamwidths between 10° and 20°, the sustainable link duration is almost negligible, suggesting that such constricted beamforming is not apt for mobile NOMA transmissions. From a beamwidth

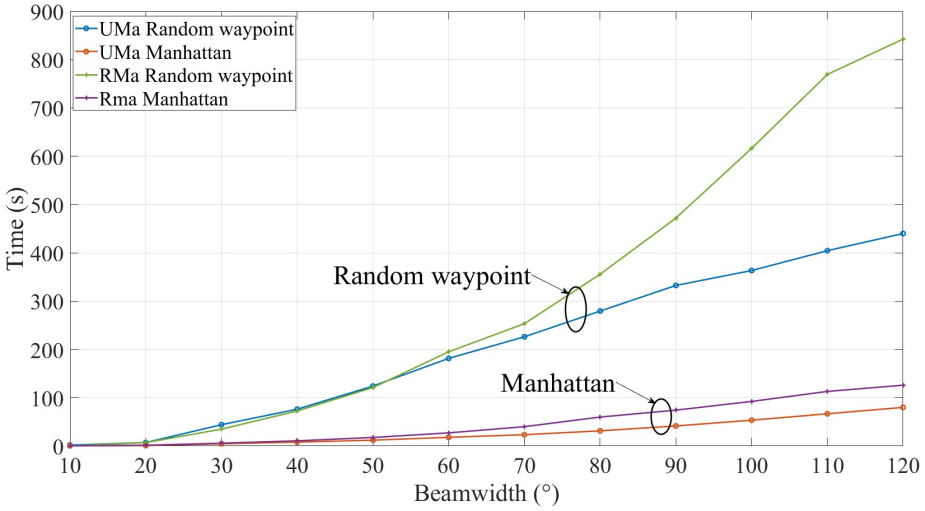

FIGURE 5.5: Impact of transmission beamwidth on link sustainability time for 3 users NOMA cluster in RMa and UMa transmission

of 20° onwards, there is a noticeable increase in sustainable link time across both mobility models and transmission zones. Predictably, the random waypoint mobility model, characterized by reduced mobility, displays an extended sustainable link duration, aligning with the observations from Figure 5.4.

When contrasting the outcomes between rural and urban settings, both environments demonstrate comparable results up to a beamwidth of 60°. Yet, when the transmission beamwidth surpasses this threshold, the sustainable link duration witnesses a more pronounced surge in rural settings. This phenomenon can be linked to diminished interference, a greater probability of LoS connections, and subsequently, reduced path loss in rural regions.

5.5 Summary

5.5.1 Contributions

This chapter has explored the significant challenges associated with maintaining user link sustainability in 5G NOMA systems. To tackle these challenges, optimization algorithms focusing on downlink N-NOMA transmission were developed. The PA technique was thoroughly evaluated under both static and dynamic channel conditions. Employing sophisticated mobility models within a 5G-compliant physical

layer simulator, the results revealed substantial improvements in link sustainability. These enhancements were evident in various deployment scenarios, and also positively impacted other key QoS metrics, such as convergence time.

5.5.2 Limitations

The PA algorithm utilizes BER to assess the quality of transmission, and adjust power ratio accordingly. However, BER is not typically available in real transmission systems. The algorithm can be adjusted to work with transmission quality index or other available parameters. Yet, the extent of potential performance loss due to the absence of BER feedback has not been explored in this study. Future work will involve substituting BER with an available feedback parameter to enable more precise analysis.

5.5.3 Future Work

The outcome of this chapter shows considerable promise in developing comprehensive resource allocation strategies for N-NOMA, taking into account pivotal network parameters such as PA, data rate, and NOMA layer reallocation. These elements are fundamental in fine-tuning the performance of NOMA, yet they present substantial challenges, particularly under dynamic channel conditions and varying receiver mobility. A critical aspect for further exploration is the latency issue, which currently limits the deployment of highly accurate algorithms due to their need for prolonged optimization times. Addressing the intricate, non-convex problem of simultaneously meeting all receiver QoS requirements is anticipated to significantly broaden the applicability and effectiveness of NOMA in a diverse array of service delivery scenarios and applications.

Chapter 6

Conclusion and Future Research Directions

6.1 Research Summary

This thesis delved deep into the world of wireless communication, exploring the exciting potential of NOMA. Think of NOMA as a super-efficient way to handle radio signals, promising to be a game-changer for our future communication systems. Many researchers, before me, had highlighted how fantastic this system could be, especially when compared to its older sibling, OMA. Some even went a step further, integrating a version of it into broadcast standards. But as the exploration went deeper, some challenges were noticed, especially when trying to make it work seamlessly with the newest 5G technologies. Despite its promise, getting NOMA to work perfectly in real-world scenarios is not straightforward. Think of it as having a supercar but not having the right roads to drive it on yet. The big goal? To create a wireless system that brings out the best in NOMA while working harmoniously with 5G's advanced features. As this journey wraps up, it becomes clear that the task ahead is to bridge the gap between the awesome potential of NOMA and the practical realities of current technologies.

Chapter 3 delved into the intricacies of the LDM-OFDM system model, emphasizing its compatibility with IoT and UE. The consistency of the analytical models with simulations across different QAM configurations was confirmed, though the model uses a fixed power ratio based on QAM order. A surface positioning model

was also introduced to monitor receiver movement, calculating key metrics like distance to the BS and the angle of transmission. This data aids in assessing the SNR at the receiver. Based on the model evaluations, an adaptive PA was developed to adjust the power ratio between the layers to changing UE channel conditions. This adaptability is crucial for the EL's sensitivity to channel variations. The model is developed further to incorporate IoT mobility. Additionally, the derived simulation model incorporated Random waypoint, Manhattan, and Freeway mobility pattern for evaluation. These comparisons highlighted the benefits of varying beam widths based on receiver positioning and provided insights for future research.

Chapter 4 presents a novel 5G NR-compliant NOMA design, which has significant implications for wireless communication research. Central to this design is its efficient integration of N-NOMA in the transceiver framework. This configuration allows for an exhaustive performance evaluation, encompassing a broad set of parameters. The chapter undertakes a detailed analysis of various components, including MIMO precoding, modulation schemes, and coding rates. This analysis provides a renewed understanding of non-orthogonal access technology, clarifying overlooked areas and addressing extant gaps in the literature. A marked departure from traditional practices is the replacement of multi-layer sequential combiners with a more efficient one-shot N-NOMA multiplexing method. This change, necessitated by the need to reduce transmission latency and to simplify the architecture of the transceiver, represents a significant development. Furthermore, the chapter introduces a refined BER expression adept at assessing both residual and non-residual errors in N-NOMA layers. Validating these theoretical perspectives, simulations conducted using a 5G NR-compliant link level simulator are incorporated. These results underscore the robustness of the proposed design and demonstrate the potential of N-NOMA to serve a wider user base.

Chapter 5 ventures into the intricate domain of user link sustainability in 5G NOMA systems, spotlighting its inherent challenges. In response to these hurdles, the chapter introduces tailored optimization algorithms with a keen emphasis on downlink N-NOMA transmission. The potency of the PA technique is brought under the lens, evaluated across both static and dynamic channel landscapes. Leveraging sophisticated mobility models implemented within a 5G-compliant physical

layer simulator, the results paint a promising picture. They indicate significant advancements in link sustainability and other paramount QoS indicators, including convergence time across diverse channel conditions. It is important to acknowledge that these advancements require extra feedback and control data for both transmission and reception. However, the promising aspect is their capability to be smoothly integrated within existing channels.

Throughout this research journey, the focus has been on pushing the boundaries of wireless communication, particularly in the realm of 5G NOMA systems. From an in-depth analysis of the LDM-OFDM system in Chapter 3, laying the foundation for understanding the interface between IoT and UE, to the unveiling of an innovative 5G NR-compliant NOMA design in Chapter 4, the narrative is one of exploration and innovation. Chapter 5 then grapples with the tangible challenges of user link sustainability, offering optimization strategies to enhance downlink N-NOMA transmission. Collectively, this work underscores a committed quest for knowledge, aiming to usher in advancements that could reshape the future of wireless communications.

6.2 Research Objective Achievements

The achievements regarding the research objectives mentioned in chapter 1 is as follow:

1. **Investigate LDM-OFDM Framework:** This objective has been successfully met by developing a transceiver model tailored for both IoT devices and regular users. Through rigorous testing, it was observed that the CL layer performs efficiently in low-data-rate transmissions, requiring approximately 15 dB less SNR. In contrast, the EL layer excels in delivering high-data-rate services. The results affirm the feasibility of LDM for meeting diverse communication needs, making it a promising solution for the heterogeneous requirements of future IoT and user scenarios.

2. **Develop & Evaluate N-NOMA-5G Transceiver** The N-NOMA-5G transceiver was successfully developed and evaluated, aligning with 3GPP standards. The

optimized architecture showed a marked improvement in performance under low SNR conditions. Specifically, it needed 60% less SNR to achieve comparable BER rates with existing models. A new one-shot multiplexing technique was implemented, reducing the processing time by 52%. This is particularly significant as the number of NOMA layers increases, underscoring the architecture's scalability and efficiency.

3. **Formulate Analytical Models:** The objective of formulating analytical models was met by successfully deriving specialized BER expressions for both CL and N-NOMA. In the case of CL, the model accounts for LL interference, providing highly accurate predictions for various power ratios and receiver mobility conditions. In the context of N-NOMA, the BER model considered both UL (residual) and LL (non-residual) interference effects on performance. These models demonstrated over 90% accuracy when compared to transmission simulation results, validating their reliability for real-world applications.

4. **Assess Mobility Impact for Unicast Transmission:** The objective to assess the impact of receiver mobility on unicast transmission was successfully addressed. A novel surface mobility system was developed to evaluate the influence of mobility on IoT-user pair connectivity across different types of environments: urban, rural, and motorway. Findings indicated that IoT movement emerged as the primary factor, contributing to about 70% of all link terminations. This underscores the need for effective mobility management strategies for maintaining IoT connectivity. Additionally, the study went a step further to introduce a 3D mobility model consistent with 3GPP standards. This model provided deeper insights into the varying mobility patterns that could be encountered in both urban and rural scenarios, thereby broadening the scope of our understanding of mobility impact on unicast transmissions.

5. **Optimize PA:** The objective to optimize PA was effectively achieved through the development of an adaptive PA strategy. Utilizing a greedy algorithm that operates on real-time feedback from the receiver, this strategy showed marked improvements in NOMA cluster sustainability. For mobile users, the algorithm led to an impressive 40% enhancement in link sustainability, making it

significantly more robust against changing conditions. Furthermore, for static users, the system was able to quickly converge to the optimal PA settings, doing so within 12 iterations.

6.3 Research Limitations

This study acknowledges the following limitations regarding the developed models and techniques:

1. The N-NOMA BER analytical model is constructed based on the assumption that both residual and non-residual interferences adhere to a Gaussian distribution. This simplification may not account for other potential interference patterns and their impacts.

2. The current model does not factor in gains from channel coding. Such gains could notably enhance the BER and diminish the occurrence of residual error events. This could lead to underestimations of system performance in real-world applications where channel coding is implemented.

3. The analytical model operates under a worst-case scenario during events of imperfect SIC. Specifically, it assumes that the transmitted QAM symbol and the erroneously decoded QAM symbol are diagonally opposite end. This approach is designed to capture the upper bound of interference but may not always be representative of typical interference events.

4. While the developed PA technique adjusts the power ratio with incremental or decremental units, a more dynamic method could be adopted. Predicting and applying the optimal power ratio, rather than relying on gradual shifts, could enhance system sustainability and reduce initial connection establishment time.

6.4 Future Work

Enhancing NOMA Receiver Design in the 5G Transceiver Model

While this study has significantly optimized the transmitter design, there remains a considerable challenge in the domain of NOMA: the design complexity of low-power, low-latency transmission receivers. This stems from the prevailing SIC technique. Current methodologies demand the lower NOMA layer receiver to sequentially decode all the UL symbols, systematically eliminating the interference of successive ULs. Consequently, this process not only is power-intensive, but also time-consuming. Additionally, receivers must provision buffers for the incoming NOMA signals. A more streamlined, one-shot detection technique could greatly amplify NOMA's potential across diverse service deliveries. In the next phase of research following the completion of the PhD, the focus will be on delving deeper into exploring alternative interference cancellation strategies for NOMA, with particular emphasis on varied clustering techniques.

Augmenting the Analytical Model

Another key focus of the upcoming research is the refinement of the analytical model. The goal is to formulate a model that quantifies error reduction potential, correlating it with the LDPC coding rate. Achieving this would facilitate its integration into the existing analytical framework, further incorporating the impact of the coding rate. Moreover, there is a vision to refine the model to estimate anticipated residual interference instead of the existing maximal residual interference, aiming to enhance its precision.

Reinforcing NOMA Link Sustainability and User Fairness through Advanced Resource Allocation

The advancements made in link sustainability through the proposed method set the stage for detailed resource allocation strategies specifically designed for N-NOMA.

The task of enhancing NOMA's performance regarding user fairness involves adjusting reconfigurable network parameters: PA, data rate (determined by modulation scheme), and allocations within the NOMA layers. Crafting an optimal NOMA setup, especially in the face of dynamic channel conditions and receiver mobility, stands out as a significant challenge in bolstering NOMA link robustness. However, the intricate interactions among these parameters and their collective impact on NOMA's effectiveness are riddled with complexities. Furthermore, given the emphasis on minimizing latency, it is crucial to avoid algorithms that entail extended optimization durations. Balancing all these intricacies while ensuring each receiver's QoS requirements are fulfilled represents a multifaceted, non-convex issue. Tackling these challenges calls for rigorous research, and the findings might prove instrumental in shaping the future trajectory of NOMA in wireless ecosystems.

Appendix A

GitHub Repositories

1. **Random Waypoint Mobility Model**: GitHub Link
2. **Manhattan Mobility Model**: GitHub Link
3. **Freeway Mobility Model**: GitHub Link
4. **One-Shot NOMA Multiplexer**: GitHub Link
5. **Dynamic Power Allocation**:GitHub Link
6. **LOS Decision Simulator**: GitHub Link
7. **5G N-NOMA Simulator for Mobile user**: GitHub Link

Bibliography

[1] J. A. Adebusola, A. A. Ariyo, O. A. Elisha, A. M. Olubunmi, and O. O. Julius, "An overview of 5G technology," in *2020 International Conference in Mathematics, Computer Engineering and Computer Science (ICMCECS)*. IEEE, 2020, pp. 1–4.

[2] S. Mattisson, "Overview of 5G requirements and future wireless networks," in *ESSCIRC 2017-43rd IEEE European Solid State Circuits Conference*. IEEE, 2017, pp. 1–6.

[3] X. Lin, "An overview of 5G advanced evolution in 3GPP release 18," *IEEE Communications Standards Magazine*, vol. 6, no. 3, pp. 77–83, 2022.

[4] H. Fourati, R. Maaloul, and L. Chaari, "A survey of 5G network systems: challenges and machine learning approaches," *International Journal of Machine Learning and Cybernetics*, vol. 12, pp. 385–431, 2021.

[5] Ericsson. (2022) Ericsson mobility report q2 2022 update. [accessed May 2023]. [Online]. Available: https://www.ericsson.com/4a4be7/assets/local/reports-papers/mobility-report/documents/2022/ericsson-mobility-report-q2-2022.pdf

[6] W. H. Chin, Z. Fan, and R. Haines, "Emerging technologies and research challenges for 5G wireless networks," *IEEE Wireless Communications*, vol. 21, no. 2, pp. 106–112, 2014.

[7] M. Abd-Elnaby, G. G. Sedhom, E.-S. M. El-Rabaie, and M. Elwekeil, "NOMA for 5G and beyond: literature review and novel trends," *Wireless Networks*, vol. 29, no. 4, pp. 1629–1653, 2023.

[8] Cisco. (2023) Annual internet report. [accessed June 2023]. [Online]. Available: https://www.cisco.com/c/en/us/solutions/collateral/executive-perspectives/annual-internet-report/white-paper-c11-741490.html

[9] G. Flagship. 6g flagship. [accessed July 2023]. [Online]. Available: https://www.6gflagship.com/

[10] L. Dai, B. Wang, Z. Ding, Z. Wang, S. Chen, and L. Hanzo, "A survey of non-orthogonal multiple access for 5G," *IEEE communications surveys & tutorials*, vol. 20, no. 3, pp. 2294–2323, 2018.

[11] S. Han, T. Xie, and I. Chih-Lin, "Greener physical layer technologies for 6g mobile communications," *IEEE Communications Magazine*, vol. 59, no. 4, pp. 68–74, 2021.

[12] Y. Liu, S. Zhang, X. Mu, Z. Ding, R. Schober, N. Al-Dhahir, E. Hossain, and X. Shen, "Evolution of NOMA toward next generation multiple access (NGMA) for 6G," *IEEE Journal on Selected Areas in Communications*, vol. 40, no. 4, pp. 1037–1071, 2022.

[13] Y. Saito, Y. Kishiyama, A. Benjebbour, T. Nakamura, A. Li, and K. Higuchi, "Non-orthogonal multiple access (NOMA) for cellular future radio access," in *2013 IEEE 77th vehicular technology conference (VTC Spring)*. IEEE, 2013, pp. 1–5.

[14] L. Zhang, W. Li, Y. Wu, Y. Xue, E. Sousa, S.-I. Park, J.-Y. Lee, N. Hur, and H.-M. Kim, "Using non-orthogonal multiplexing in 5G-MBMS to achieve broadband-broadcast convergence with high spectral efficiency," *IEEE Transactions on Broadcasting*, 2020.

[15] E. Iradier, J. Montalban, L. Fanari, P. Angueira, L. Zhang, Y. Wu, and W. Li, "Using NOMA for enabling broadcast/unicast convergence in 5G networks," *IEEE Transactions on Broadcasting*, 2020.

[16] Y. Xue, A. Alsohaily, E. Sousa, W. Li, L. Zhang, and Y. Wu, "Using layered division multiplexing for mixed unicast-broadcast service delivery in 5G," in *2019*

IEEE International Symposium on Broadband Multimedia Systems and Broadcasting (BMSB). IEEE, 2019, pp. 1–6.

[17] Z. Ding, P. Fan, and H. V. Poor, "Impact of user pairing on 5G nonorthogonal multiple-access downlink transmissions," *IEEE Transactions on Vehicular Technology*, vol. 65, no. 8, pp. 6010–6023, 2015.

[18] L. Zhang, W. Li, Y. Wu, K. Salehian, S. Laflèche, Z. Hong, S.-I. Park, H. M. Kim, J.-Y. Lee, N. Hur *et al.*, "Using layered-division-multiplexing to deliver multi-layer mobile services in ATSC 3.0," *IEEE Transactions on Broadcasting*, vol. 65, no. 1, pp. 40–52, 2018.

[19] E. Iradier, A. Abuin, R. Cabrera, I. Bilbao, J. Montalban, P. Angueira, S. Kwon, N. Hur, and S.-I. Park, "Advanced NOMA-based RRM schemes for broadcasting in 5G mmwave frequency bands," *IEEE Transactions on Broadcasting*, vol. 68, no. 1, pp. 143–155, 2021.

[20] S. Ahn, S.-I. Park, J.-Y. Lee, N. Hur, Y. Wu, L. Zhang, W. Li, and J. Kim, "Large-scale network analysis on NOMA-aided broadcast/unicast joint transmission scenarios considering content popularity," *IEEE Transactions on Broadcasting*, vol. 66, no. 4, pp. 770–785, 2020.

[21] 3rd Generation Partnership Project, "Study on non-orthogonal multiple access (NOMA) for NR (release 16)," Technical Specification Group Radio Access Network, Technical Report 3GPP TR 38.812 V16.0.0, 2018. [Online]. Available: https://portal.3gpp.org/desktopmodules/Specifications/SpecificationDetails.aspx?specificationId=3236

[22] Z. Zhang, Y. Xiao, Z. Ma, M. Xiao, Z. Ding, X. Lei, G. K. Karagiannidis, and P. Fan, "6G wireless networks: Vision, requirements, architecture, and key technologies," *IEEE Vehicular Technology Magazine*, vol. 14, no. 3, pp. 28–41, 2019.

[23] C.-X. Wang, X. You, X. Gao, X. Zhu, Z. Li, C. Zhang, H. Wang, Y. Huang, Y. Chen, H. Haas *et al.*, "On the road to 6G: Visions, requirements, key technologies and testbeds," *IEEE Communications Surveys & Tutorials*, 2023.

[24] M. Z. Chowdhury, M. Shahjalal, S. Ahmed, and Y. M. Jang, "6G wireless communication systems: Applications, requirements, technologies, challenges, and research directions," *IEEE Open Journal of the Communications Society*, vol. 1, pp. 957–975, 2020.

[25] K. David and H. Berndt, "6g vision and requirements: Is there any need for beyond 5g?" *IEEE vehicular technology magazine*, vol. 13, no. 3, pp. 72–80, 2018.

[26] H. Tataria, M. Shafi, A. F. Molisch, M. Dohler, H. Sjöland, and F. Tufvesson, "6G wireless systems: Vision, requirements, challenges, insights, and opportunities," *Proceedings of the IEEE*, vol. 109, no. 7, pp. 1166–1199, 2021.

[27] Y. Liu, Z. Qin, M. Elkashlan, Z. Ding, A. Nallanathan, and L. Hanzo, "Nonorthogonal multiple access for 5G and beyond," *Proceedings of the IEEE*, vol. 105, no. 12, pp. 2347–2381, 2017.

[28] Z. Ding, Y. Liu, J. Choi, Q. Sun, M. Elkashlan, I. Chih-Lin, and H. V. Poor, "Application of non-orthogonal multiple access in LTE and 5G networks," *IEEE Communications Magazine*, vol. 55, no. 2, pp. 185–191, 2017.

[29] S. R. Islam, N. Avazov, O. A. Dobre, and K.-S. Kwak, "Power-domain non-orthogonal multiple access (NOMA) in 5G systems: Potentials and challenges," *IEEE Communications Surveys & Tutorials*, vol. 19, no. 2, pp. 721–742, 2016.

[30] S.-I. Park, J.-Y. Lee, B.-M. Lim, S. Kwon, J.-H. Seo, H. M. Kim, N. Hur, and J. Kim, "Field comparison tests of LDM and tdm in ATSC 3.0," *IEEE Transactions on Broadcasting*, vol. 64, no. 3, pp. 637–647, 2018.

[31] C. Regueiro, J. Montalban, J. Barrueco, M. Velez, P. Angueira, Y. Wu, L. Zhang, S.-I. Park, J.-Y. Lee, and H. M. Kim, "LDM core services performance in ATSC 3.0," *IEEE Transactions on Broadcasting*, vol. 62, no. 1, pp. 244–252, 2016.

[32] M. Earnshaw, K. Shelby, H. Lee, Y. Oh, and M. Simon, "Physical layer framing for ATSC 3.0," *IEEE Transactions on Broadcasting*, vol. 62, no. 1, pp. 263–270, 2016.

[33] X. Xu, Y. Liu, X. Mu, Q. Chen, H. Jiang, and Z. Ding, "Artificial intelligence enabled NOMA toward next generation multiple access," *IEEE Wireless Communications*, vol. 30, no. 1, pp. 86–94, 2023.

[34] G. Wunder, P. Jung, M. Kasparick, T. Wild, F. Schaich, Y. Chen, S. Ten Brink, I. Gaspar, N. Michailow, A. Festag *et al.*, "5GNOW: non-orthogonal, asynchronous waveforms for future mobile applications." *IEEE Communications Magazine*, vol. 52, no. 2, pp. 97–105, 2014.

[35] Y. Liu, W. Yi, Z. Ding, X. Liu, O. A. Dobre, and N. Al-Dhahir, "Developing NOMA to next generation multiple access: Future vision and research opportunities," *IEEE Wireless Communications*, 2022.

[36] L. Dai, B. Wang, Y. Yuan, S. Han, I. Chih-Lin, and Z. Wang, "Non-orthogonal multiple access for 5G: solutions, challenges, opportunities, and future research trends," *IEEE Communications Magazine*, vol. 53, no. 9, pp. 74–81, 2015.

[37] J. P. Lemayian and J. M. Hamamreh, "Recurrent neural network-based channel prediction in mMIMO for enhanced performance in future wireless communication," in *2020 International Conference on UK-China Emerging Technologies (UCET)*. IEEE, 2020, pp. 1–4.

[38] B. Clerckx, Y. Mao, R. Schober, E. A. Jorswieck, D. J. Love, J. Yuan, L. Hanzo, G. Y. Li, E. G. Larsson, and G. Caire, "Is NOMA efficient in multi-antenna networks? a critical look at next generation multiple access techniques," *IEEE Open Journal of the Communications Society*, vol. 2, pp. 1310–1343, 2021.

[39] M. Cheng, W. Lin, and T. Matsumoto, "Down-link NOMA with successive refinement for binary symmetric source transmission," *IEEE Transactions on Communications*, vol. 68, no. 12, pp. 7927–7937, 2020.

[40] A. Maatouk, M. Assaad, and A. Ephremides, "Minimizing the age of information: NOMA or OMA?" in *IEEE INFOCOM 2019-IEEE Conference on Computer Communications Workshops (INFOCOM WKSHPS)*. IEEE, 2019, pp. 102–108.

[41] Z. Chen, Z. Ding, X. Dai, and R. Zhang, "An optimization perspective of the superiority of NOMA compared to conventional OMA," *IEEE Transactions on Signal Processing*, vol. 65, no. 19, pp. 5191–5202, 2017.

[42] Z. Wei, J. Guo, D. W. K. Ng, and J. Yuan, "Fairness comparison of uplink NOMA and OMA," in *2017 IEEE 85th vehicular technology conference (VTC Spring)*. IEEE, 2017, pp. 1–6.

[43] Z. Wei, L. Yang, D. W. K. Ng, J. Yuan, and L. Hanzo, "On the performance gain of NOMA over OMA in uplink communication systems," *IEEE Transactions on Communications*, vol. 68, no. 1, pp. 536–568, 2019.

[44] J. Ghosh, I.-H. Ra, S. Singh, H. Haci, K. A. Al-Utaibi, and S. M. Sait, "On the comparison of optimal NOMA and OMA in a paradigm shift of emerging technologies," *IEEE Access*, vol. 10, pp. 11 616–11 632, 2022.

[45] M. Zeng, A. Yadav, O. A. Dobre, G. I. Tsiropoulos, and H. V. Poor, "On the sum rate of MIMO-NOMA and MIMO-OMA systems," *IEEE Wireless communications letters*, vol. 6, no. 4, pp. 534–537, 2017.

[46] Y. Saito, A. Benjebbour, Y. Kishiyama, and T. Nakamura, "System-level performance evaluation of downlink non-orthogonal multiple access (NOMA)," in *2013 IEEE 24th Annual International Symposium on Personal, Indoor, and Mobile Radio Communications (PIMRC)*. IEEE, 2013, pp. 611–615.

[47] Y. Cai, Z. Qin, F. Cui, G. Y. Li, and J. A. McCann, "Modulation and multiple access for 5G networks," *IEEE Communications Surveys & Tutorials*, vol. 20, no. 1, pp. 629–646, 2017.

[48] S. Islam, M. Zeng, and O. A. Dobre, "NOMA in 5G systems: Exciting possibilities for enhancing spectral efficiency," *arXiv preprint arXiv:1706.08215*, 2017.

[49] Y. Zhang, H. Cao, M. Zhou, and L. Yang, "Spectral efficiency maximization for uplink cell-free massive MIMO-NOMA networks," in *2019 IEEE International Conference on Communications Workshops (ICC Workshops)*. IEEE, 2019, pp. 1–6.

[50] A. Benjebbour, K. Saito, A. Li, Y. Kishiyama, and T. Nakamura, "Non-orthogonal multiple access (NOMA): concept and design," *Signal processing for 5G: Algorithms and implementations*, pp. 143–168, 2016.

[51] X. Chen, A. Benjebbour, A. Li, and A. Harada, "Multi-user proportional fair scheduling for uplink non-orthogonal multiple access (NOMA)," in *2014 IEEE 79th Vehicular Technology Conference (VTC Spring)*. IEEE, 2014, pp. 1–5.

[52] A. Li, Y. Lan, X. Chen, and H. Jiang, "Non-orthogonal multiple access (NOMA) for future downlink radio access of 5G," *China Communications*, vol. 12, no. Supplement, pp. 28–37, 2015.

[53] K. Wang, T. Zhou, T. Xu, H. Hu, and X. Tao, "Asymmetric adaptive modulation for uplink NOMA systems," *IEEE Transactions on Communications*, vol. 69, no. 11, pp. 7222–7235, 2021.

[54] M. S. Ali, H. Tabassum, and E. Hossain, "Dynamic user clustering and power allocation for uplink and downlink non-orthogonal multiple access (NOMA) systems," *IEEE access*, vol. 4, pp. 6325–6343, 2016.

[55] Y. Xu, G. Wang, B. Li, and S. Jia, "Performance of D2D aided uplink coordinated direct and relay transmission using NOMA," *IEEE Access*, vol. 7, pp. 151 090–151 102, 2019.

[56] M. Ganji, X. Zou, and H. Jafarkhani, "Asynchronous transmission for multiple access channels: Rate-region analysis and system design for uplink NOMA," *IEEE Transactions on Wireless Communications*, vol. 20, no. 7, pp. 4364–4378, 2021.

[57] L. Zhang, J. Liu, M. Xiao, G. Wu, Y.-C. Liang, and S. Li, "Performance analysis and optimization in downlink NOMA systems with cooperative full-duplex relaying," *IEEE Journal on Selected Areas in Communications*, vol. 35, no. 10, pp. 2398–2412, 2017.

[58] H. Tabassum, M. S. Ali, E. Hossain, M. J. Hossain, and D. I. Kim, "Uplink vs. downlink noma in cellular networks: Challenges and research directions," in

2017 IEEE 85th vehicular technology conference (VTC Spring). IEEE, 2017, pp. 1–7.

[59] S. R. Islam, M. Zeng, O. A. Dobre, and K.-S. Kwak, "Resource allocation for downlink NOMA systems: Key techniques and open issues," *IEEE Wireless Communications*, vol. 25, no. 2, pp. 40–47, 2018.

[60] F. Fang, J. Cheng, and Z. Ding, "Joint energy efficient subchannel and power optimization for a downlink NOMA heterogeneous network," *IEEE Transactions on Vehicular Technology*, vol. 68, no. 2, pp. 1351–1364, 2018.

[61] X. Zhang and M. Haenggi, "The performance of successive interference cancellation in random wireless networks," *IEEE Transactions on Information Theory*, vol. 60, no. 10, pp. 6368–6388, 2014.

[62] K. Higuchi and A. Benjebbour, "Non-orthogonal multiple access (NOMA) with successive interference cancellation for future radio access," *IEICE Transactions on Communications*, vol. 98, no. 3, pp. 403–414, 2015.

[63] Z. Ding, R. Schober, and H. V. Poor, "Unveiling the importance of SIC in NOMA systems—part 1: State of the art and recent findings," *IEEE Communications Letters*, vol. 24, no. 11, pp. 2373–2377, 2020.

[64] T. Manglayev, R. C. Kizilirmak, Y. H. Kho, N. Bazhayev, and I. Lebedev, "NOMA with imperfect SIC implementation," in *IEEE EUROCON 2017-17th International Conference on Smart Technologies*. IEEE, 2017, pp. 22–25.

[65] M. S. Islam, R. Abozariba, D. Mi, M. Patwary, D. He, and A. T. Asyhari, "Design and evaluation of multi-layer NOMA on NR physical layer for 5G and beyond," *IEEE Transactions on Broadcasting*, pp. 1–15, 2023.

[66] S. Gamal, M. Rihan, S. Hussin, A. Zaghloul, and A. A. Salem, "Multiple access in cognitive radio networks: From orthogonal and non-orthogonal to rate-splitting," *IEEE Access*, vol. 9, pp. 95 569–95 584, 2021.

[67] L. Zhu, J. Zhang, Z. Xiao, X. Cao, and D. O. Wu, "Optimal user pairing for downlink non-orthogonal multiple access (NOMA)," *IEEE Wireless Communications Letters*, vol. 8, no. 2, pp. 328–331, 2018.

[68] S. Rezvani, E. A. Jorswieck, R. Joda, and H. Yanikomeroglu, "Optimal power allocation in downlink multicarrier NOMA systems: Theory and fast algorithms," *IEEE Journal on Selected Areas in Communications*, vol. 40, no. 4, pp. 1162–1189, 2022.

[69] I.-H. Lee and H. Jung, "User selection and power allocation for downlink NOMA systems with quality-based feedback in rayleigh fading channels," *IEEE Wireless Communications Letters*, vol. 9, no. 11, pp. 1924–1927, 2020.

[70] J. Wang, B. Xia, K. Xiao, and Z. Chen, "Performance analysis and power allocation strategy for downlink NOMA systems in large-scale cellular networks," *IEEE Transactions on Vehicular Technology*, vol. 69, no. 3, pp. 3459–3464, 2020.

[71] Y. Zhang, X. Zhao, S. Geng, Z. Zhou, P. Qin, L. Zhang, and L. Yang, "Power allocation algorithms for stable successive interference cancellation in millimeter wave NOMA systems," *IEEE Transactions on Vehicular Technology*, vol. 70, no. 6, pp. 5833–5847, 2021.

[72] L. Pang, W. Wu, Y. Zhang, Y. Yuan, Y. Chen, A. Wang, and J. Li, "Joint power allocation and hybrid beamforming for downlink mmwave-NOMA systems," *IEEE Transactions on Vehicular Technology*, vol. 70, no. 10, pp. 10 173–10 184, 2021.

[73] M. Liaqat, K. A. Noordin, T. Abdul Latef, and K. Dimyati, "Power-domain non orthogonal multiple access (PD-NOMA) in cooperative networks: an overview," *Wireless Networks*, vol. 26, pp. 181–203, 2020.

[74] P. N. Thakre and S. B. Pokle, "A survey on power allocation in pd-noma for 5g wireless communication systems," in *2022 10th International Conference on Emerging Trends in Engineering and Technology-Signal and Information Processing (ICETET-SIP-22)*. IEEE, 2022, pp. 1–5.

[75] A. Al Khansa, Y. Yin, G. Gui, and H. Sari, "Power-domain NOMA or NOMA-2000?" in *2019 25th Asia-Pacific Conference on Communications (APCC)*. IEEE, 2019, pp. 336–341.

[76] Z. Liu and L.-L. Yang, "Sparse or dense: A comparative study of code-domain NOMA systems," *IEEE Transactions on Wireless Communications*, vol. 20, no. 8, pp. 4768–4780, 2021.

[77] C. Chen, Y. Yang, X. Deng, P. Du, H. Yang, Z. Chen, and W.-D. Zhong, "NOMA for MIMO visible light communications: A spatial domain perspective," in *2019 IEEE Global Communications Conference (GLOBECOM)*. IEEE, 2019, pp. 1–6.

[78] A. Yadav, C. Quan, P. K. Varshney, and H. V. Poor, "On performance comparison of multi-antenna HD-NOMA, SCMA, and PD-NOMA schemes," *IEEE Wireless Communications Letters*, vol. 10, no. 4, pp. 715–719, 2020.

[79] S. I. Park, Y. Wu, L. Zhang, J. Montalban, J.-Y. Lee, P. Angueira, S. Kwon, H. M. Kim, N. Hur, and J. Kim, "Low complexity layered division multiplexing system for the next generation terrestrial broadcasting," in *2015 IEEE International Symposium on Broadband Multimedia Systems and Broadcasting*. IEEE, 2015, pp. 1–3.

[80] Y. Wu, B. Rong, K. Salehian, and G. Gagnon, "Cloud transmission: A new spectrum-reuse friendly digital terrestrial broadcasting transmission system," *IEEE Transactions on Broadcasting*, vol. 58, no. 3, pp. 329–337, 2012.

[81] L. Zhang, W. Li, Y. Wu, X. Wang, S.-I. Park, H. M. Kim, J.-Y. Lee, P. Angueira, and J. Montalban, "Layered-division-multiplexing: Theory and practice," *IEEE Transactions on Broadcasting*, vol. 62, no. 1, pp. 216–232, 2016.

[82] D. Gómez-Barquero and O. Simeone, "LDM versus FDM/TDM for unequal error protection in terrestrial broadcasting systems: An information-theoretic view," *IEEE Transactions on Broadcasting*, vol. 61, no. 4, pp. 571–579, 2015.

[83] H. Kim, J. Kim, S.-I. Park, J.-y. Lee, S. Kwon, and N. Hur, "Capacity analysis and improvement of ldm-based Multiple-PLP configurations in ATSC 3.0," *IEEE Transactions on Broadcasting*, 2021.

[84] L. Zhang, Y. Wu, W. Li, H. M. Kim, S.-I. Park, P. Angueira, J. Montalban, and M. Velez, "Channel capacity distribution of layer-division-multiplexing system for next generation digital broadcasting transmission," in *2014 IEEE International Symposium on Broadband Multimedia Systems and Broadcasting*. IEEE, 2014, pp. 1–6.

[85] L. Zhang, Y. Wu, W. Li, K. Salehian, S. Lafleche, X. Wang, S. I. Park, H. M. Kim, J.-y. Lee, N. Hur *et al.*, "Layered-division multiplexing: An enabling technology for multicast/broadcast service delivery in 5G," *IEEE Communications Magazine*, vol. 56, no. 3, pp. 82–90, 2018.

[86] J. Zhao, O. Simeone, D. Gunduz, and D. Gómez-Barquero, "Non-orthogonal unicast and broadcast transmission via joint beamforming and LDM in cellular networks," in *2016 IEEE Global Communications Conference (GLOBECOM)*. IEEE, 2016, pp. 1–6.

[87] Y. Liu, Z. Qin, Y. Cai, Y. Gao, G. Y. Li, and A. Nallanathan, "UAV communications based on non-orthogonal multiple access," *IEEE Wireless Communications*, vol. 26, no. 1, pp. 52–57, 2019.

[88] S. Zhang, Y. Zeng, and R. Zhang, "Cellular-enabled UAV communication: A connectivity-constrained trajectory optimization perspective," *IEEE Transactions on Communications*, vol. 67, no. 3, pp. 2580–2604, 2018.

[89] W. Yi, Y. Liu, E. Bodanese, A. Nallanathan, and G. K. Karagiannidis, "A unified spatial framework for UAV-aided mmwave networks," *IEEE Transactions on Communications*, vol. 67, no. 12, pp. 8801–8817, 2019.

[90] T. Hou, Y. Liu, Z. Song, X. Sun, and Y. Chen, "Exploiting NOMA for UAV communications in large-scale cellular networks," *IEEE Transactions on Communications*, vol. 67, no. 10, pp. 6897–6911, 2019.

[91] X. Mu, Y. Liu, L. Guo, J. Lin, and Z. Ding, "Energy-constrained UAV data collection systems: NOMA and OMA," *IEEE Transactions on Vehicular Technology*, vol. 70, no. 7, pp. 6898–6912, 2021.

[92] W. Mei and R. Zhang, "Uplink cooperative NOMA for cellular-connected UAV," *IEEE Journal of Selected Topics in Signal Processing*, vol. 13, no. 3, pp. 644–656, 2019.

[93] X. Mu, Y. Liu, L. Guo, and J. Lin, "Non-orthogonal multiple access for air-to-ground communication," *IEEE Transactions on Communications*, vol. 68, no. 5, pp. 2934–2949, 2020.

[94] Y. Liu, X. Liu, X. Gao, X. Mu, X. Zhou, O. A. Dobre, and H. V. Poor, "Robotic communications for 5g and beyond: Challenges and research opportunities," *IEEE Communications Magazine*, vol. 59, no. 10, pp. 92–98, 2021.

[95] X. Mu, Y. Liu, L. Guo, J. Lin, and R. Schober, "Intelligent reflecting surface enhanced indoor robot path planning: A radio map-based approach," *IEEE Transactions on Wireless Communications*, vol. 20, no. 7, pp. 4732–4747, 2021.

[96] X. Gao, Y. Liu, and X. Mu, "Trajectory and passive beamforming design for IRS-aided multi-robot NOMA indoor networks," in *ICC 2021-IEEE International Conference on Communications*. IEEE, 2021, pp. 1–6.

[97] N. H. Mahmood, S. Böcker, A. Munari, F. Clazzer, I. Moerman, K. Mikhaylov, O. Lopez, O.-S. Park, E. Mercier, H. Bartz *et al.*, "White paper on critical and massive machine type communication towards 6G," *arXiv preprint arXiv:2004.14146*, 2020.

[98] J.-B. Seo, B. C. Jung, and H. Jin, "Performance analysis of NOMA random access," *IEEE Communications Letters*, vol. 22, no. 11, pp. 2242–2245, 2018.

[99] Z. Ding, R. Schober, P. Fan, and H. V. Poor, "Simple semi-grant-free transmission strategies assisted by non-orthogonal multiple access," *IEEE Transactions on Communications*, vol. 67, no. 6, pp. 4464–4478, 2019.

[100] C. Zhang, Y. Liu, W. Yi, Z. Qin, and Z. Ding, "Semi-grant-free NOMA: Ergodic rates analysis with random deployed users," *IEEE Wireless Communications Letters*, vol. 10, no. 4, pp. 692–695, 2020.

[101] Y. Mao, C. You, J. Zhang, K. Huang, and K. B. Letaief, "A survey on mobile edge computing: The communication perspective," *IEEE communications surveys & tutorials*, vol. 19, no. 4, pp. 2322–2358, 2017.

[102] Z. Ding, P. Fan, and H. V. Poor, "Impact of non-orthogonal multiple access on the offloading of mobile edge computing," *IEEE Transactions on Communications*, vol. 67, no. 1, pp. 375–390, 2018.

[103] F. Wang, J. Xu, and Z. Ding, "Multi-antenna NOMA for computation offloading in multiuser mobile edge computing systems," *IEEE Transactions on Communications*, vol. 67, no. 3, pp. 2450–2463, 2018.

[104] Z. Song, Y. Liu, and X. Sun, "Joint radio and computational resource allocation for NOMA-based mobile edge computing in heterogeneous networks," *IEEE Communications Letters*, vol. 22, no. 12, pp. 2559–2562, 2018.

[105] Y. Wu, L. P. Qian, K. Ni, C. Zhang, and X. Shen, "Delay-minimization nonorthogonal multiple access enabled multi-user mobile edge computation offloading," *IEEE Journal of Selected Topics in Signal Processing*, vol. 13, no. 3, pp. 392–407, 2019.

[106] Y. Liu, X. Liu, X. Mu, T. Hou, J. Xu, M. Di Renzo, and N. Al-Dhahir, "Reconfigurable intelligent surfaces: Principles and opportunities," *IEEE communications surveys & tutorials*, vol. 23, no. 3, pp. 1546–1577, 2021.

[107] Q. Wu, S. Zhang, B. Zheng, C. You, and R. Zhang, "Intelligent reflecting surface-aided wireless communications: A tutorial," *IEEE Transactions on Communications*, vol. 69, no. 5, pp. 3313–3351, 2021.

[108] M. Di Renzo, A. Zappone, M. Debbah, M.-S. Alouini, C. Yuen, J. De Rosny, and S. Tretyakov, "Smart radio environments empowered by reconfigurable intelligent surfaces: How it works, state of research, and the road ahead," *IEEE journal on selected areas in communications*, vol. 38, no. 11, pp. 2450–2525, 2020.

[109] Y. Liu, X. Mu, X. Liu, M. Di Renzo, Z. Ding, and R. Schober, "Reconfigurable intelligent surface-aided multi-user networks: Interplay between NOMA and RIS," *IEEE Wireless Communications*, vol. 29, no. 2, pp. 169–176, 2022.

[110] S. Zhang and R. Zhang, "Intelligent reflecting surface aided multi-user communication: Capacity region and deployment strategy," *IEEE Transactions on Communications*, vol. 69, no. 9, pp. 5790–5806, 2021.

[111] X. Mu, Y. Liu, L. Guo, J. Lin, and R. Schober, "Joint deployment and multiple access design for intelligent reflecting surface assisted networks," *IEEE Transactions on Wireless Communications*, vol. 20, no. 10, pp. 6648–6664, 2021.

[112] C. Wu, Y. Liu, X. Mu, X. Gu, and O. A. Dobre, "Coverage characterization of STAR-RIS networks: NOMA and OMA," *IEEE Communications Letters*, vol. 25, no. 9, pp. 3036–3040, 2021.

[113] Y. Liu, X. Mu, J. Xu, R. Schober, Y. Hao, H. V. Poor, and L. Hanzo, "STAR: Simultaneous transmission and reflection for 360° coverage by intelligent surfaces," *IEEE Wireless Communications*, vol. 28, no. 6, pp. 102–109, 2021.

[114] X. Mu, Y. Liu, L. Guo, J. Lin, and R. Schober, "Simultaneously transmitting and reflecting (STAR) RIS aided wireless communications," *IEEE Transactions on Wireless Communications*, vol. 21, no. 5, pp. 3083–3098, 2021.

[115] X. Mu, Y. Liu, L. Guo, J. Lin, and N. Al-Dhahir, "Exploiting intelligent reflecting surfaces in NOMA networks: Joint beamforming optimization," *IEEE Transactions on Wireless Communications*, vol. 19, no. 10, pp. 6884–6898, 2020.

[116] G. Yang, X. Xu, Y.-C. Liang, and M. Di Renzo, "Reconfigurable intelligent surface-assisted non-orthogonal multiple access," *IEEE Transactions on Wireless Communications*, vol. 20, no. 5, pp. 3137–3151, 2021.

[117] M. Fu, Y. Zhou, Y. Shi, and K. B. Letaief, "Reconfigurable intelligent surface empowered downlink non-orthogonal multiple access," *IEEE Transactions on Communications*, vol. 69, no. 6, pp. 3802–3817, 2021.

[118] R. Hadani and A. Monk, "OTFS: A new generation of modulation addressing the challenges of 5G," *arXiv preprint arXiv:1802.02623*, 2018.

[119] P. Raviteja, Y. Hong, E. Viterbo, and E. Biglieri, "Practical pulse-shaping waveforms for reduced-cyclic-prefix OTFS," *IEEE Transactions on Vehicular Technology*, vol. 68, no. 1, pp. 957–961, 2018.

[120] K. R. Murali and A. Chockalingam, "On OTFS modulation for high-doppler fading channels," in *2018 Information Theory and Applications Workshop (ITA)*. IEEE, 2018, pp. 1–10.

[121] Z. Ding, R. Schober, P. Fan, and H. V. Poor, "OTFS-NOMA: An efficient approach for exploiting heterogenous user mobility profiles," *IEEE Transactions on Communications*, vol. 67, no. 11, pp. 7950–7965, 2019.

[122] Z. Ding, "Robust beamforming design for OTFS-NOMA," *IEEE Open Journal of the Communications Society*, vol. 1, pp. 33–40, 2019.

[123] Y. Sun, D. W. K. Ng, Z. Ding, and R. Schober, "Optimal joint power and subcarrier allocation for full-duplex multicarrier non-orthogonal multiple access systems," *IEEE Transactions on Communications*, vol. 65, no. 3, pp. 1077–1091, 2017.

[124] Z. Ding, P. Fan, and H. V. Poor, "On the coexistence between full-duplex and NOMA," *IEEE Wireless Communications Letters*, vol. 7, no. 5, pp. 692–695, 2018.

[125] X. Yue, Y. Liu, S. Kang, A. Nallanathan, and Z. Ding, "Spatially random relay selection for full/half-duplex cooperative NOMA networks," *IEEE Transactions on Communications*, vol. 66, no. 8, pp. 3294–3308, 2018.

[126] ——, "Exploiting full/half-duplex user relaying in NOMA systems," *IEEE Transactions on Communications*, vol. 66, no. 2, pp. 560–575, 2017.

[127] X. Zhang, Q. Gao, C. Gong, and Z. Xu, "User grouping and power allocation for NOMA visible light communication multi-cell networks," *IEEE communications letters*, vol. 21, no. 4, pp. 777–780, 2016.

[128] L. Yin, W. O. Popoola, X. Wu, and H. Haas, "Performance evaluation of non-orthogonal multiple access in visible light communication," *IEEE Transactions on Communications*, vol. 64, no. 12, pp. 5162–5175, 2016.

[129] C. Chen, W.-D. Zhong, H. Yang, and P. Du, "On the performance of MIMO-NOMA-based visible light communication systems," *IEEE Photonics Technology Letters*, vol. 30, no. 4, pp. 307–310, 2017.

[130] U. Ghafoor, M. Ali, H. Z. Khan, A. M. Siddiqui, and M. Naeem, "NOMA and future 5G & B5G wireless networks: A paradigm," *Journal of Network and Computer Applications*, vol. 204, p. 103413, 2022.

[131] A. A. Bipon, A. Osman, M. S. Islam, A. T. Asyhari, and R. Abozariba, "Pathfinder: End-to-end automation of coverage mapping of 4G/5G networks at street level," in *2023 20th Annual IEEE International Conference on Sensing, Communication, and Networking (SECON)*. IEEE, 2023, pp. 375–377.

[132] Nokia. 5G core. Accessed: June 2022. [Online]. Available: https://www.nokia.com/networks/core/5g-core

[133] MathWorks, "5G toolbox documentation: NR PDSCH throughput. https://uk.mathworks.com/help/5g/ug/nr-pdsch-throughput.html#NewRadioPDSCHThroughputExample-13," 2020, [accessed June 2020].

[134] "Physical channels and modulation," 2020, 3GPP TR 38.901 version 16.2.0 Release 16. [Online]. Available: https://www.etsi.org/deliver/etsi_ts/138200_138299/138211/16.02.00_60/ts_138211v160200p.pdf

[135] J. H. Bae, A. Abotabl, H.-P. Lin, K.-B. Song, and J. Lee, "An overview of channel coding for 5G NR cellular communications," *APSIPA transactions on signal and information processing*, vol. 8, p. e17, 2019.

[136] K. Arora, J. Singh, and Y. S. Randhawa, "A survey on channel coding techniques for 5G wireless networks," *Telecommunication Systems*, vol. 73, pp. 637–663, 2020.

[137] MATLAB, "5G Toolbox," https://uk.mathworks.com/products/5g.html, accessed: November, 2021.

[138] "5G; Study on channel model for frequencies from 0.5 to 100 GHz," 2020, 3GPP TR 38.901 version 16.1.0 Release 16. [Online]. Available: https://www.etsi.org/deliver/etsi_tr/138900_138999/138901/16.01.00_60/tr_138901v160100p.pdf

[139] Y. O. Imam-Fulani, N. Faruk, O. A. Sowande, A. Abdulkarim, E. Alozie, A. D. Usman, K. S. Adewole, A. A. Oloyede, H. Chiroma, S. Garba *et al.*, "5G frequency standardization, technologies, channel models, and network deployment: Advances, challenges, and future directions," *Sustainability*, vol. 15, no. 6, p. 5173, 2023.

[140] A. S. M. Mohammed, A. I. A. Taman, A. M. Hassan, and A. Zekry, "Deep learning channel estimation for OFDM 5G systems with different channel models," *Wireless Personal Communications*, vol. 128, no. 4, pp. 2891–2912, 2023.

[141] R. Abozariba, E. Davies, M. Broadbent, and N. Race, "Evaluating the real-world performance of 5G fixed wireless broadband in rural areas," in *2019 IEEE 2nd 5G World Forum (5GWF)*. IEEE, 2019, pp. 465–470.

[142] M. S. Islam, M. Patwary, R. Tait, and E. Peytchev, "Layer division multiplexing for 5G DL transmission within ultra-dense heterogeneous networks," in *2020 IEEE 91st Vehicular Technology Conference (VTC2020-Spring)*. IEEE, 2020, pp. 1–7.

[143] M. S. Islam, R. Abozariba, A. T. Asyhari, M. Patwary, and M. A. Matin, "Feasibility of ldm to serve user-iot pairs in the future wireless network," in *A Glimpse Beyond 5G in Wireless Networks*. Springer, 2022, pp. 231–253.

[144] J. Hayes, A. Aneiba, and M. Gaber, "SymbIoT: towards an extensible blockchain integration testbed for IIoT," in *Proceedings of the 1st Workshop on Enhanced Network Techniques and Technologies for the Industrial IoT to Cloud Continuum*, 2023, pp. 8–14.

[145] J. Hayes, A. Aneiba, M. Gaber, M. S. Islam, and R. Abozariba, "FBA-SDN: a federated byzantine approach for blockchain-based collaborative intrusion detection in edge SDN," in *2023 IEEE International Conference on Communications Workshops (ICC Workshops)*. IEEE, 2023, pp. 427–433.

[146] M. Razaak, H. Kerdegari, E. Davies, R. Abozariba, M. Broadbent, K. Mason, V. Argyriou, and P. Remagnino, "An integrated precision farming application based on 5G, UAV and deep learning technologies," in *Computer Analysis of Images and Patterns: CAIP 2019 International Workshops, ViMaBi and DL-UAV, Salerno, Italy, September 6, 2019, Proceedings 18*. Springer, 2019, pp. 109–119.

[147] M. Patwary, S. K. Sharma, S. Chatzinotas, Y. Chen, M. Abdel-Maguid, R. Abd-Alhameed, J. Noras, and B. Ottersten, "Universal intelligent small cell (UnIS-Cell) for next generation cellular networks," *Digital Communications and Networks*, vol. 2, no. 4, pp. 167–174, 2016.

[148] B. Sklar, *Digital communications: fundamentals and applications*. Pearson, 2021.

[149] F. Khan, Z. Pi, and S. Rajagopal, "Millimeter-wave mobile broadband with large scale spatial processing for 5G mobile communication," in *2012 50th annual allerton conference on communication, control, and computing (Allerton)*. IEEE, 2012, pp. 1517–1523.

[150] N. Deng and M. Haenggi, "A fine-grained analysis of millimeter-wave device-to-device networks," *IEEE Transactions on Communications*, vol. 65, no. 11, pp. 4940–4954, 2017.

[151] J. Li, X. Li, A. Wang, and N. Ye, "Beamspace MIMO-NOMA for millimeter-wave broadcasting via full-duplex d2d communications," *IEEE Transactions on Broadcasting*, vol. 66, no. 2, pp. 545–554, 2020.

[152] M. Roy and H. Jamadagni, "Performance analysis of MQAM-OFDM based WLAN in presence of zigbee interference in AWGN and rayleigh fading channel," in *2009 Sixth International Conference on Information Technology: New Generations*. IEEE, 2009, pp. 1178–1183.

[153] M. K. Simon and M. S. Alouini, *Digital Communication over Fading Channels: A unified Approach to Performance Analysis*. Wiley, 2000.

[154] C. E. Shannon, "A mathematical theory of communication," *The Bell system technical journal*, vol. 27, no. 3, pp. 379–423, 1948.

[155] E. Garro, J. J. Giménez, D. Gómez-Barquero, and S.-I. Park, "Performance evaluation of layer division multiplexing (LDM) combined with time frequency slicing (TFS)," in *2015 IEEE International Symposium on Broadband Multimedia Systems and Broadcasting*. IEEE, 2015, pp. 1–5.

[156] E. Arruti, M. Mendicute, and M. Barrenechea, "QoS in industrial wireless networks using LDM," in *2017 IEEE International Workshop of Electronics, Control, Measurement, Signals and their Application to Mechatronics (ECMSM)*. IEEE, 2017, pp. 1–6.

[157] R. Kumar and M. Dave, "Mobility models and their affect on data aggregation and dissemination in vehicular networks," *Wireless personal communications*, vol. 79, no. 3, pp. 2237–2269, 2014.

[158] M. K. Naeem, R. Abozariba, M. Asaduzzaman, and M. Patwary, "Towards the mobility issues of 5G-NOMA through user dissociation and re-association control," in *2020 IEEE 21st International Symposium on" A World of Wireless, Mobile and Multimedia Networks"(WoWMoM)*. IEEE, 2020, pp. 427–432.

[159] ——, "Mobility support for MIMO-NOMA user clustering in next-generation wireless networks," *IEEE Transactions on Mobile Computing*, 2022.

[160] S. Zhang, K. Peng, and J. Song, "Performance analysis and power allocation for spatial modulation-aided MIMO-LDM with finite alphabet inputs," *IEEE Transactions on Broadcasting*, 2022.

[161] A. Akbar, S. Jangsher, and F. A. Bhatti, "NOMA and 5G emerging technologies: A survey on issues and solution techniques," *Computer Networks*, vol. 190, p. 107950, 2021.

[162] E. C. Cejudo, H. Zhu, and J. Wang, "Resource allocation in multicarrier NOMA systems based on optimal channel gain ratios," *IEEE Transactions on Wireless Communications*, vol. 21, no. 1, pp. 635–650, 2021.

[163] R. Abozariba, M. K. Naeem, M. Patwary, M. Seyedebrahimi, P. Bull, and A. Aneiba, "NOMA-based resource allocation and mobility enhancement framework for IoT in next generation cellular networks," *IEEE Access*, vol. 7, pp. 29 158–29 172, 2019.

[164] H. Yahya, E. Alsusa, and A. Al-Dweik, "Exact BER analysis of NOMA with arbitrary number of users and modulation orders," *IEEE Transactions on Communications*, vol. 69, no. 9, pp. 6330–6344, 2021.

[165] S. I. Park, J.-Y. Lee, S. Myoung, L. Zhang, Y. Wu, J. Montalbán, S. Kwon, B.-M. Lim, P. Angueira, H. M. Kim *et al.*, "Low complexity layered division multiplexing for ATSC 3.0," *IEEE Transactions on broadcasting*, vol. 62, no. 1, pp. 233–243, 2016.

[166] G.-R. Barb, M. Otesteanu, G. Budura, and C. Balint, "Performance evaluation of tdl channels for downlink 5g mimo systems," in *2019 International Symposium on Signals, Circuits and Systems (ISSCS)*. IEEE, 2019, pp. 1–4.

[167] A. M. Pessoa, B. Sokal, C. F. e Silva, T. F. Maciel, A. L. de Almeida, D. A. Sousa, Y. C. Silva, and F. R. P. Cavalcanti, "Cdl-based channel model for 5g mimo systems in remote rural areas," in *2019 16th International Symposium on Wireless Communication Systems (ISWCS)*. IEEE, 2019, pp. 21–26.

[168] A. Goldsmith, *Wireless communications*. Cambridge University Press, 2005.

[169] G. H. Golub and C. F. Van Loan, *Matrix computations*. JHU press, 2013.

[170] J. H. Winters, "The diversity gain of transmit diversity in wireless systems with rayleigh fading," *IEEE transactions on vehicular technology*, vol. 47, no. 1, pp. 119–123, 1998.

[171] MATLAB, "NR PDSCH Throughput," https://uk.mathworks.com/help/5g/ug/nr-pdsch-throughput.html, accessed: May 25, 2023.